The role of *MIRNA156* and *MIRNA157* during floral transition at the shoot apical meristem

Inaugural-Dissertation

zur

Erlangung des Doktorgrades
der
Mathematisch-Naturwissenschaftlichen
Fakultät der Universität zu Köln

vorgelegt von

Adrian Roggen
Aus Bergisch Gladbach

Köln, August 2022

The role of *MIRNA156* and *MIRNA157* during floral transition at the shoot apical meristem

Inaugural-Dissertation

zur

Erlangung des Doktorgrades

der

Mathematisch-Naturwissenschaftlichen Fakultät

der Universität zu Köln

vorgelegt von

Adrian Hermann Roggen

Aus Bergisch Gladbach

Köln, 2022

Die vorliegende Arbeit wurde am Max-Planck-Institut für Pflanzenzüchtungsforschung in Köln in der Abteilung für Entwicklungsbiologie der Pflanzen (Direktor Prof. Dr. G. Coupland), Arbeitsgruppe Prof. Dr. George Coupland durchgeführt.

The work described in this thesis was conducted at the Max Planck Institute for Plant Breeding Research in the Department of Plant Developmental Biology (Director: Prof. Dr. George Coupland) under the supervision of Prof. Dr. George Coupland.

Berichterstatter (Gutachter):	**Prof. Dr. George Coupland**
	Prof. Dr. Ute Höcker
Prüfungsvorsitzender**:**	**Prof. Dr. Martin Hülskamp**
Tag der mündlichen Prüfung:	**29. November 2022**

MAX-PLANCK-INSTITUT
FÜR PFLANZENZÜCHTUNGSFORSCHUNG

1. Abstract

Developmental transitions are periods of change between phases of greater stability and they enable multicellular organisms to drastically alter their mode of growth. Developmental transitions are subject to strict regulation, often involving small molecules termed microRNAs (miRNAs) that repress target genes post-transcriptionally. In *Arabidopsis thaliana* (Arabidopsis), miRNA156 controls developmental timing both during vegetative and reproductive growth. Its targets are members of the *SQUAMOSA PROMOTER BINDING PROTEIN-LIKE (SPL)* family of transcription factors, which includes the floral integrator *SPL15* that promotes flowering under non-inductive conditions. Plants expressing miR156-resistant *SPL15 (rSPL15)* transition prematurely, whereas those that overexpress miR156 are late flowering. In seedlings, miR156 is highly abundant and rapidly decreases as plants grow, thus setting the rate of developmental progression and contributing to the control of flowering time.

Two closely related *MIR156* and *MIR157* families, consisting of eight and four genes respectively, encode isoforms of miR156 in Arabidopsis. Of these, *MIR156A, MIR156C*, *MIR157A* and *MIR157C* are the most abundant and show age-dependent expression patterns. The roles of *MIR156* and *MIR157* in flowering are often described synonymously and a detailed analysis of their functions during floral transition is currently lacking. Taking advantage of small RNA-sequencing and CRISPR/Cas9-induced mutants, I characterised the relationship among *MIR156* and *MIR157* genes and their individual contributions towards floral transition. I observed different dynamics in miR156 and miR157 abundance over time that was also reflected in photoperiod-dependent flowering phenotypes of mutants. Strikingly, mutations in *MIR157* genes affected inflorescence development after floral transition, a phenotype that resembled that of *rSPL15* plants, but not *mir156* mutants. The mechanistic basis for this phenotype was then investigated by performing genetic interaction studies and confocal imaging. The spatial expression pattern of SPL15 and FRUITFULL, which act downstream of miR156, was not altered in *mir157* mutants, whereas their temporal expression was accelerated. The combination of *mir157* and *fruitfull* mutations had synergistic effects on inflorescence development.

Ultimately, this work provides a more detailed understanding of the role of miR156 isoforms at the shoot apex in antagonizing flowering under non-inductive conditions and demonstrates that in particular, *MIR157* genes have specific functions in inflorescence development.

Table of Contents

2. Introduction

2.1. MicroRNAs and developmental transitions

The field of developmental biology involves the study of the complexities of coordinating growth in multi-cellular organisms. Multicellular life arose several times during evolution, and independently in animals and plants (Grosberg and Strathmann, 2007). Despite the great diversification across the tree of life, recurring developmental themes can be identified. One of these is the characterisation of development as a series of successive transitions. In a broad sense, developmental transitions can be defined as occurrences of greater changes between phases of relative stability (Connell and Furman, 1984). A typical feature of multicellular life is the differentiation of specialised tissues, in which cells are programmed to fulfil specific functions (Grosberg and Strathmann, 2007). The development of a complex morphology with multiple tissues requires tight regulation in space and time. Thus, developmental transitions are characterised by responsiveness to a multitude of environmental and endogenous cues, which are integrated by master regulators (Kaufmann and Airoldi, 2018).

MicroRNAs are a class of small RNAs (sRNAs) that often function as negative regulators of transcription factors with major roles in development. These short molecules are generated from the processing of precursor transcripts and contribute to post-transcriptional gene silencing (PTGS). Their mode of action involves complementary base pairing with target transcripts that leads to the degradation of the mRNA or blocking of its translation. The activity of miRNAs can shape the spatial (Skopelitis et al., 2017) or temporal expression patterns of target genes (Nodine and Bartel, 2010) and is proposed to confer robustness to developmental transitions (Ebert and Sharp, 2012).

The concept of miRNAs emerged from studying developmental stages of the nematode *Caenorhabditis elegans* (Lee et al., 1993; Ruvkun et al., 2004; Wightman et al., 1993). The *C. elegans* life cycle encompasses four successive larval stages (Rougvie and Moss, 2013). The *LIN-14* protein is expressed during the first larval stage and its abundance decreases before the transition to the second stage (Ruvkun and Giusto, 1989). Different mutations in the *lin-14* gene led to both gain- and loss-of-

function alleles with opposite effects on developmental timing. The *lin-4* gene was identified as a negative regulator of *LIN-14* protein abundance, whereas *lin-14* transcription and polyadenylation remained unaffected (Olsen and Ambros, 1999). The *lin-4* gene product is a 22-nucleotide miRNA that has a complementary binding site in the 3′ untranslated region (3′UTR) of *lin-14.* Mutations that disrupted the *lin-4* binding site were causal for *lin-14* gain-of-function alleles. Thus, a miRNA switch is responsible for the timing of larval developmental transition. The second miRNA that was discovered, let-7, is widely conserved among species in addition to nematodes. Orthologues of let-7 are present in the genomes of Drosophila, humans and maritime sponges (Pasquinelli et al., 2000). This finding led to miRNAs being acknowledged as more ubiquitous regulators of developmental transitions.

Molecular cloning and bioinformatic analyses led to the identification of a plethora of miRNA families in plants (Llave et al., 2002a; Park et al., 2002; Reinhart et al., 2002; Rhoades et al., 2002). Plant miRNAs are central to a variety of developmental processes, which is also reflected by the pleiotropic or lethal phenotypes of mutants in miRNA biogenesis (Clarke et al., 1999; Han et al., 2004; Kidner and Martienssen, 2004; Park et al., 2002). Processes that involve miRNA-mediated regulation include embryogenesis, leaf development, stem cell maintenance and flowering (Laufs et al., 2004; Nodine and Bartel, 2010; Palatnik et al., 2003; Wu and Poethig, 2006; Wu et al., 2006). Analogously to the developmental regulatory function of lin-4 and let-7 miRNAs in *C. elegans*, miRNA156 (miR156) is a plant-specific miRNA that regulates morphological changes during vegetative growth and the age at which plants become competent to flower (Bergonzi et al., 2013; Wang et al., 2009; Wu et al., 2009).

2.2. Floral transition and inflorescence architecture in *Arabidopsis thaliana*

One of the most important events in the plant life cycle is floral transition, when the identity of the apical meristem is switched from vegetative growth to reproductive growth. An extensive reliance on post-embryonic development and modular architecture are traits that distinguish land plants from animals. Upon germination, a seedling consists of a limited number of organs – two cotyledons, an hypocotyl and a primary root – all of which are established during embryogenesis. The shoot apical

meristem (SAM), located at the junction between the cotyledons and hypocotyl, is the specialised tissue from which all aerial organs derive. Its stereotypical morphology consists of a central zone at the apex, a peripheral zone at the flanks and a rib zone subtending the central zone (Barton, 2010; Bowman and Eshed, 2000). In the central zone, a population of pluripotent stem cells is maintained, and lateral organ primordia are initiated within the peripheral zone. The rib zone gives rise to the stem and associated vasculature (Basile et al., 2017). During vegetative growth, the *Arabidopsis thaliana* (hereafter Arabidopsis) SAM is relatively flat and initiates leaf primordia in a spiral phyllotaxis (Bernier, 1988; Lee et al., 2009). Internode elongation is suppressed, leading to a characteristic rosette growth habit. Axillary meristems are initiated at the boundaries between leaf primordia and the SAM. In vegetative plants, this initiation occurs acropetally at a distance from the SAM. After the SAM initiates a few leaf primordia, the axillary meristems enter a paradormant state until reproductive development begins (Grbić and Bleecker, 2000; Long and Barton, 2000; Stirnberg et al., 1999).

The transition to flowering is associated with marked changes in SAM and shoot morphology (Kinoshita et al., 2020; Lyndon and Battey, 1985; Tal et al., 2017). At an early stage of the transition, the number and size of cells within the SAM increases. This leads to a rapid increase in the height of the meristem, which adopts a domed structure that reduces in height again once floral transition is completed (Jacqmard et al., 2003; Kinoshita et al., 2020; Kwiatkowska, 2008; Tal et al., 2017). The apical meristem is now termed an inflorescence meristem (IM) and the identity of initiated primordia changes, which occurs in two phases (Hempel and Feldman, 1994; Pouteau and Albertini, 2009; Talbert et al., 1995). In the first phase (I1), the youngest primordia develop into cauline leaves. The internodes between the cauline leaves rapidly elongate, which drives the bolting of the main shoot. Axillary meristems are initiated in the axils of cauline leaves immediately at the SAM and remain active to generate outgrowing secondary inflorescences.

The second phase of floral transition (I2) involves flower production. The axillary meristems now acquire a floral meristem identity and generate floral buds. The associated subtending leaf, termed a bract, is initiated at the SAM, but its outgrowth is subsequently repressed (Baum and Day, 2004; Karim et al., 2009; Long and Barton,

2000). Under non-optimal conditions and in some mutant genotypes, the bracts develop and subtend the flowers (Liljegren et al., 1999; Tooke et al., 2005). After a period of producing siliques, the inflorescence meristem ceases to initiate organs and enters proliferative arrest (Balanzà et al., 2018). In annual plants, inflorescence development is also the last phase of the life cycle, which ends with whole-plant senescence after the production of seeds.

2.3. Genetic basis of the floral transition in Arabidopsis

Flowering time is controlled by several gene regulatory networks that converge on a small number of floral integrators (Pajoro et al., 2014). Independent of the specific pathway that initiates floral transition, floral development involves the sustained expression of the floral meristem identity genes *APETALA1* (*AP1*) and *LEAFY* (*LFY*) in developing floral primordia at the SAM (Liljegren et al., 1999). These genes are activated by a set of MADS-box transcription factors, including *SUPPRESSOR OF OVEREXPRESSION OF CONSTANS1* (*SOC1*) and *FRUITFULL* (*FUL*) (Immink et al., 2012; Teper-Bamnolker and Samach, 2005; Torti and Fornara, 2012).

On the basis of their flowering response to photoperiod, plants can be characterised as either short-day, day-neutral or long-day (Thomas and Vince-Prue, 1996). The major model plant species Arabidopsis is an annual Brassicaceae that flowers most rapidly in long days containing more than 12 hours of day light. This day-length response contributes to the rapid-cycling growth habit, and is controlled genetically by the photoperiodic pathway. The effectors of this pathway are the two paralogous master regulators *FLOWERING LOCUS T* (*FT*) and *TWIN SISTER OF FT* (*TSF*) (Figure 2.1). Both genes are transcriptionally activated in response to long days by the circadian-clock-controlled CONSTANS (CO) protein (Samach et al., 2000; Suárez-López et al., 2001; Valverde et al., 2004; Yamaguchi et al., 2005). This occurs in phloem companion cells of the leaf vasculature around 12- 16 hours after dawn (Böhlenius et al., 2006; Chen et al., 2018b; Corbesier et al., 2007; Yamaguchi et al., 2005). The FT and TSF proteins are then loaded into the phloem transport stream and are translocated to the SAM, where they initiate floral transition (Corbesier et al., 2007; Liu et al., 2019; Mathieu et al., 2007). FT and TSF are unable to bind DNA, but they

induce transcriptional changes at the SAM during floral transition, by each interacting with the bZIP transcription factor FD and 14-3-3 scaffolding proteins to form the florigen activation complex (FAC) (Abe et al., 2005, 2019; Taoka et al., 2011). Because the *FT/TSF* and *FD* expression domains are physically distinct in the plant, long-distance movement of the FT protein is essential for FAC formation (Abe et al., 2019; Corbesier et al., 2007). At the SAM, the complex directly induces the expression of *SOC1*, *FUL* and *AP1* and indirectly induces *LFY* (Collani et al., 2019; Romera-Branchat et al., 2020).

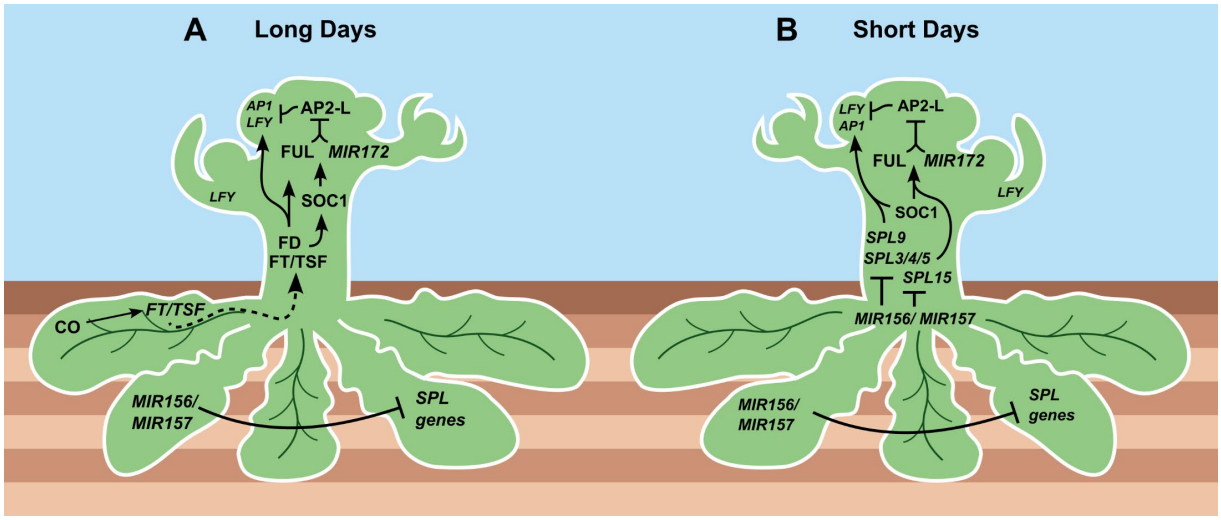

Figure 2.1. Schematic representation of floral induction under long days and short days. A) The photoperiod pathway activates *FT/TSF* expression in leaves under long days. B) SPL transcription factors play a central role in promoting flowering under non-inductive conditions. CONSTANS (CO), *FLOWERING LOCUS T/ TWIN SISTER OF FT* (*FT/TSF*), FD transcription factor (FD), *SQUAMOSA PROMOTER BINDING PROTEIN-LIKE* (SPL), FRUITFULL (FUL), SUPPRESSOR OF OVEREXPRESSION OF CO 1 (SOC1), LEAFY (LFY), *APETALA1* (*AP1*).

If the day length is shorter than that required for *FT/TSF* activation in leaves, floral transition is activated via alternative pathways. The functional interaction between *SOC1* and *SQUAMOSA PROMOTER BINDING PROTEIN-LIKE 15 (SPL15)*, which encodes a plant-specific transcription factor of the SPL family, plays a central role in promoting flowering under non-inductive conditions. Together, SOC1 and SPL15, promote floral transition by integrating signalling from the gibberellin (gibberellic acid, GA) and age pathways of flowering (Hyun et al., 2016, 2019; Jung et al., 2012). Both *spl15* and *soc1* mutants flower late under short days and show a reduced sensitivity to exogenous GA application (Hyun et al., 2016; Moon et al., 2003). Gibberellins are essential for flowering in short-day conditions (Wilson et al., 1992), and the exogenous

application of GA accelerates flowering, which partially depends on SPL15 function under short days (Blázquez et al., 1998; Galvão et al., 2012; Hyun et al., 2016). The perception of the developmental age of the plant is integrated at the level of *SPL15* and closely related *SPL* genes that are targeted by the miR156 and miR157 post-transcriptional repressors (Hyun et al., 2016; Jung et al., 2012; Wang et al., 2009).

2.4. The SPL family of transcription factors and their roles in vegetative phase change and the age pathway of flowering

The SPL transcription factors form a family of plant-specific developmental regulators (Klein et al., 1996; Xie et al., 2006). Phylogenetically, the family is subdivided into at least eight clades, of which four predate the diversification of land plants (Preston and Hileman, 2013). Out of the 17 *SPL* genes present in the Arabidopsis genome, in total 11 (SPL2/ SPL3/ SPL4 /SPL5/ SPL6/ SPL8/ SPL9/ SPL10/ SPL13A/ SPL13B and SPL15) are targets of miR156. The conserved miR156-binding sites are located within the coding sequence or the 3′UTR. After binding to complementary sequences in target transcripts, miR156 represses the function of *SPL* genes by either inducing the degradation of their transcripts or by interfering with their translation (Song et al., 2019). The prevalent mechanism of miRNA repression varies according to targets; targets, such as *SPL3* can be subject to both mechanisms (Gandikota et al., 2007). The translational repression of target mRNAs reduces the ratio of protein level to mRNA abundance. Although some miRNAs are involved in spatially regulating their target genes, miR156 has been proposed to be a quantitative regulator (Nodine and Bartel, 2010; Wang et al., 2008).

The regulation of *SPL* genes by miR156 is conserved among land plants (Arazi et al., 2005; Axtell et al., 2007; Cho et al., 2012). A high miR156 level in young plants prevent the precocious expression of miR156-responsive SPL transcription factors (Bergonzi et al., 2013; He et al., 2018; Hyun et al., 2016). The abundance of miR156 then decreases with progressing developmental age. This mechanism also provides the basis of the age signalling pathway that regulates the timing of vegetative development and flowering in distantly related Angiosperms. The relationship between SPL genes and miR156/miR157 has been described in species such as tobacco (Feng et al., 2016), trees (Wang et al., 2011), grasses (Chuck et al., 2010; Jiao et al., 2010; Liu et al., 2017; Miura et al., 2010; Xie et al., 2006) and mosses (Cho et al., 2012).

During vegetative phase change, SPL transcription factors confer changes in leaf morphology. These include trichomes on the abaxial side of leaves, promoting leaf serration and leaf blade growth (Schwab et al., 2005; Wu and Poethig, 2006). Constitutive overexpression of *MIR156* genes inhibits *SPL* function and extends the juvenile phase. Accordingly, *MIR156* overexpressors develop smaller leaves with a round shape and long petioles (Schwab et al., 2005; Wu and Poethig, 2006). *SPL* genes fulfil similar functions in grasses. In maize, the heterochronic *corngrass* mutant shows an extended juvenile phase and increased branching phenotypes, which are caused by *MIR156* overexpression from tandem duplicated genes (Chuck et al., 2007).

In Arabidopsis, decrease in the level of miR156 allows the accumulation of the floral integrator SPL15 at the SAM that cooperates with SOC1 to activate *FUL* and *MIR172B* expression (Hyun et al., 2016). miR172 represses a set of genes encoding APETALA2-LIKE (AP2-LIKE) transcription factors that act as floral repressors during vegetative growth, and the expression dynamic of miR172 is broadly anti-correlated with that of miR156 (Aukerman and Sakai, 2003; Chen, 2004; Lian et al., 2021; Ó'Maoiléidigh et al., 2021; Wu et al., 2009). Following the induction of miR172 expression, the level of inhibitory AP2-LIKE floral inhibitor proteins is reduced in the SAM, which allows floral transition to proceed (Lian et al., 2021; Ó'Maoiléidigh et al., 2021; Sang et al., 2022; Wu and Poethig, 2006). In parallel, FUL represses *AP2-LIKE* genes via directly binding their promoters (Balanzà et al., 2018).

Other members of the SPL family also participate in floral transition. The closest paralogue of *SPL15* is *SPL9* (Preston and Hileman, 2013). Loss of *SPL9* function enhances the *spl15-1* mutant late-flowering phenotype, but single *spl9* mutants show only a slight delay in flowering time (Hyun et al., 2016). This might be due to the divergent spatial expression domains of both genes. Although *SPL15* is expressed throughout the SAM, *SPL9* expression localises to the peripheral zone, which suggests that both genes possess divergent functions (Hyun et al., 2016). Whereas *SPL15* expression induces floral transition at the central zone, SPL9 might directly activate *AP1* expression at the peripheral zone (Hyun et al., 2016; Yamaguchi et al., 2014).

The closely related SPL3, SPL4 and SPL5 (SPL3/4/5) proteins form a separate clade within the SPL family and are the smallest SPL proteins (Preston and Hileman, 2013). All three proteins retain the SBP DNA-binding domain and can bind DNA, but they

lacked transactivation activity in protoplast experiments (Gandikota et al., 2007; Jung et al., 2016; Xing et al., 2010). To exert their regulatory function, these small SPL proteins might interact with other transcription factors.

Similar to *SPL9* and *SPL15*, *SPL3, SPL4* and *SPL5* contribute to floral induction, which is best studied in long days. The expression of *SPL3, SPL4* and *SPL5* (*SPL3*/*4*/*5*) is upregulated during floral transition at the shoot apex (Olas et al., 2019; Torti et al., 2012). *In situ* hybridisation experiments showed that *SPL3* transcripts localise to the periphery of the shoot apex, whereas *SPL4* and *SPL5* mRNAs are present in the rib zone of the SAM (Olas et al., 2019; Wang et al., 2009). Evidence suggests that the function of the three paralogues might be more relevant to floral induction under long days than are *SPL9* and *SPL15.* When wild-type plants are transferred from short-day to long-day conditions, a rapid upregulation of floral meristem identity genes including *AP1*, *FUL* and *LFY* occurs via the FT/TSF pathway. In *spl9 spl15* double mutants, the induction of *LFY* was delayed, but the mutations did not affect the responses of *AP1* and *FUL* to day length (Jung et al., 2016). By contrast, the simultaneous knockdown of *SPL3/4/5* expression additionally suppressed the upregulation of *AP1* and *FUL* (Jung et al., 2016). The SPL transcription factors bind to a GTAC core motif (Birkenbihl et al., 2005; Cardon et al., 1999; Liang et al., 2008; Yamasaki et al., 2009). Chromatin Immuno-precipitation (ChiP) and *in vitro* experiments indicate that SPL3/4/5 directly bind to GTAC motifs in the *AP1*, *FUL* and *LFY* promoters (Wang et al., 2009; Xie et al., 2020a; Yamaguchi et al., 2009). Binding of SPL3 to SOC1 and FT was also detected in *SPL3* overexpressors (Kim et al., 2012; Wang et al., 2009; Yamaguchi et al., 2009). However, the induction of *FT* expression in response to long days was not altered in these plants (Jung et al., 2016).

Consistent with the induction of SPL3/4/5 during floral transition, their overexpression causes early flowering. The rate of leaf initiation is reduced in plants with enhanced SPL9 or SPL15 levels, but is unaffected by changes SPL3/4/5 activity (Cardon et al., 1997; Hyun et al., 2016; Schwarz et al., 2008; Wang et al., 2008, 2009; Wu and Poethig, 2006). The *spl3 spl4 spl5* triple loss-of-function mutant produces significantly more rosette leaves than wild type (Xie et al., 2020a). The interaction with the photoperiodic pathway might occur at the protein level. SPL3/4/5 can physically interact with FD, but SPL9 or SPL15 cannot. The ability of *SPL3* overexpression lines to accelerate

flowering in response to long-day exposure depends on the presence of functional FD (Jung et al., 2016).

A role in the regulation of flowering time was additionally suggested for SPL10, SPL11 and SPL13, which might also regulate the expression of *MIR172* precursors (Wu et al., 2009, 2006). In addition to flowering, SPL transcription factors are involved in several of other developmental processes such as leaf development (Yamaguchi et al., 2009), shoot maturation (Schwarz et al., 2008; Wang et al., 2008) and stress responses (Chao et al., 2017; Stief et al., 2014; Zhou and Tang, 2018).

2.5. Developmental regulation of *MIR156* and *MIR157* precursors

MicroRNA156 is a 20- or 21-nucleotide-long sRNA that has been described as a developmental timer (Wu et al., 2009). It is encoded by the two closely related *MIR156* and *MIR157* gene families, which contain eight and four precursor genes respectively (Chorostecki et al., 2017; Jones-Rhoades and Bartel, 2004). The major miR156 isoform is 20 nucleotides long, whereas the predominant miR157 isoform is 21 nucleotides long (He et al., 2018). The sequence of these mature miRNAs differs by only three nucleotides, which leads to near-perfect complementarity to *SPL* transcripts, with a single mismatch each (Gandikota et al., 2007; He et al., 2018).

MIRNA families often encompass several genes that encode functionally equivalent miRNAs (Jones-Rhoades and Bartel, 2004). This renders the genetic analysis via complete loss-of-function mutants challenging. Prior to the advent of CRISPR/Cas9-mediated mutagenesis, the function of *MIR156* and *MIR157* genes was studied in T-DNA mutants (He et al., 2018; Yang et al., 2013; Yu et al., 2013) and various transgenic lines. These included plants overexpressing *MIR156* genes (Jung et al., 2011; Schwab et al., 2005; Wu and Poethig, 2006), artificial *MIM156/MIM157* target mimicries (Franco-Zorrilla et al., 2007; Todesco et al., 2010) or miR156/miR157-resistant *SPL* (*rSPL*) genes (Barrera-Rojas et al., 2019; Hyun et al., 2016; Wang et al., 2009). Plants overexpressing *MIM156/MIM157* and *rSPL* showed consistent phenotypes and were opposite to that of *MIR156*-overexpressing plants and *spl* mutants (Hyun et al., 2016;

Schwarz et al., 2008; Todesco et al., 2010; Wu and Poethig, 2006; Yamaguchi et al., 2009).

Four genes – *MIR156A*, *MIR156C*, *MIR157A* and *MIR157C* – are thought to generate the majority of mature miR156/miR157 (He et al., 2018). The miRNA156 was first identified as the master regulator of vegetative phase change, a term that collectively describes changes in leaf morphology, photosynthetic rate and competence to flower during vegetative growth (Bäurle and Dean, 2006; Poethig, 2013; Wang et al., 2011). A correlation between the level of miR156 and vegetative phase change is functionally conserved in various land plants such as perennial trees and grasses (Chuck et al., 2007; Jiao et al., 2010; Wang et al., 2011).

The dynamic abundance of miR156 provides a marker of developmental age. The miRNA is highly expressed in developing seeds and juvenile plants, but expression gradually decreases in shoot apices and successive leaf primordia (Cheng et al., 2021; He et al., 2018; Plotnikova et al., 2019; Wu et al., 2009). The manipulation of miR156/miR157 abundance alters the onset of vegetative phase change and the transition to flowering. Although miR156 overexpression extends the juvenile phase and delays flowering, depletion of miR156 results in precocious expression of adult traits and early flowering (Wu et al., 2009; Yang et al., 2013; Yu et al., 2013).

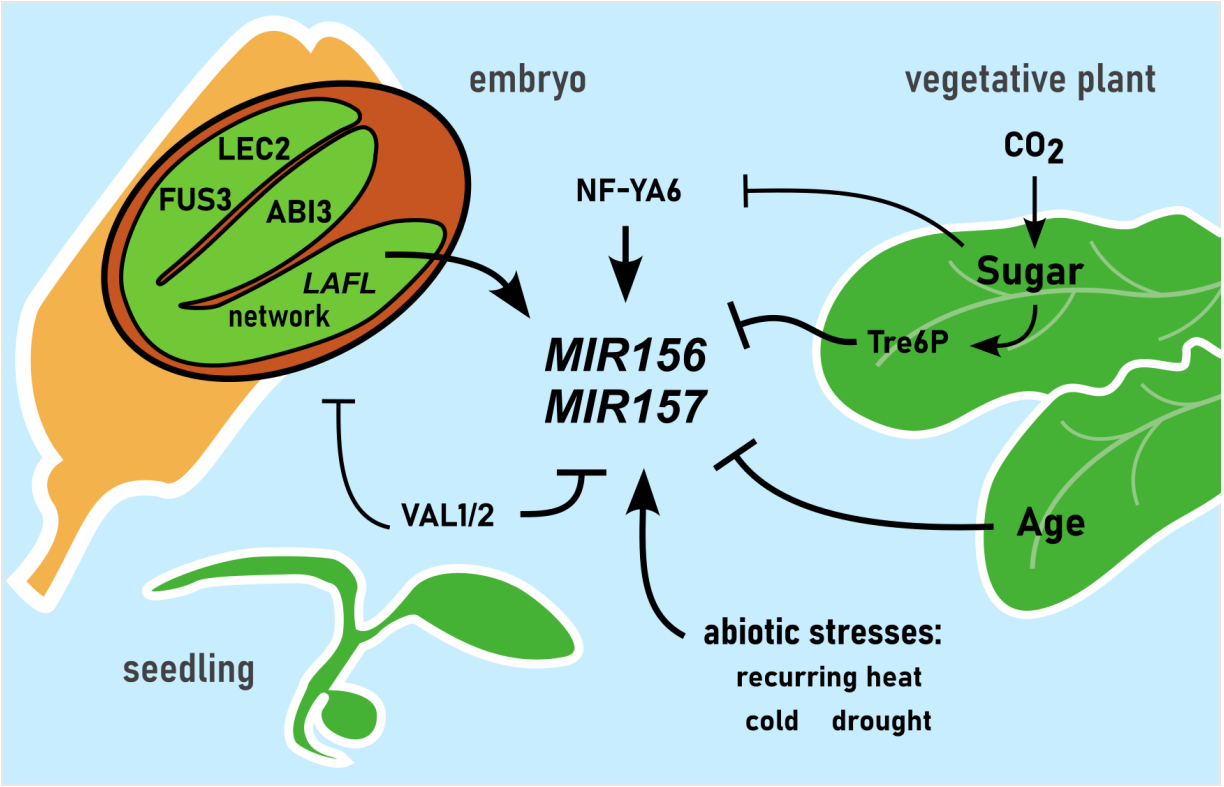

Figure 2.2. Factors that regulate *MIR156* and *MIR157* precursors during development. Known regulators are expressed during embryogenesis, germination or vegetative growth. Arrowheads indicate activation, bars represent repressive regulation. *LAFL* gene regulatory network [*LEAFY COTYLEDON1* (*LEC1*), *ABSISIC ACID INSENSITIVE 3* (*ABI3*), *FUSCA3* (FUS3) and *LEAFY COTYLEDON2* (*LEC2*)], VIVIPAROUS/ABI3-LIKE1 and 2 (VAL1/2), Trehalose-6-Phosphate (Tre6P), NUCLEAR FACTOR Y subunit A6 (NF-YA6).

The precise mechanisms that regulate the stereotypical expression pattern of miR156 are subject to active research and to date, several direct regulators of *MIR156* genes have been described. Notably, several members of the LAFL [*LEAFY COTYLEDON1* (*LEC1*), *ABSISIC ACID INSENSITIVE 3* (*ABI3*), *FUSCA3* (FUS3) and *LEAFY COTYLEDON2* (*LEC2*)] gene regulatory network that governs embryogenesis and seed maturation (Jia et al., 2014) activate specific *MIR156* genes. For example, the B3-type transcription factors LEC2, FUS3 and ABI3 bind to RY motifs in the promoters of *MIR156A* and *MIR156C* and induce their expression (Gao et al., 2022; Tian et al., 2020; Wang and Perry, 2013). In addition, ABI3 promotes the expression of *MIR156D* during early embryogenesis (Tian et al., 2020); thus, high miR156 expression is established during the earliest stages of development.

Expression of miR156 in the embryo probably suppresses SPL10 and SPL11 activity, which prevents precocious maturation of the seed (Nodine and Bartel, 2010; Rodrigues

and Miguel, 2017; Willmann et al., 2011). Upon germination, the influence of the LAFL network diminishes, in part due to transcriptional repression by another set of B3-type transcription factors, VIVIPAROUS/ABI3-LIKE1 and 2 [VAL1, VAL2 (Chen et al., 2018a; Suzuki et al., 2007; Tsukagoshi et al., 2007; Zhou et al., 2013b)]. The VAL1 and VAL2 proteins might also be involved in the repression of *MIR156* precursors (Fouracre et al., 2021; Picó et al., 2015). VAL1/ VAL2 are transcriptional repressors that recruit the polycomb repressive complex 2 (PRC2), which deposits the repressive histone3 lysine 27 trimethylation (H3K27me3) mark at target loci (Förderer et al., 2016; Mozgova and Hennig, 2015; Pengelly et al., 2013). Direct physical interaction between VAL proteins and PRC2 components has been demonstrated *in vivo* (Chen et al., 2018a; Yuan et al., 2021).

The expression of *MIR156* precursors and therefore the abundance of mature miR156 is also epigenetically regulated. In wild-type plants, the deposition of repressive H3K27me3 marks at *MIR156* loci progressively increases during vegetative development, which is correlated with a decrease in *MIR156* expression (Picó et al., 2015; Xu et al., 2016a). Experimental data from the use of transgenic reporter lines suggests that RY motifs in *MIR156* promoters function in this process. Mutation of these binding sites led to a marked increase in *MIR156* expression during vegetative development, which is consistent with the repressive function of VAL proteins (Fouracre et al., 2021). Double mutants carrying weak alleles of *val1* and *val2* express *MIR156A and MIR156C* at elevated levels (Fouracre et al., 2021; Picó et al., 2015). Chromatin remodellers such as *PICKLE* might also participate in the epigenetic regulation of *MIR156* (Hu et al., 2022; Xu et al., 2016b).

In the epigenetic mutants described above, miR156 abundance continues to follow the characteristic temporal decrease observed in wild type (Fouracre et al., 2021; Xu et al., 2016a, 2016b). Currently, two physiological concepts exist to explain the temporal regulation. The first concept is based on endogenous sugars that accumulate during vegetative growth as a consequence of increased photosynthetic activity (Buendía-Monreal and Gillmor, 2017; Yang et al., 2013; Yu et al., 2013). Experiments on plants with altered photosynthetic ability showed changes in miR156 expression. In chlorophyll-deficient plants, miR156 expression is elevated (Yang et al., 2013; Yu et al., 2013). Similarly, the physical removal of leaves promotes miR156 expression.

Elevated atmospheric CO_2 levels accelerate the rate of photosynthesis (Leakey et al., 2009). An sRNA sequencing experiment performed in these conditions showed a reduction in miR156 abundance, whereas the miR172 level increased (May et al., 2013). Recently, NY-A8, a subunit of the trimeric NUCLEAR FACTOR Y complex was reported to upregulate *MIR156* precursors (Zhao et al., 2020). The *NF-YA8* gene is highly expressed in juvenile leaves and is also repressed in response to sugar treatment. Exogenous application of sugars also represses miR156 levels, mainly through reduction of *MIR156A* and *MIR156C* (Yang et al., 2013; Yu et al., 2013).

In Arabidopsis, sucrose levels are correlated with the downstream signalling molecule trehalose-6-phosphate (Tre6P), which is primarily synthesised by Tre6P SYNTHETHASE 1 (TPS1) (Fichtner and Lunn, 2021). The function of TPS1 is essential during embryogenesis but not essential during later development (Eastmond et al., 2002; Wahl et al., 2013). Recovered *tps1* mutants express miR156 at a significantly higher level than wild-type plants and this affects both the timing of vegetative phase change and floral transition (Ponnu et al., 2020; Wahl et al., 2013).

A second concept links the decrease in *MIR156C* expression to the rate of cell division at the SAM (Cheng et al., 2021). During embryogenesis, transcription of a *MIR156C* reporter did not decrease at the quiescent apical meristem. After germination, *MIR156C* expression declined within the central and peripheral zones of the SAM, but it remained constant within the rib zone. This difference was attributed to varying rates of cell division. In roots, treatment with cell-cycle inhibitors and transferal of plants to low temperatures stabilised *MIR156C* reporter expression. Thus, the rate of cell division might be instructive for the age-related decrease in the level of *MIR156C*.

Environmental signals also modulate the expression of *MIR156* precursors. Exposure of juvenile plants to cold prevents the gradual decrease in the miR156 level in wild type (Bergonzi et al., 2013; Hyun et al., 2019). This mechanism plays an important role in the perennial life cycle of *Arabis alpina,* where it ensures that flowering only occurs in mature, established plants. Additionally, miR156 levels are affected by ambient temperature (Kim et al., 2012), recurring heat stress (Stief et al., 2014), and salt or drought stress (Cui et al., 2014).

2.6. Evolutionary conservation of *MIR156* and *MIR157* genes

Despite these divergences in the mature sequence, limited information is available concerning when or how the two *MIR* families separated during evolution.

Although *MIR156* family members are represented in all land plants (Arazi et al., 2005; Axtell et al., 2007; Cho et al., 2012), some studies suggest that the *MIR157* family is dicot-specific (Guo et al., 2020; Wang et al., 2006). Consistent with this, the *MIR157* family is absent from *Oryza sativa* and probably from other grasses (Guo et al., 2020; Wang et al., 2006). Two putative *MIR157* orthologues have been reported in *Zea mays* on the basis of a simple basic local alignment (blast) search. However, no orthologous sequences were identified in five other grasses (Chorostecki et al., 2017).

All members of the *MIR156* and *MIR157* gene families of Arabidopsis are present in almost all other Brassicacae species tested (Chorostecki et al., 2017; Fahlgren et al., 2010). Within these families, several inter- and intrachromosomal duplication events are retraceable. For *MIR156,* the most recent duplication gave rise to *MIR156A* and *MIR156C,* which is evidenced by a highly conserved microsynteny among neighbouring genes (Maher et al., 2006). The genes also show the strongest expression among *MIR156* family members in Arabidopsis (He et al., 2018). *MIR156D* forms an outgroup to *MIR156A/C* and might have arisen from a large-scale duplication event with *MIR156H*. The same event might also have generated *MIR156E* and *MIR156F*. On the basis of the conservation of flanking genes, the oldest precursor appears to be *MIR156G,* whose locus weakly resembles only that of *MIR156E* (Maher et al., 2006). Furthermore, *MIR156B* is distantly related to *MIR156F.*

The evolutionary relationship among *MIR157* genes has been reconstructed via comparative promoter analysis (Wang et al., 2006). *MIR157A* and *MIR157C* are the most strongly expressed *MIR157* genes in Arabidopsis and generate the majority of mature miR157 (He et al., 2018). *MIR157A* and *MIR157B* are youngest genes in the family. They reside on the same Arabidopsis chromosome arm and are separated by a distance of only 4 kb. Their origin by duplication might be caused by a transposable element that is inserted between them (Wang et al., 2006). Fewer similarities are shared by the promoter regions of *MIR157C* and *MIR157D* than are shared by *MIR157A* and *MIR157B*. The *MIR157C* and *MIR157D* genomic loci are located in

duplicated segments of chromosomes 1 and 3 and the three flanking protein-coding genes show conserved synteny (Maher et al., 2006; Wang et al., 2006).

A comparison between targeted and non-targeted *SPL* genes in angiosperms revealed that targeted genes are generally present in more copies than non-targeted genes (Li et al., 2020). In transcriptome datasets, the expression of non-targeted *SPLs* was more similar to that of house-keeping genes, whereas miR156-regulated *SPLs* exhibited more dynamic temporal expression patterns, suggesting that their recruitment to more complex physiological processes might have occurred during evolution (Li et al., 2020).

2.7. MicroRNA biogenesis and function in plants

MIRNA genes possess characteristics common for RNA Polymerase II (RNAP II) - transcribed genes, such as those that contain a TATA-box promoter and a polyadenylation signal (Xie et al., 2005). The occurrence of introns and transcript splicing is also prevalent among precursors.

The mature miRNA and its miRNA* complementary sequence are encoded by inverted-repeat sequences, which fold into imperfect double-stranded hairpin structures after transcription of primary-microRNAs (pri-miRNAs, Kurihara and Watanabe, 2004; Song et al., 2019). This conformation is recognized by the DICER-like 1 (DCL1) processing machinery that catalyses the miRNA maturation process via two cleavage steps in the nucleus (Park et al., 2005). Processing of plant miRNAs can occur in distinct modes, depending on the pri-miRNA structure.

In the base-to-loop processing mode, DCL1 recognises a 15- to 17- nucleotide long stem segment below the miRNA/miRNA* duplex that defines the position of the first cut. After cleavage, the second cut is initiated at a distance of 21 nucleotides and the miRNA/miRNA* duplex is released (Bologna et al., 2013; Mateos et al., 2010; Werner et al., 2010; Zhu et al., 2013). The helicase domain of DCL1 functions as a motor that relocates the substrate between successive cleavage events (Wei et al., 2021). The base-to-loop mode of miRNA biogenesis resembles the mechanism found in animals.

During loop-to-base processing, the first cut is initiated below the terminal loop (Addo-Quaye et al., 2008; Bologna et al., 2009, 2013). Precursors processed from the loop contain a structured double-stranded RNA region above the miRNA/miRNA* duplex that defines the first cleavage position (Chorostecki et al., 2017; Kim et al., 2016; Moro et al., 2018). Processing then proceeds towards the base of the precursor. Due to functional constraints, the mode by which a precursor is processed can be deduced from evolutionary signatures (Chorostecki et al., 2017). Base-to-loop processed precursors are highly conserved below the miRNA/miRNA* duplex and the length of the terminal loop is variable. By contrast, the stem segment is less conserved in loop-to-base substrates. Here, the length and structure of the terminal loop is consistent across species (Chorostecki et al., 2017). All members of the *MIR156* and *MIR157* families are processed in a loop-to-base manner. The hairpin structure in miR157c is unusually long for pri-miRNAs processed this way. Moreover, it ends in a terminally branched loop that was previously associated with unproductive cuts (Moro et al., 2018; Zhu et al., 2013). Experimental data suggest that although processing of miR157c pri-miRNAs is productive, the biogenesis of miR157a and miR157b, which contain smaller, unbranched loops, is more efficient. Replacement of the stem loop with a shorter variant also led to more efficient processing (Moro et al., 2018).

The RNA-binding proteins HYPONASTIC LEAVES 1 (HYL1) and SERRATE (SE) form a core part of the DCL1 processing machinery. Their role is to promote the precision and accuracy of pri-miRNA processing (Dong et al., 2008; Han et al., 2004; Iwata et al., 2013; Kurihara and Watanabe, 2004; Kurihara et al., 2006; Vazquez et al., 2004; Yang et al., 2006). Via its intrinsically disordered domains, SE additionally possesses a scaffolding function. Driven by SE condensation (Fang and Spector, 2007; Li et al., 2021b; Xie et al., 2021), DCL1 complexes aggregate into membrane-less nuclear organelles termed dicing bodies (D-bodies). These are physically distinct from Cajal-bodies, the sites of mRNA processing (Fang and Spector, 2007; Song et al., 2007). Null mutants of *dcl1* and double *se* and *hyl* mutants are embryo lethal (Schauer et al., 2002; Yang et al., 2006).

Several lines of evidence suggest that pre-miRNA processing occurs co-transcriptionally (Wei et al., 2021). Many plant *MIRNA* genes, including *MIR156A* and *MIR156C,* carry introns that are spliced out during transcription. Several components

of the miRNA processing machinery, notably DCL1, HYL1 and SE, also contribute to the splicing process (Laubinger et al., 2008; Li et al., 2021a; Raczynska et al., 2014). DCL1 complexes were observed to colocalise with *MIR* loci (Fang et al., 2015), which might be mediated by interaction with transcription factors (Wang et al., 2013; Zhang et al., 2013) and subunits of both the mediator (Cambiagno et al., 2021) and elongator complexes (Fang et al., 2015).

The final outcome of DCL1 processing is an imperfect miRNA/miRNA* duplex with an overhang of two nucleotides at the 3’ ends (Mateos et al., 2010). After methylation, which protects the duplex from degradation (Baranauskė et al., 2015), the guide strand is selected and loaded into AGO proteins. Selection of the correct guide strand is promoted by proteins such as HYL1 on the basis of the lower thermodynamic stability of the 5′ end, whereas the passenger strand is usually degraded (Eamens et al., 2009; Manavella et al., 2012).

ARGONAUTE (AGO) proteins and associated sRNAs form the central unit of RNA-induced silencing complexes (RISCs, Vaucheret, 2008). Ten AGO proteins are present in Arabidopsis, which can be phylogenetically grouped into three major clades: AGO1/ AGO5/AGO10, AGO2/AGO3/AGO7 and AGO4/AGO6/AGO8/AGO9 (Vaucheret, 2008; Zhang et al., 2015). The majority of miRNAs, including miR156 and miR157, are loaded into AGO1 (Joshua-Tor and Hannon, 2011; Rogers and Chen, 2013; Zhang et al., 2015). AGO5 and AGO10 additionally preferentially bind to 21-nucleotide-long miRNAs. Recently, it was reported that AGO5 loads and interacts with miR156 to regulate flowering at the SAM (Roussin-Léveillée et al., 2020).

The fate of an sRNA is determined by its 5’ terminal nucleotide (Mi et al., 2008), for which AGO proteins have binding affinities. For example, AGO1 has a strong preference for 5′ uracil, whereas AGO2 preferentially binds 5′ adenosine and AGO5 has the highest affinity for 5′ cytosine. By changing the 5′ terminal nucleotide, it is possible to send an sRNA to a different complex (Mi et al., 2008; Thieme et al., 2012). Structural properties of the miRNA/miRNA* duplex also contribute to the sorting process (Zhang et al., 2014). Loading of the AGO proteins occurs mainly in the nucleus, and the presence of both nuclear import and export signals allows the shuttling of AGO complexes. A recently identified cytosolic pool of unloaded miRNA suggests that the

availability of AGO proteins may be a limiting factor. (Bologna et al., 2018; Dalmadi et al., 2019). Some AGO loading might also take place outside of the nucleus.

Once it is assembled, the RISC complex is relocated to the cytosol, where it functions. AGO1-associated miRNAs function by inducing cleavage of targets or by blocking their translation into proteins (Brodersen et al., 2008; Llave et al., 2002b). In Arabidopsis, the AGO proteins AGO1, AGO2, AGO4, AGO7 and AGO10 show cleavage activity (Li et al., 2013; Qi et al., 2006; Zhu et al., 2013), whereas AGO1, AGO2, AGO7 and AGO10 also mediate translational repression (Fátyol et al., 2016; Qi et al., 2006; Zhu et al., 2011).

The repression of transcripts via cleavage does not depend on components that are required for translational repression (Brodersen et al., 2008; Li et al., 2013; Yang et al., 2012). Conversely, cleavage-deficient AGO1 proteins are able to efficiently carry out translational repression (Arribas-Hernández et al., 2016).

To exert translational repression, AGO1 associates with polysomes found at the rough endoplasmatic reticulum (Lanet et al., 2009; Li et al., 2013). There, it interacts with cytosolic HYL1 and the integral membrane protein ALTERED MERISTEM PROGRAM1 (Lanet et al., 2009; Li et al., 2013; Yang et al., 2021). Interaction with the RISC complex then prevents the recruitment of targeted transcripts to membrane-bound polysomes (Li et al., 2013).

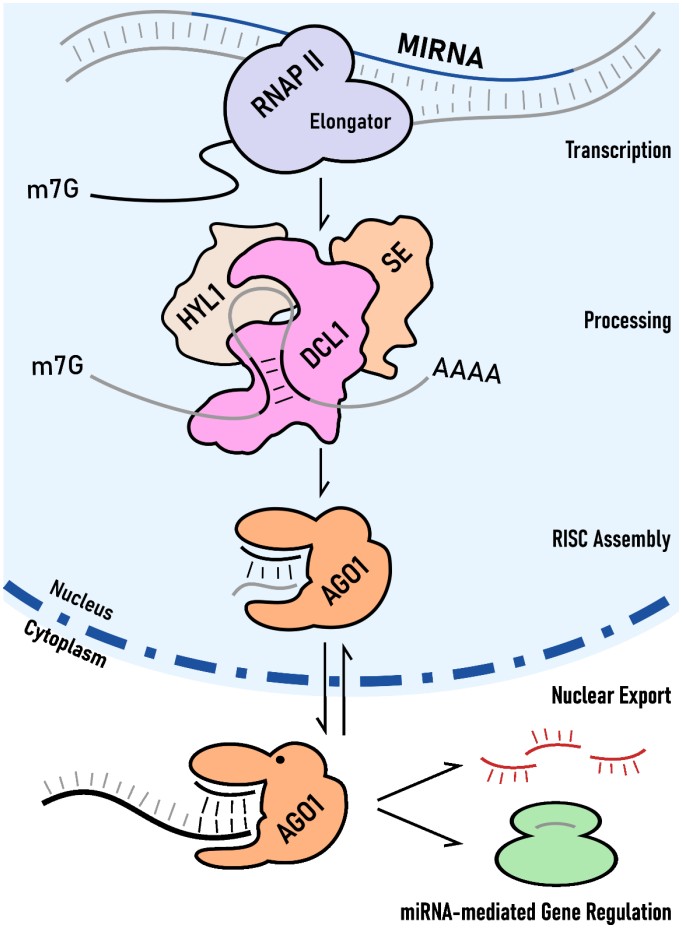

Figure 2.3. MicroRNAs are transcribed from precursor genes and undergo nuclear maturation catalysed by the DICER-LIKE 1 (DCL1) complex. The transcript forms a hairpin structure, which is processed by DCL1 in cooperation with HYPONASTIC LEAVES (HYL1) and SERRATE (SE). The mature miRNA is loaded into ARGONAUTE1 and translocated to the cytosol, where it engages in post-transcriptional gene silencing (following Bologna et al., 2018).

2.8. Aim of the thesis

In total, twelve genes encode miR156/miR157 isoforms in Arabidopsis. Of these, *MIR156A/C* and *MIR157A/C* are the most abundant and regulate phase transition during vegetative growth, with *MIR156* precursors playing a more prominent role (He et al., 2018). The relative contribution of *MIR156* and *MIR157* to floral transition is less clear, because they are often described synonymously in this context (Wang et al., 2009). Moreover, although vegetative phase change occurs in leaves (Yang et al., 2011), flowering under non-inductive conditions is initiated at the SAM (Hyun et al., 2016; Wang et al., 2009). The overall aim of this thesis is therefore to dissect the role of miR156 and miR157 in repressing flowering at the shoot meristem.

I used sRNA-sequencing to compare the abundance of miR156 and miR157 over time in plants grown in inductive and non-inductive photoperiods. Confocal imaging of reporter lines allowed me to characterise the spatio-temporal expression patterns of individual *MIR156* and *MIR157* genes. The aim of combining these approaches with the analysis of CRISPR/Cas9-induced mutants was to identify *MIR156* and *MIR157* genes that contribute to the bolting process under different photoperiods. In addition, the comparative analyses of plants with enhanced SPL activity and the genetic interactions with downstream factors, enabled me to integrate the insights into the current framework of the age pathway of flowering.

3. The expression patterns of *MIR156* and *MIR157*

3.1. Introduction

The levels of miR156 and miR157 are developmentally regulated and decrease over time in apices and successive leaf primordia (Bergonzi et al., 2013; Cheng et al., 2021; He et al., 2018; Wang et al., 2009). The expression of *MIR156/ MIR157* genes decreases more slowly in short days than in long days, and short days also delay flowering in Arabidopsis (Figure 3.1). However, the level of miR156 is regulated independently from the photoperiodic pathway and is unaffected by *ft tsf* mutations (Wang et al., 2009).

Limited information is available on the relative importance of mature miR156 and miR157 in regulating flowering time. Constitutive overexpression of miR156 delays flowering (Roussin-Léveillée et al., 2020; Schwab et al., 2005), but it is unclear which of the native *MIR156* and *MIR157* promoters are relevant for floral transition. When sRNA samples derived from total RNA extractions were sequenced, a higher abundance of miR157 than miR156 was observed in vegetative apices from 11-day-old, long-day-grown plants (He et al., 2018). This was consistent with the observed higher expression of *MIR157A* and *MIR157C* precursors relative to that of *MIR156* counterparts. However, northern blot analysis of miRNAs extracted from isolated AGO1 proteins showed that miR156 and miR157 were equally abundant (He et al., 2018), which the authors explained by different AGO1 loading efficiencies.

To date, the only available detailed spatio-temporal expression pattern for *MIR156* and *MIR157* genes at the SAM is that for *MIR156C* (Cheng et al., 2021). The expression patterns of *MIR156A*, *MIR156B* and *MIR157A* in the embryo, young leaves and pollen were reported recently (Gao et al., 2022). Moreover, the spatial expression of *MIR156H*, *MIR157C* and *MIR157D* was characterised during early anther development (Xing et al., 2011).

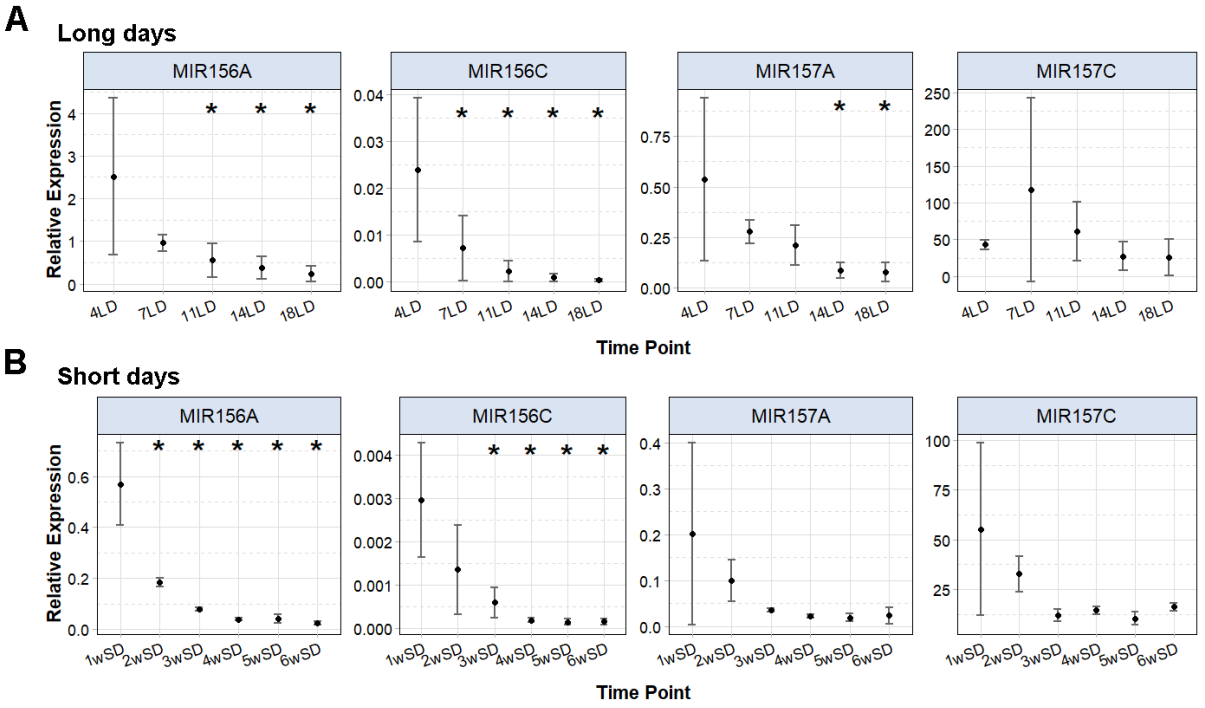

Figure 3.1. Expression analysis of *MIR156* and *MIR157* genes in apices of A) long-day grown and B) short-day-grown Col-0 plants. The graph shows qRT-PCR expression data from total RNA for *MIR156A*/*MIR156C* and *MIR157A*/*MIR157C* calculated as delta Ct relative to expression of the *PEROXIN4* gene. Expression values are shown along a time course for each growth condition. Asterisks denote significant differences compared with the first time point in the series as measured by a one-factor ANOVA with $p < 0.05$.

This chapter describes two approaches taken to further characterise *MIR156* and *MIR157* with a focus on their roles in floral transition. The first approach compared the levels of miR156 and miR157 between apices of plants grown in long days and short days in a time-resolved sRNA sequencing experiment (Figure 3.2). The approach employed the TraPR method, which allowed the specific isolation of all AGO-bound sRNA-molecules, including miRNAs (Grentzinger et al., 2020). In contrast to methods based on total RNA extraction coupled with size-exclusion gel electrophoresis, the TraPR method uses a column-based approach to bind free RNA, while allowing the specific elution of AGO proteins from tissue extracts. A second step extracts sRNAs directly from the AGO-complexes. This approach minimises the amount of fragmented mRNA molecules within the sRNA fraction and enriches for functional sRNAs that engage in PTGS.

The second approach consisted of describing the spatio-temporal expression patterns of selected *MIR156* and *MIR157* precursors in detail by confocal imaging. The analysis

focussed on the expression patterns in the SAM, which is relevant for the age pathway of flowering.

3.2. Small RNA sequencing revealed different expression dynamics of miR156 and miR157 families

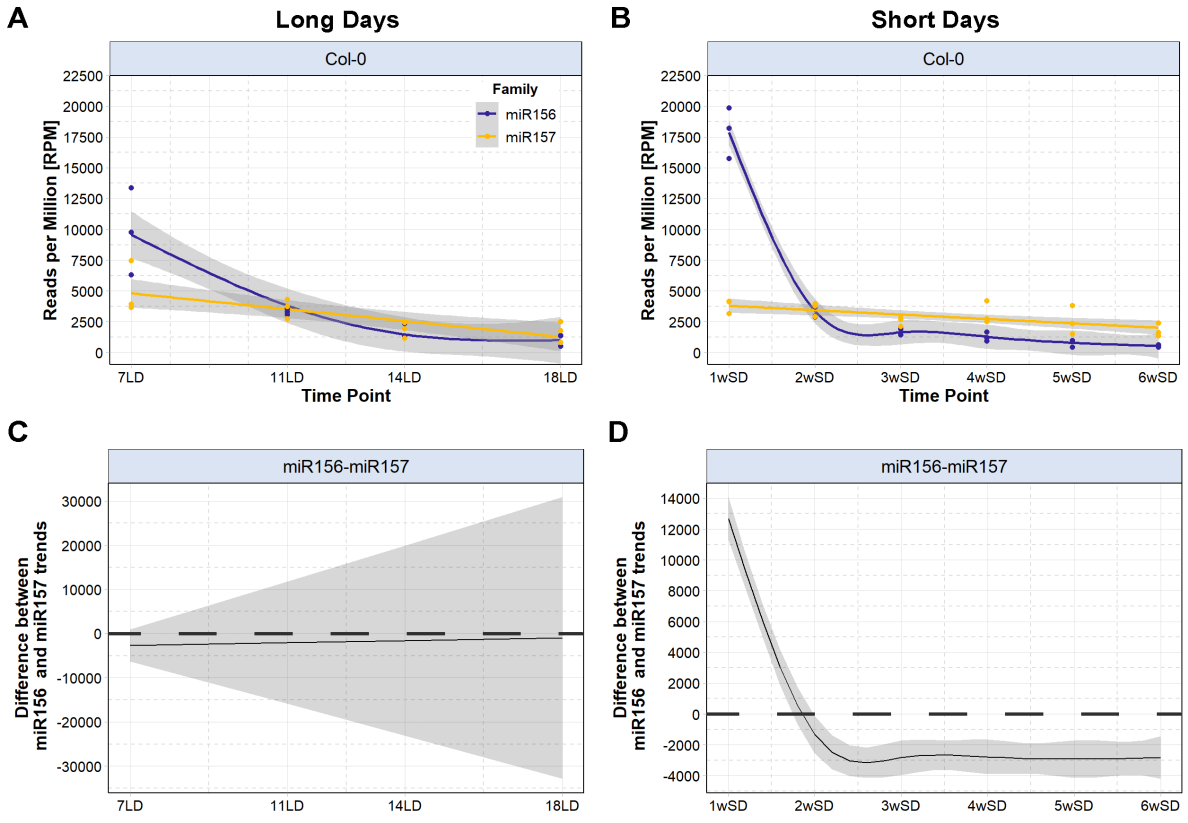

Figure 3.2. Quantification of mature miR156 (blue) and miR157 (orange) expression levels by small RNA sequencing of wild type (Col-0) apices grown under long and short day photoperiods. A) Long day time course comparing miR156 and miR157 levels in wild type plants after 7, 9, 11, 14 and 18 long days (7LD to18LD). B) Short-day time course with samples collected after 1 to 6 weeks (1wSD to 6wSD). Data points represent three independent biological replicates. Lines represent fitted generalised additive models. Shaded areas represent approximate, 95% confidence intervals. C and D) Differences between miR156 and miR157 trends plotted in A and B and associated 95% confidence intervals. The differences are statistically significant, when the confidence interval excludes zero. The sRNA sequencing experiment was analysed in collaboration with Dr. Vidya Oruganti.

Because the age pathway of flowering is more important under non-inductive conditions than inductive conditions, the experimental design incorporated a comparison between long- and short-day time courses for Col-0 (Figure 3.2). Three replicates were harvested per time point. In short days, sampling occurred weekly from

one to six weeks after germination (1wSD to 6wSD, Figure 3.2). Most *MIR156* precursors encode the same miR156 isoform and *MIR157A* to *MIR157C* encode the same miR157 isoform (Jones-Rhoades and Bartel, 2004); therefore miRNA expression patterns were analysed at the family level.

At 1wSD, miR156 was expressed at a high level, which was approximately fourfold higher than that of miR157 (Figure 3.2B). By 2wSD, the miR156 abundance decreased sharply, from about 17,000 reads per million (RPM) to circa 3,000 RPM. At the same time points, miR157, levels remained stable, resulting in equal amounts of both miRNAs at 2wSD. As development progressed, miR156 levels continued to decrease but at a slower rate. Overall, the dynamics of miR156 expression in short-day-grown shoot apices was consistent with the previously reported exponential decrease in miR156 in leaf primordia (He et al., 2018). By contrast, miR157 expression was less dynamic. Between 1wSD and 6wSD, miR157 abundance approximately halved, as a result of a more or less steady rate of decrease. This also changed the relationship between the amounts of the two related miRNAs. From 3wSD onwards, miR157 expression was consistently higher than that of miR156. The differences in miR156 and miR157 levels were statistically significant (Figure 3.2D).

In LDs, apices were harvested at 7, 11, 14 and 18 days after germination (7LD to 18LD, Figure 3.2A). Similarly to in short days, miR156 was more abundant than miR157 one week after germination (7LD). At 11LD, miR156 and miR157 levels were equal, which in both cases was lower than at 7LD. The level of miR156 and miR157 further decreased at 14LD, but showed only a slight decrease at 18LD. Thus, miR156 was expressed more highly during early vegetative growth but decreased to a similar level as miR157 as development progressed. In contrast to their relative expression in short days, miR157 was not statistically significantly more abundant than miR156 during the experiment in long days (Figure 3.2C).

3.3. Characterisation of the spatial expression pattern of *MIR156* and *MIR157* precursors

The sRNA sequencing experiment confirmed the dynamic temporal change in miR156 expression that was reported in the literature and a less dynamic change for miR157. To understand how these dynamic changes occur at the SAM, the spatial expression patterns of selected *MIR156* and *MIR157* genes were analysed by confocal imaging. The analysis focussed on the *MIR156A::GFP* reporter that was provided by the group of Jia-Wei Wang (Gao et al., 2022), the *MIR156C::VENUS:GUS* (*MIR156C::VNG*) and *MIR156B::VNG* reporters that were generated in the Coupland group and the *MIR157A::VNG* and *MIR157D::VNG* reporters that were created as part of this thesis. All *MIR156* and *MIR157* reporters contained the entire intergenic sequences of the *MIR* locus and a nuclear-localised fluorophore that replaced the miRNA-encoding hairpin structure.

The *MIR156A* and *MIR156C* reporters were expressed in a similar pattern, in a broad domain throughout apices of young seedlings in both short-day (Figure 3.3A and B) and long-day conditions (Figure 3.3C). Consistent with the temporal decrease in mature miR156 levels, *MIR156A* and *MIR156C* reporter expression decreased with increasing plant age, and this decrease occurred more rapidly in long days than in short days. Although the expression of both reporters decreased at the SAM and in newly formed primordia, strong signal remained in older regions of the shoot (11LD in Figure 3.3A and B). The reported expression domain of *MIR156A* differed from that of *MIR156C* at the central zone of the SAM. In both growth conditions, *MIR156C::VNG* expression was present in the central zone at one week after germination, before being expressed in the more distal rib zone at later time points. By contrast, *MIR156A::GFP* reporter expression was absent from the central zone throughout the long-and short-day time courses.

The expression pattern of the *MIR156B::VNG* reporter was analysed under short-day conditions (Figure 3.3C). It differed from that of *MIR156A* and *MIR156C* reporters by being very specific and spatially stable over time. At the SAM, the expression of *MIR156B::VNG* reporter was exclusively localised to the L1-layer and no signal was present in deeper layers of the meristem. Strikingly, the otherwise ubiquitously expressed VNG protein was not detected at the tip of the SAM. Outside of the meristem,

the expression domain extended into the epidermis of leaf primordia. At 7wSD, the SAM completed floral transition and at this time point, the *MIR156B::VNG* reporter was also expressed in the floral primordia emerging from the peripheral zone.

The miR156-targeted *SPL9* and *SPL15* genes contribute to the regulation of shoot branching (Xie et al., 2020b; Zhang et al., 2020). For example, the *spl9 spl15* double mutant produces more rosette branches (Schwarz et al., 2008; Xie et al., 2020b). To analyse whether *MIR156* reporters might be expressed in relevant tissues, the spatial expression patterns of *MIR156A::GFP, MIR156B::VNG* and *MIR156C::VNG* were assessed in rosettes of six-week-old, short-day-grown plants (Figure 3.4). At this time point, the SAM undergoes floral transition, which releases axillary buds from apical dominance. To access the meristems in the axils of older rosette leaves, cross-sections of the rosette base perpendicular to the main shoot were prepared. Sections of the *pSPL15::9AV:SPL15* reporter line were also included for comparison.

The dissected samples allowed the study of reporter gene expression patterns in petioles of mature rosette leaves and their axillary buds. Expression of the *MIR156A::GFP* reporter was present in older rosette leaves. The strongest expression was observed in the epidermis. Weak reporter signal was present throughout the petiole cross-section, and the signal intensity increased towards the adaxial side. In cross-sections that included the leaf blade, strong *MIR156A::GFP* expression was observed in secondary veins of the leaf vasculature, but no signal was detectable in midveins. Similarly, no expression of the *MIR156A::GFP* reporter was observed in axillary meristems, which is consistent with the absence of *MIR156A::GFP* expression at the shoot apex.

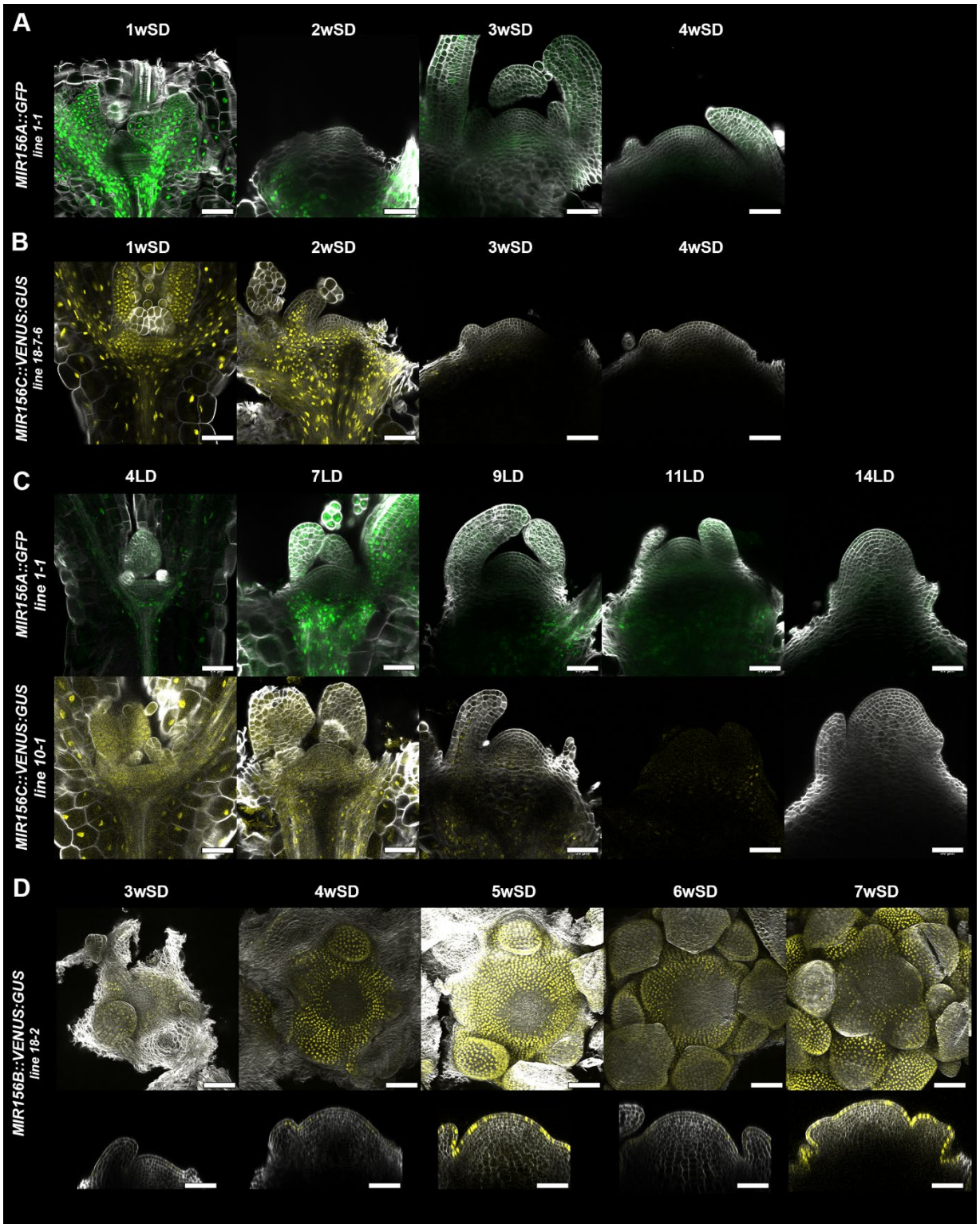

Figure 3.3. Confocal images of *MIR156* transcriptional reporter expression at the shoot apical meristem under short- and long-day conditions A) *MIR156A::GFP* and B) *MIR156C::VNG* reporter expression in short days. C) *MIR156A::GFP* and *MIR156C::VNG* reporter expression in long days. D) Maximum intensity projection and reconstructed cross-section of the *MIR156B::VNG* reporter line in short days. Scale bars represent 50 µm in all panels. The same microscope imaging parameters were used within a time course. Images are representative of three to five analysed samples.

Expression of *MIR156C::VNG* was also present in petioles of older rosette leaves. Contrary to expression of *MIR156A::GFP*, *MIR156C::VNG* was expressed most strongly in abaxial regions and was excluded from the epidermis. In young leaf primordia produced by axillary meristems, *MIR156C::VNG* was also expressed at the lateral edges of the developing leaf blade, but was absent from the meristem.

The activity of *MIR156B::VNG* in axillary meristems mirrored the pattern observed at the SAM. Strong signal localised to the L1 layer of the meristem and to the epidermis of leaf primordia. In mature leaves, epidermal *MIR156B* expression localised to the abaxial side of the midrib and the lateral edges of the leaf blade, whereas no signal was detected in the intermittent regions. Similarly, VNG signal was notably absent from leaf vasculature and other inner tissue layers.

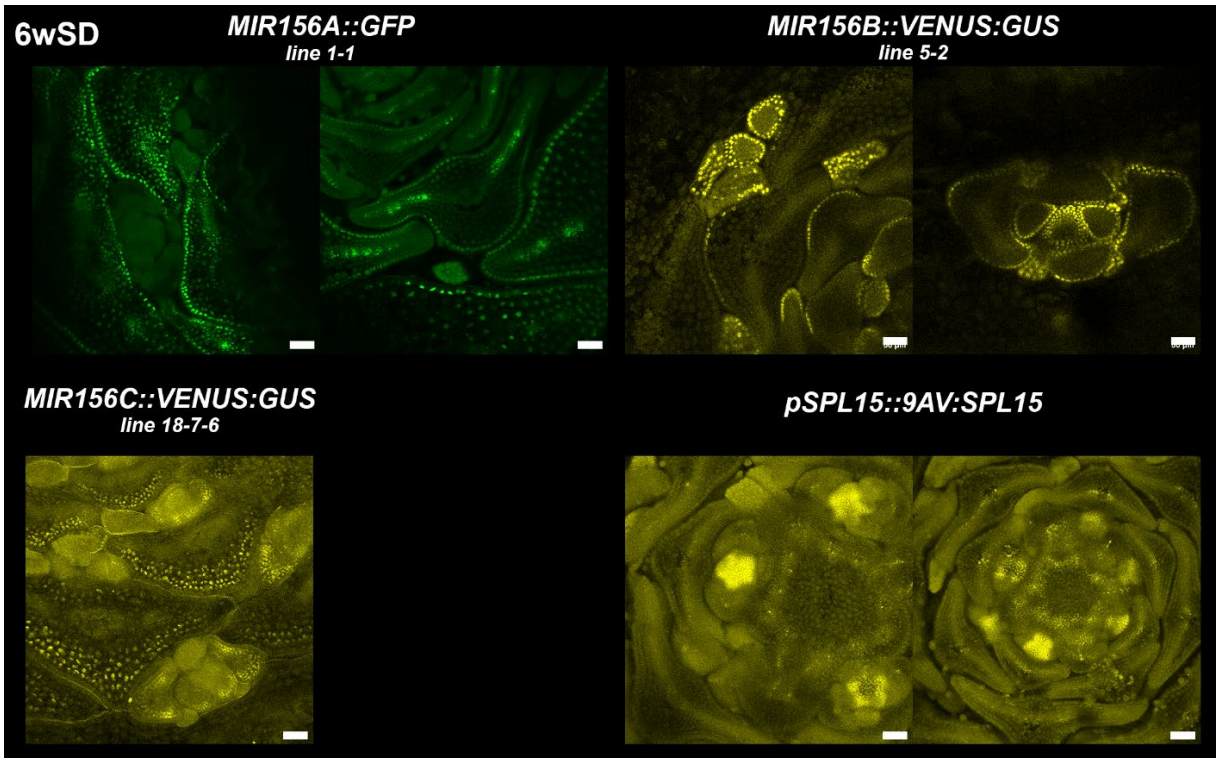

Figure 3.4. Expression pattern of *MIR156A*, *MIR156B*, *MIR156C* and *pSPL15::9AV:SPL15* reporters in cross-sections of six-week-old, short-day-grown rosettes. Confocal images of basal cross sections of whole rosettes that reveal axillary meristems and petioles of associated leaves. Signal intensities are not comparable among lines. Scale bars indicate 50 µm.

The *pSPL15::9AV:SPL15* construct reports SPL15 protein accumulation after post-transcriptional regulation by miR156 (Hyun et al., 2016). At 6wSD, *pSPL15::9AV:SPL15* was strongly expressed in the meristems of lateral shoots, but

expression was absent from incipient primordia, which is a pattern similar to that at the SAM. At the basal main shoot stem, SPL15 protein accumulated in specific vascular strands. In older leaves, expression was located to the leaf midveins, where no expression of *MIR156A*, *MIR156*B or *MIR156*C reporters was detected.

The expression of the *MIR157A::VNG* and *MIR157D::VNG* reporters in apices was analysed in a short-day time course (Figure 3.5). At 1wSD, strong *MIR157A::VNG* activity was observed in the vasculature of leaves and the hypocotyl (Figure 3.5A and C). The expression domain did not include the SAM, but expression was present in the subtending tissue. Starting from 2wSD, *MIR157A::VNG* expression appeared in cell clusters below young and incipient leaf primordia at the peripheral zone (Figure 3.5A). In older primordia, the *MIR157A::VNG* reporter was expressed in inner layers of the leaf base, which are associated with developing vasculature (Figure 3.5C). Expression was absent from outer layers or distal regions of the leaf. Both *MIR157A::VNG* transgenic lines analysed reported similar expression domains. The intensity of *MIR157A::VNG* expression decreased with time and was lowest at 6wSD.

During vegetative growth, the *MIR157D::VNG* reporter was not expressed at the SAM (Figure 3.5B). Reporter activity was present in the distal half of more developed leaves in proximity to differentiating leaf veins. In mature roots, individual cell files expressed the *MIR157D::VNG* reporter in the cortex. These cells were not associated with differentiated xylem. Over the course of the experiment, only one transgenic line transitioned to flowering. In the transitioning shoot, *MIR157D::VNG* was expressed at the boundary between the axillary meristem and cauline leaf (Figure 3.5B). Additional samples were harvested at 8wSD (Figure 3.5C), at which time point the abaxial base of mature cauline leaves strongly expressed the *MIR157D::VNG* reporter. Expression of *MIR157D::VNG* was also observed in axillary shoots, in a few cells located at the boundary between the leaf and axillary meristem. Similarly, *MIR157D::VNG* signal was detected at the boundary between floral organs of stage 7 flowers (after Smyth et al., 1990).

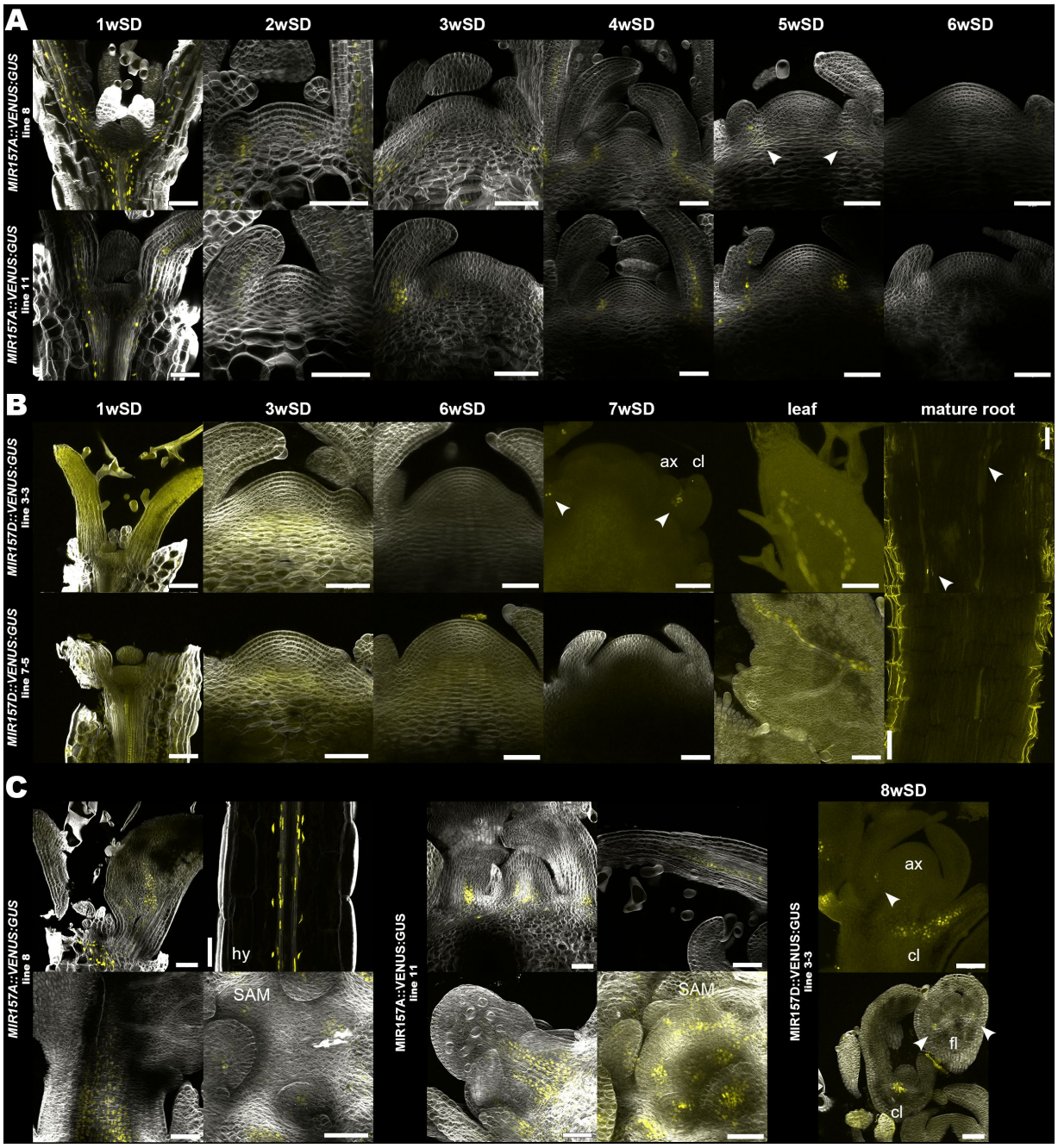

Figure 3.5. Confocal images of *MIR157A::VENUS:GUS* and *MIR157D::VENUS:GUS* expression at the SAM. A) Expression patterns of *MIR157A::VNG.* Two independent lines were analysed in the T2 generation that segregated for the transgene in an approximate 3:1 ratio. B) Confocal images of two homozygous *MIR157D::VNG* reporter lines showing no expression at the SAM. Two independent lines are depicted that were homozygous for a single-insertion transgene. Samples were harvested from one week to seven weeks in short days (1wSD to 7wSD). C) Additional tissues showing *MIR157A::VNG* and *MIR157D::VNG* expression. The experiment was a collaboration with Dr. Yohanna Miotto. Between 5 to 10 samples were harvested per line and time point. The scales represent 50 µm in all images. Abbreviations: ax = axillary meristem, cl = cauline leaf, fl = flower, SAM = shoot apical meristem.

In the age pathway of flowering, miR172 acts downstream of miR156 and represses *AP2-L* floral repressors (Lian et al., 2021; Ó'Maoiléidigh et al., 2021; Sang et al., 2022). *MIR172* precursors are activated by several SPL transcription factors (Hyun et al., 2016; Xie et al., 2020b). The *mir172a-2 mir172b-3 mir172d-3* (*mir172abd*) triple mutant is late flowering in long days (Ó'Maoiléidigh et al., 2021). To investigate the temporal expression of *MIR156C* in the context of late flowering and to test whether feedback regulation occurs, the *MIR156C::VNG* reporter was introduced to *mir172abd.* Reporter gene expression was then analysed in a long-day time course by confocal imaging (Figure 3.6).

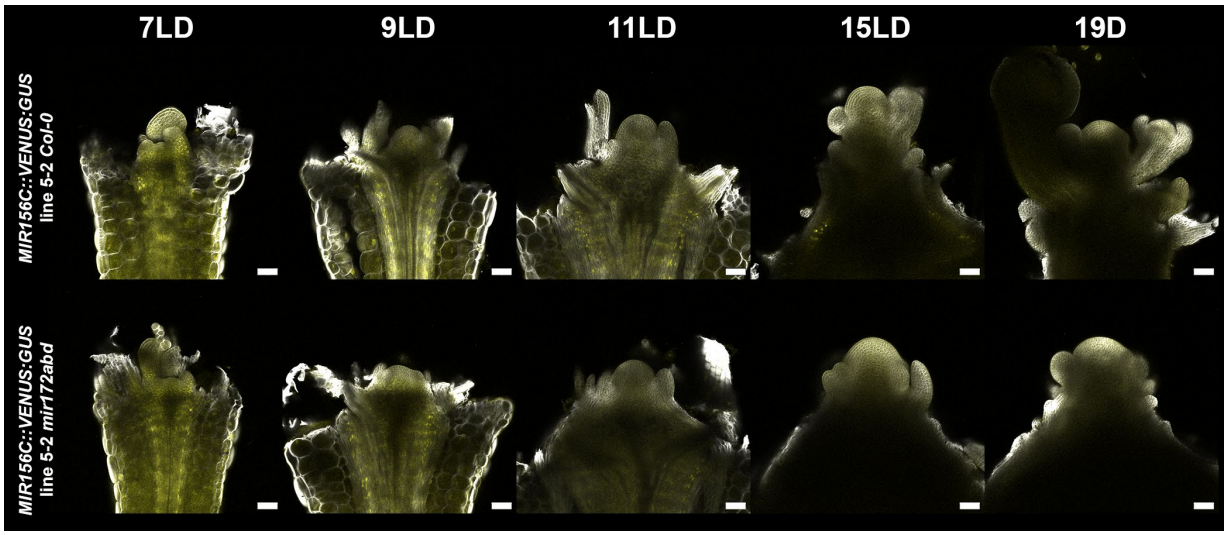

Figure 3.6. *MIR156C::VENUS:GUS* expression pattern in late-flowering *mir172a-2 mir172b-3 mir172d-3* (*mir172abd*) mutants harvested from 7 to 19 long days (7LD to 19LD). Images are representative of three to five harvested samples. The scale bar represents 50 µm in all panels.

At 7LDs, *MIR156C::VNG* was expressed throughout apices: Expression was observed in the SAM and leaf primordia, and additionally in the hypocotyl and vasculature. At 11LD, the wild-type SAM domed, whereas *mir172abd* mutants reached a similar morphology at 15LD. However, there was no discernible difference in *MIR156C::VNG* expression between wild type and *mir172abd*. *MIR156C::VNG* signal disappeared from the SAM but remained in the older shoot, which was difficult to image simultaneously with the SAM due to the tissue thickness.

3.4. Conclusion

Small-RNA sequencing revealed that in apices miR156 is initially more highly expressed than miR157, but its abundance decreases at a significantly faster rate. As a consequence, miR156 and miR157 reach equal abundance in both long-day and short-day conditions. Only in short days did miR157 become more abundantly expressed than miR156 before floral transition occurred. The different expression dynamics of miR156 and miR157 were consistent with the expression patterns of *MIR156* and *MIR157* reporters. In young apices, both *MIR156A* and *MIR156C* reporters showed broad and strong expression that decreased with age. By contrast, the analysed *MIR157A* and *MIR157D* reporters were less abundant in apices. However, *MIR157C* had the strongest expression according to qRT-PCR analysis and its spatial expression pattern was not analysed.

Confocal imaging revealed limited expression of *MIR156* and *MIR157* precursors at the SAM. Although *MIR156A* was not expressed within the central zone, the expression of *MIR156C* was initially strong in this domain but gradually disappeared during development. This gradual decrease in expression also occurred in the late-flowering *mir172abd* mutant in long days. Therefore, the temporal dynamics of *MIR156C* might not directly correlate with floral induction and there was no evidence for the activation of *MIR156C* expression by AP2-L.

In short days, the *MIR157A* reporter was expressed in small cell clusters situated at the peripheral zone below young and incipient primordia. This expression pattern did not change markedly during vegetative growth but expression decreased in older plants. Expression of the *MIR157D* reporter was absent from the SAM during vegetative growth but was present specifically in distal regions of expanding leaves. The *MIR157D* reporter activity was associated with vascular strands; therefore, *MIR157D* expression might be involved in prepatterning vascular veins, which would be consistent with its localisation to the distal part of the leaf. *MIR157A* might fulfil a similar role in prepatterning vascular tissue that connects incipient leaf primordia with the shoot.

The *pSPL15::9AV:SPL15* reporter was expressed in meristems and in the vasculature of six-week-old rosettes. *MIR156A*, *MIR156B* and *MIR156C* reporter expression

localised to older rosette leaves and leaf primordia of axillary meristems. MIR156A was also expressed in leaf vasculature but the overlap of its expression domain with that of *pSPL15::9AV:SPL15* was limited.

4. The closely related *MIR156* and *MIR157* families have distinct roles in the regulation of flowering time

4.1. Introduction

The strongest flowering promoting pathway in the long-day plant Arabidopsis is the photoperiodic pathway. In experimental settings, long days are simulated by 16 hours of continuous light followed by 8 hours of darkness. Short-day conditions, which do not induce *FT/TSF* expression in leaves, commonly consist of 8 hours of light followed by 16 hours of darkness (Samach et al., 2000; Valverde et al., 2004; Yamaguchi et al., 2005). In these non-inductive conditions, SPL15 and SOC1 promote floral transition at the SAM by cooperatively activating *MIR172* and *FUL* expression (Hyun et al., 2016; Wang et al., 2009). Photoperiod-insensitive mutants grown in long days flower at a similar time as wild type plants grown in short days (Samach et al., 2000; Yamaguchi et al., 2005). The sRNA sequencing experiment described in the previous chapter revealed that the abundance of miR156 or miR157 changes during development. Moreover, although miR156 and miR157 are equally abundant during floral transition in long days, the expression of miR157 becomes dominant during vegetative growth in short days.

To dissect the contribution of individual *MIR156* and *MIR157* genes to the age pathway of flowering, CRISPR/Cas9-induced *mir156* and *mir157* mutant alleles were generated in the Coupland group (Figure 4.1A). This chapter describes the characterisation of the vegetative and flowering-time phenotypes of these *mir156* and *mir157* mutants. The impact of mutant alleles on miR156/miR157 biogenesis was assessed by sRNA sequencing. In addition to the analysis of flowering time in long and short days, the expression of genes involved in floral transition was analysed, as well as the spatio-temporal expression pattern of SPL15 and FUL translational reporters.

4.2. Characterisation of novel CRISPR/Cas9 induced *mir156* and *mir157* mutants

The CRISPR/Cas9- induced *mir156* and *mir157* alleles carry deletions in sequences encoding the pri-miRNA hairpin structure (Figure 4.1A). At the *MIR156C, MIR157A,*

and *MIR157C* loci, deletions additionally affect the miRNA or miRNA* sequence. At *MIR157D,* CRISPR/Cas9 editing caused a 1.18kb deletion that covered the entire pri-miR157d sequence. *MIR157A* and *MIR157B* are located in proximity to each other on chromosome 1, and the *mir157a* and *mir157b* alleles were generated within a single plant.

The effect of deletion alleles on vegetative growth was analysed for the *mir156ac*, *mir157cd* and *mir157abc* mutant combinations, and controls were Col-0 and plants expressing *rSPL15* (Figure 4.1). The rosette leaf morphology of wild-type plants changes gradually during vegetative growth, which is known as vegetative phase change (Kerstetter and Poethig, 1998; Tsukaya et al., 2000). Cotyledons and juvenile leaves have a near-circular leaf blade and short petioles. Successive leaves appear more elongated along the proximal–distal axis and become increasingly serrated (Figure 4.1B). To compare the vegetative development of wild type, *mir156* and *mir157* mutants, the ratio between leaf length and width (length/width ratio, LWR, Figure 4.1C) was calculated for all leaves of plants grown for four weeks in short days.

Differences in the morphology of the first leaves formed were observed among genotypes. For wild type, the LWR increased incrementally from the second to the sixth leaf, where it reached a maximum (upper dotted line in Figure 4.1C). Subsequently, the LWR decreased in leaves that were not completely expanded at the time of harvesting. Plants carrying the *rSPL15* transgene produced fewer leaves than Col-0. The cotyledons and first two leaves of *rSPL15* plants appeared more ovate and had a greater LWR. The fifth leaf of *rSPL15* showed the maximum LWR, which was at a similar position than in wild type. From leaf six onwards, the LWR of *rSPL15* leaves decreased continuously.

The rosette leaf phenotype of *mir156ac* double mutants was most similar to that of *rSPL15* plants. Leaves one and two were longer than the equivalent leaves in Col-0, and generally appeared more advanced in morphological development. Consequently, the LWR values were close to maximum value for *mir156ac* leaves. By contrast, the increase in the LWR of *mir157cd* and *mir157abc* mutants for successive leaves was largely comparable with that of wild-type plants, but higher maximum ratios were achieved.

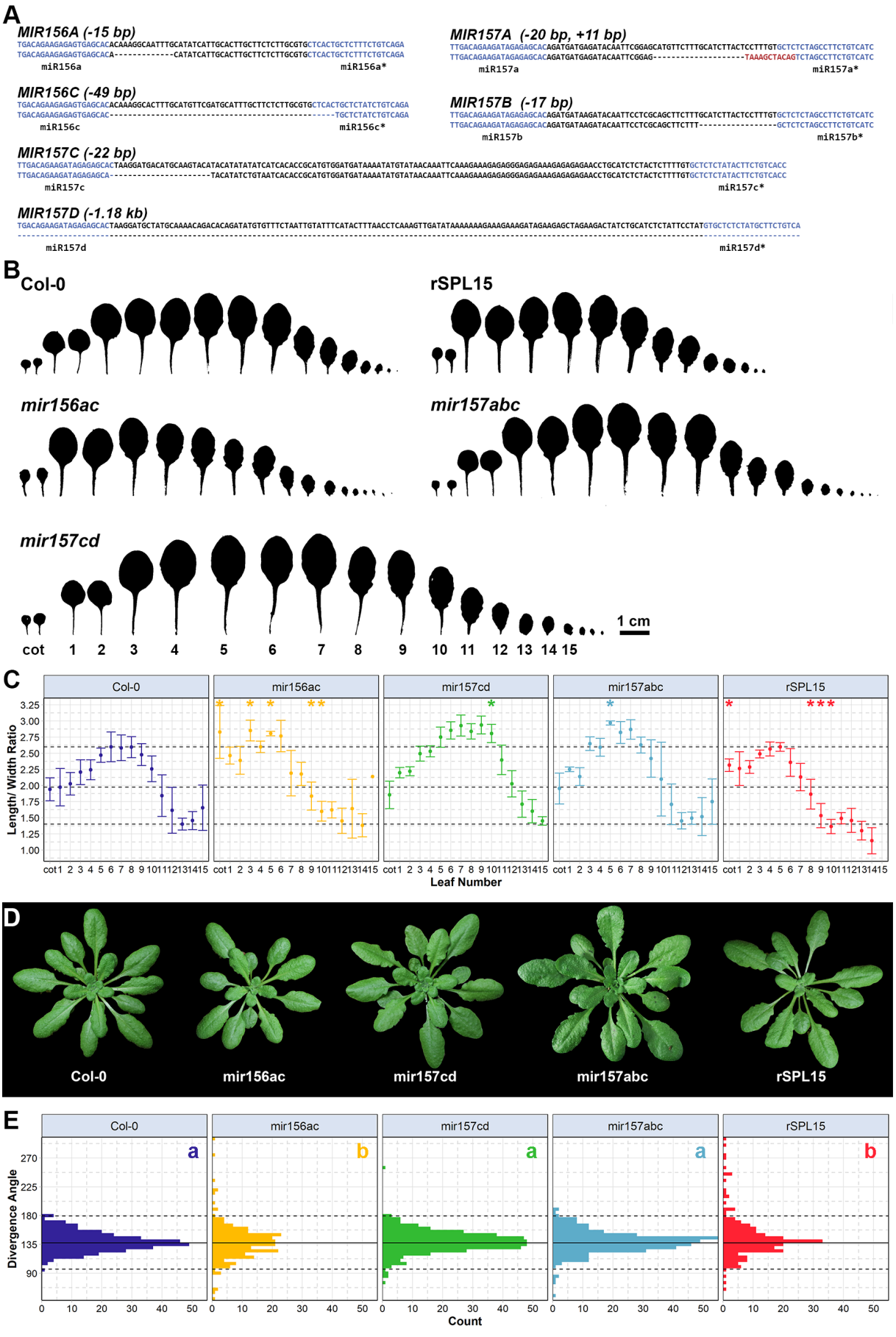
A
MIR156A (-15 bp)
miR156a
miR156a*
MIR156C (-49 bp)
miR156c
miR156c*
MIR157A (-20 bp, +11 bp)
miR157a
miR157a*
MIR157B (-17 bp)
miR157b
miR157b*
MIR157C (-22 bp)
miR157c
miR157c*
MIR157D (-1.18 kb)
miR157d
miR157d*
B
Col-0
rSPL15
mir156ac
mir157abc
mir157cd
cot 1 2 3 4 5 6 7 8 9 10 11 12 13 14 15
1 cm
C
Col-0
mir156ac
mir157cd
mir157abc
rSPL15
Length/ Width Ratio
Leaf Number
D
Col-0
mir156ac
mir157cd
mir157abc
rSPL15
E
Divergence Angle
Count
a
b
a
a
b

Figure 4.1. Novel CRISPR/Cas9-induced *mir156* and *mir157* alleles and vegetative phenotypes of precursor mutants. A) Sequence of the mutant alleles. All deletions affect the conserved hairpin-sequence that is required for the correct biogenesis of miR156 and miR157. The wild type reference sequence is shown and the mutant sequence are shown below. The miRNA and miRNA* sequences are highlighted in blue. Red letters indicate non-template insertions. B) Shapes and C) length/ width ratios (LWRs) of successive rosette leaves after four weeks in short days. Shown are the mean LWRs of three to six samples. Asterisks indicate values that differ significantly from Col-0 according to ANOVA followed by pairwise Tukey's HSD, with a Bonferroni-corrected *p*-value < 0.05. D) Rosette leaf phenotypes of five-week-old *mir156ac*, *mir157cd* and *mir157abc* mutants, Col-0 and *rSPL15* plants. E) Distribution of the divergence angle between successive rosette leaves in five-week-old plants. The horizontal line at 137.5° indicates the ideal angle, and dashed lines show the minimum and maximum angles measured for Col-0. Letters indicate statistically significant differences in variation as calculated by Levene and post-hoc Tukey's HSD tests.

Vegetative growth was also analysed in terms of leaf phyllotaxis. The leaves of wild-type plants are initiated in regular spiral patterns with an ideal divergence angle of 137.5° (thick horizontal line in Figure 4.1E; Palauqui and Laufs, 2011). Consistently, the experimental values measured for each genotype approximated the ideal angle, but differences in variation were observed (Figure 4.1E). The variation in leaf initiation angles for *mir157cd* and *mir157abc* mutants was similar to that for wild-type plants, although several individual outliers were present. The visually discontinuous phyllotaxis of *mir156ac* and *rSPL15* genotypes (Figure 4.1D) was also reflected in the increased variation in divergence angles, which was significantly greater than that of wild type and *mir157* mutants (Figure 4.1E). Therefore, *mir156ac* mutants had stronger vegetative phenotypes than *mir157* mutants that resembled those of *rSPL15* plants.

4.3. The effect of *mir156* and *mir157* mutations on the abundance of miR156 and miR157 in short days

The levels of miR156 and miR157 expression in *mir156ac*, *mir157cd* and *mir157abc* mutants were analysed in short days. Apices were harvested at one, three and six weeks and the abundance of miR156 and miR157 was compared with that in the wild-type time course described above in section 3. The abundance of miR156 in *mir156ac* mutants was significantly lower than in wild type. In absolute numbers, the strongest reduction was occurred at 1wSD, when miR156 levels in Col-0 and mutants were highest. No difference in the abundance of miR156 was observed in *mir157cd* and *mir157abc* over time compared with Col-0 and the level of miR157 in apices of *mir156ac* was similar to that in wild type (Figure 4.2).

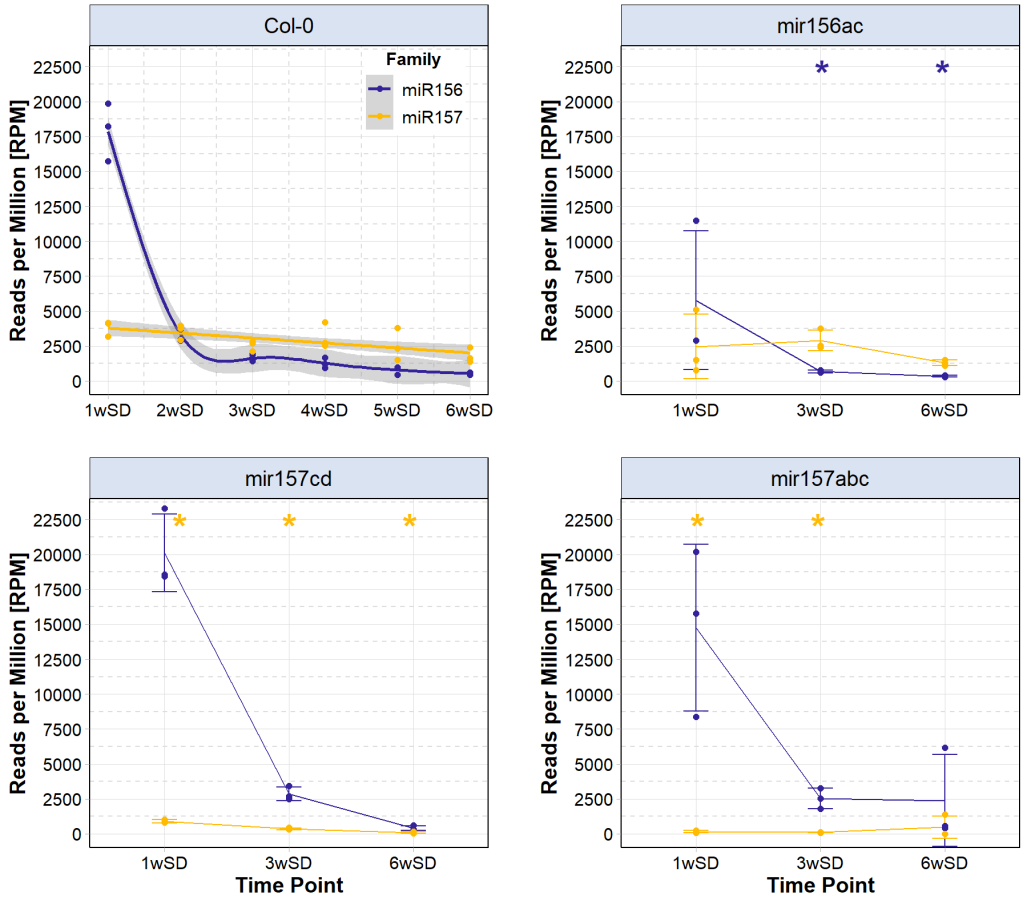

Figure 4.2. The abundance of miR156/miR157 in precursor mutants under short days over time from sRNA sequencing expressed as reads per million (RPM). The levels of miR156 (blue) and miR157 (yellow) are shown for Col-0, *mir156ac*, *mir157cd* and *mir157abc* mutants. Lines for Col-0 represent fitted generalised additive models (GAMs). Shaded areas represent 95% confidence intervals. To prevent overfitting due a low number of time points, lines in *mir156ac*, *mir157cd* and *mir157abc* panels represent the connected means instead. Asterisks denote significant differences in pairwise comparisons between mutants and Col-0, Bonferroni-adjusted $p < 0.05$. The sRNA sequencing experiment was analysed in collaboration with Dr. Vidya Oruganti. The data for the Col-0 time course are reproduced from Figure 3.2.

By contrast, the abundance of miR157 was significantly lower in *mir157cd* and *mir157abc* mutants than in Col-0 but the miR156 levels were similar. The effect of the deletion alleles therefore is miRNA family-specific. Although residual miR157 expression was present in *mir157cd* at 1wSD, virtually no miR157 reads were detected at 1wSD and 3wSD in *mir157abc*. This observation, together with the significant reduction in miR157 abundance in *mir157cd,* suggests that *MIR157C*, contributes the majority of mature miR157 molecules in short-day grown apices.

4.4. Flowering-time phenotypes of *mir156ac* and *mir157cd* mutants in long and short days.

Because the CRISPR/Cas9-induced deletions within the *MIR156* and *MIR157* genes specifically reduced either miR156 or miR157 abundance, this enabled the dissection of the relative importance of *MIR156* and *MIR157* genes during floral transition. For this, the flowering time of *mir156ac, mir157cd* and mutants was examined in long-day conditions (Figure 4.3), in which wild-type miR156 levels were reached prior to floral transition. The following flowering-related phenotypes were recorded: The time until the bolting of the main shoot occurred (days to bolting), the time until the first flower opened (days to flowering) and the number of rosette and cauline leaves.

In long days, the median time to bolting of Col-0 was 24 days and the first flower opened approximately five days later (Figure 4.3A and B). The *mir156ac* and *rSPL15* genotypes bolted significantly earlier than wild type. The variation in bolting time for the *rSPL15* phenotype was lower than that of other genotypes, but the median bolting time was similar to that of *mir156ac*. *mir156ac* also flowered earlier than wild type, but the difference in days to flowering between *rSPL15* and wild type was not significant.

One function of *SPL15* is to reduce the rate of leaf initiation (Hyun et al., 2016; Schwarz et al., 2008). Consistent with this, *rSPL15* plants had the fewest rosette leaves (Figure 4.3C). The difference in the number of rosette leaves in *rSPL15* compared with Col-0 was more extreme than the acceleration in time to bolting.

By contrast with the bolting and flowering-time phenotypes of *mir156ac* mutants, these phenotypes of *mir157cd* mutants in long days did not differ significantly from those of wild type. The number of rosette leaves was also comparable in *mir157cd* and wild type. Despite the similar flowering phenotypes of *mir157cd* and wild type, *mir157cd* mutants produced additional cauline leaves (Figure 4.3C). This was a similar, but weaker phenotype to that of *rSPL15*. Notably, the early flowering *mir156ac* mutant produced the same number of cauline leaves as wild-type plants.

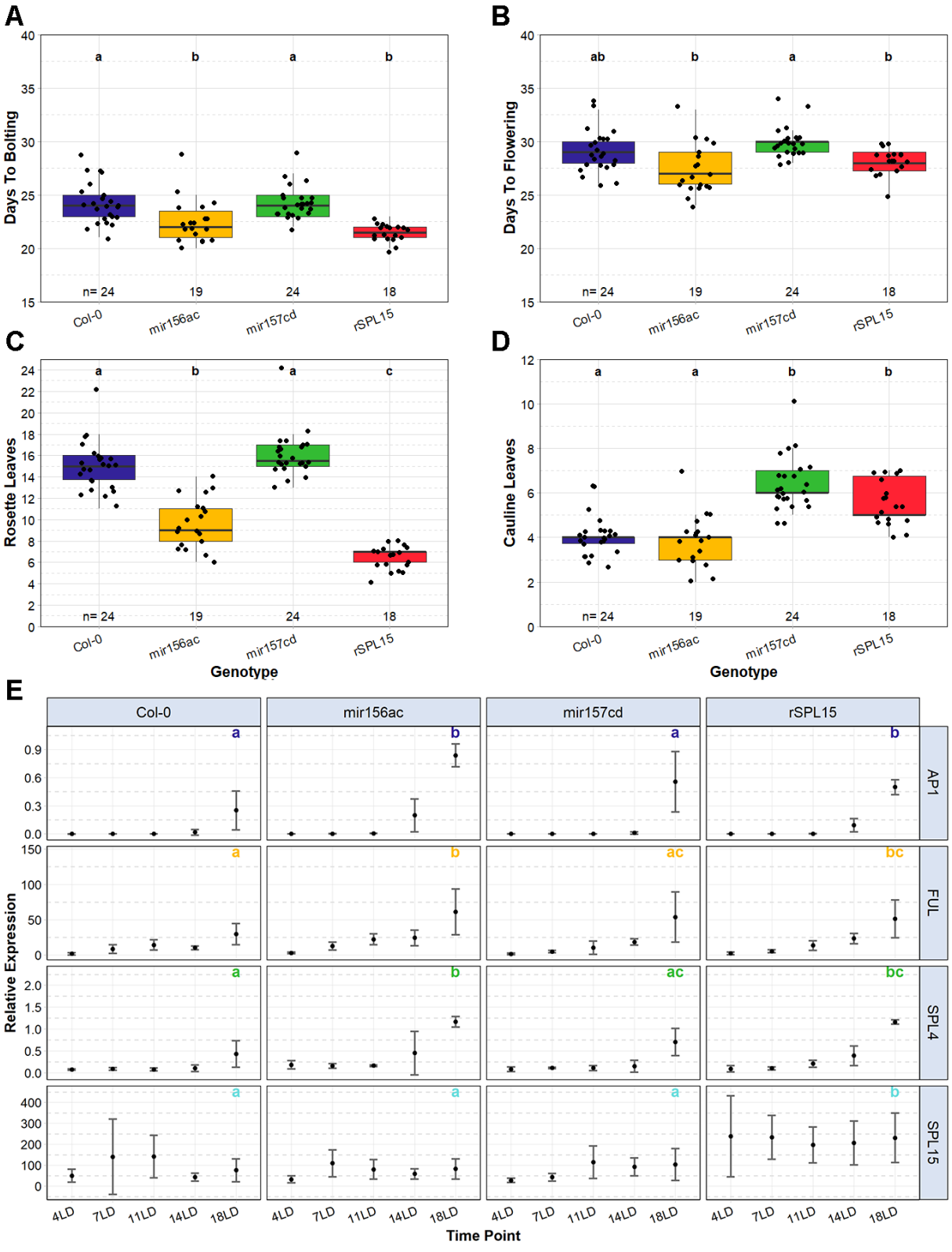

Figure 4.3. Flowering time and expression of floral meristem identity genes in *mir156ac* and *mir157cd* mutants in long days. Flowering time was measured as A) days to bolting, B) days to flowering, C) the number of rosette leaves and D) the number of cauline leaves produced. The sample size (n) is shown for each panel. E) qRT-PCR analysis of *APETALA1* (*AP1*), *FRUITFULL* (FUL), *SQUAMOSA PROMOTER BINDING PROTEIN-LIKE 4* (*SPL4*) and *SPL15* gene expressions. The expression values are relative to that of *PEROXIN4,* values are the means and standard deviations of

three replicates. Significant differences were determined by ANOVA analysis with genotype and time point as factors, followed by Tukey's HSD pairwise comparisons. Different letters indicate statistically significant differences among genotypes at $p < 0.05$.

The flowering-time phenotypes were associated with significant differences in the temporal expression patterns of the floral meristem identity genes *AP1* and *FUL* in apices (Figure 4.3E). The expression of *AP1* is specific to floral primordia initiated at the flanks of inflorescence meristems, therefore it was absent in all genotypes analysed at vegetative time points. In the early-flowering *mir156ac* and *rSPL15* genotypes, *AP1* expression was detected at 14LD and was strongly upregulated at 18LD. In wild-type and *mir157cd* apices, an elevated level of *AP1* transcripts was detected at 18LD only.

The expression of *FUL,* which is the target of several SPL transcription factors, increased steadily in all four genotypes during the experimental time course. The level of *FUL* transcription was most strongly upregulated in *mir156ac*, *mir157cd* and *rSPL15* genotypes, but *FUL* expression in *mir157cd* was not significantly different to that in wild type. The miR156/miR157 target *SPL4* was upregulated at 18LD in wild type and *mir157cd*, but was upregulated earlier and to a greater degree in *mir156ac* and *rSPL15*.

The expression of *SPL15* was also quantified, but no significant changes were detected over time (Figure 4.3E). This suggests that the miR156/miR157-mediated regulation of *SPL15* might act at the translational level. The level of *SPL15* expression was consistently higher in *rSPL15* plants than in other genotypes, but the expression level did not change over time. The endogenous *SPL15* gene is functional in *rSPL15* lines; therefore, a higher *SPL15* copy number might cause increased transcription.

The effect of *mir156* and *mir157* mutations on inflorescence height was analysed in long-day conditions (Figure 4.4). The length of I1 internodes was measured in two independent experiments. The total height of the I1 zone was calculated via the summation of individual internode lengths (Figure 4.4C). Although absolute measurements varied between experiments, *mir156ac*, *mir157cd* and *mir157abc* mutants had taller I1 zones than wild-type plants. For *mir156ac* and *mir157abc* plants, the differences in inflorescence height were statistically significant in both experiments.

Wild-type plants and *mir156ac* mutants formed a similar number of cauline leaves. By contrast, *mir157cd* mutants consistently formed more cauline leaves than *mir156ac* and wild type (Figure 4.4B). Strikingly, the number of cauline leaves of *mir157abc* triple mutants was lower than that of *mir157cd* mutants, but higher than that of wild type and *mir156ac* mutants. This suggests that *MIR157D* is involved in inflorescence development and that in this context it might be more important than *MIR157A* and *MIR157B*. Despite the greater number of I1 nodes, the I1 height of *mir157cd* and *mir157abc* was not greater than that of *mir156ac* mutants; instead, the I1 internodes of *mir157cd* and *mir157abc* shoots were reproducibly shorter than those of *mir156ac* shoots. The difference between I1 internode length of wild type and *mir157cd* was significant in the first experiment, whereas the difference in internode length between wild type and *mir157abc* was not.

The position of the longest internode of wild-type plants was either the first or the second position at the inflorescence base (Figure 4.4E). For *mir156ac* mutants, the longest internode was usually the first one and this was consistent across experiments. Thus, although the number of cauline leaves produced by *mir156ac* inflorescences was similar to that of wild type, the pattern of internode elongation appeared to be different. The position of the longest internode was more variable in *mir157cd* and *mir157abc* mutants. The position of the longest internode of *mir157abc* plants was less consistent between experiments; in one experiment, it was similar to that of *mir156ac* whereas in the other it was more similar to that of *mir157cd*. For *mir157cd* mutants, the longest internode was more often at the first position, but was otherwise among at the first three positions. Taken together, the *mir157cd* and *mir157abc* phenotype was highly consistent in terms of cauline leaf number in long days, but the internode elongation was more variable.

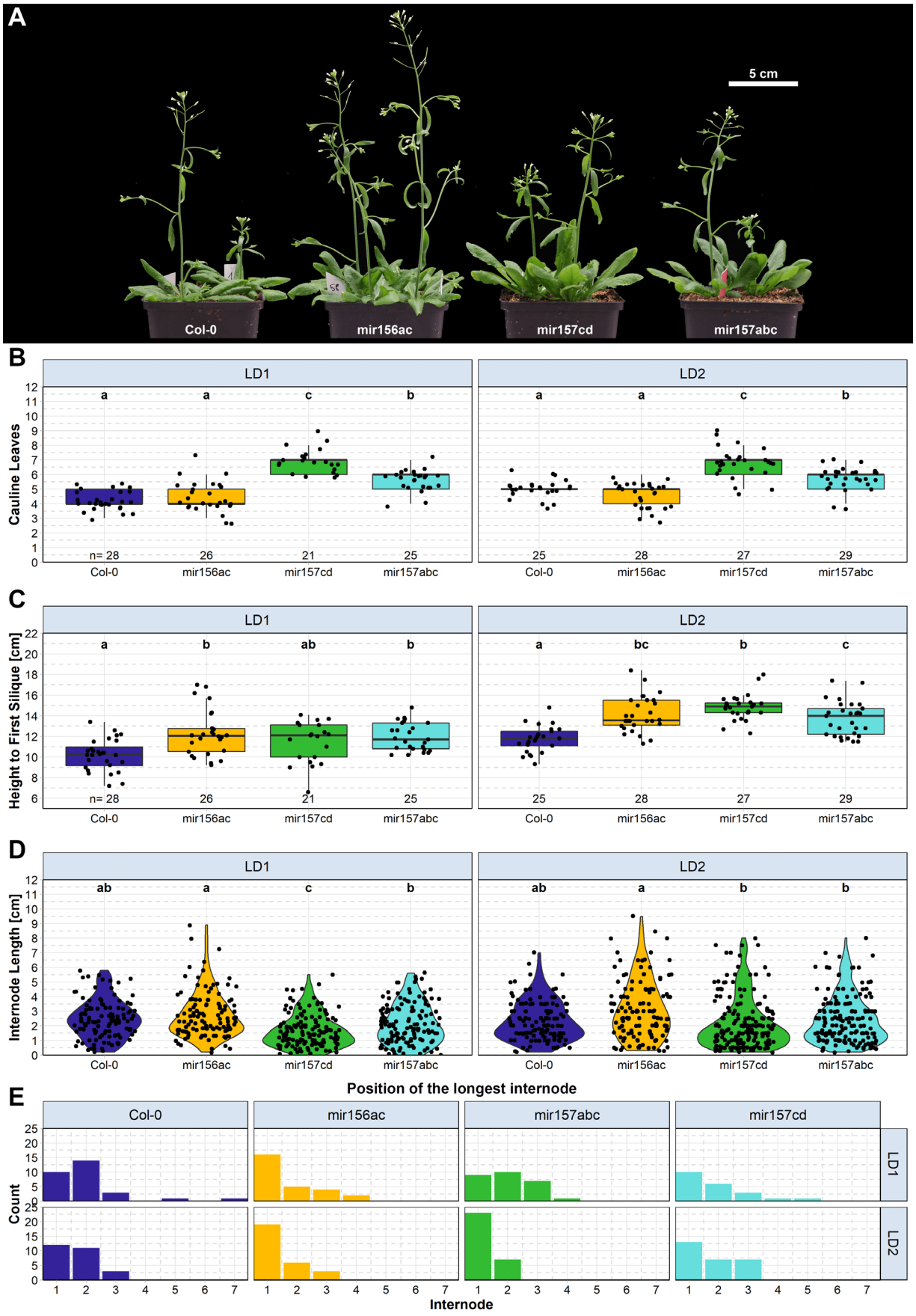
A
5 cm
Col-0
mir156ac
mir157cd
mir157abc
B
LD1
LD2
Cauline Leaves
a a c b
n= 28 26 21 25
C
Height to First Silique [cm]
a b ab b
a bc b c
D
Internode Length [cm]
ab a c b
ab a b b
Col-0
mir156ac
mir157cd
mir157abc
E
Position of the longest internode
Count
Internode
LD1
LD2

Figure 4.4. The effect of *mir156* and *mir157* mutations on inflorescence growth. A) Representative images of Col-0, *mir156ac*, *mir157cd* and *mir157abc* plants at flowering. Images correspond to the second experiment (LD2). B) Number of cauline leaves. C) Reconstructed I1 zone height calculated as the sum of I1 internode measurements plotted in D). Significance levels in B and C were determined by one-factor ANOVA followed by Tukey's HSD post-hoc tests. Sample size (n) is given at the base of the plots. D) The length of all I1 internodes of wild type (Col-0), *mir156ac*, *mir157cd* and *mir157abc* was measured in two independent experiments in long days (LD1 and LD2). Significance levels in D) were determined by the non-parametric Kruskal-Wallis test followed by Nemenyi's post-hoc test. E) Histogram showing the position of the longest I1 internode. Position 1 refers to the lowest elongated internode between the rosette and first cauline leaf.

The flowering time of *mir156ac*, *mir157cd* and *mir157abc* was then analysed in short days and compared with that of *rSPL15* and wild type (Figure 4.5). In these conditions, *rSPL15* plants were the first to bolt, approximately two weeks earlier than Col-0 (Figure 4.5A). In contrast to the bolting and flowering time of *mir156ac* in long days, *mir156ac* mutants bolted and flowered in short days at the same time as Col-0 (Figure 4.5A, B). Notably, *mir157cd* and *mir157abc* bolted significantly earlier than wild type, but later than *rSPL15* plants. The opening of the first flower occurred at about the same time in all three genotypes, which suggests that the formation of mature flowers takes longer in *rSPL15* than in *mir157cd* and *mir157abc*. The delay in flowering time of wild type compared with that of *rSPL15* was also less extreme than the difference in time to bolting.

The number of rosette leaves produced prior to flowering was similar for wild type, *mir156ac* and *mir157cd*, whereas *mir157abc* produced fewer leaves than wild type and *mir156ac* (Figure 4.5C). Plants carrying the *rSPL15* transgene initiated the fewest rosette leaves. Similarly to in long days, the number of cauline leaves in short days was highest in *rSPL15*, followed by *mir157cd* (Figure 4.5D). Col-0, *mir156ac* and *mir157abc* produced a similar number of cauline leaves, although the variation was greater for the latter two genotypes.

The expression of *AP1*, *FUL* and *SPL4* was analysed in one- to six-week-old apices (Figure 4.5E). Throughout the time course, *AP1* expression was barely detectable in wild type and *mir156ac* samples, suggesting that floral transition had not occurred at 6wSD. By contrast, the level of *AP1* expression increased in six-week-old apices of *mir157cd* and *mir157abc*. Due to variation among replicates, the difference in *AP1* expression from that of Col-0 was only significant in *mir157abc* plants. The expression levels of *FUL* and *SPL4* were significantly higher in *mir157cd* and *mir157abc* mutants

than in wild type. This suggests that at 6wSD these two genotypes were undergoing floral transition.

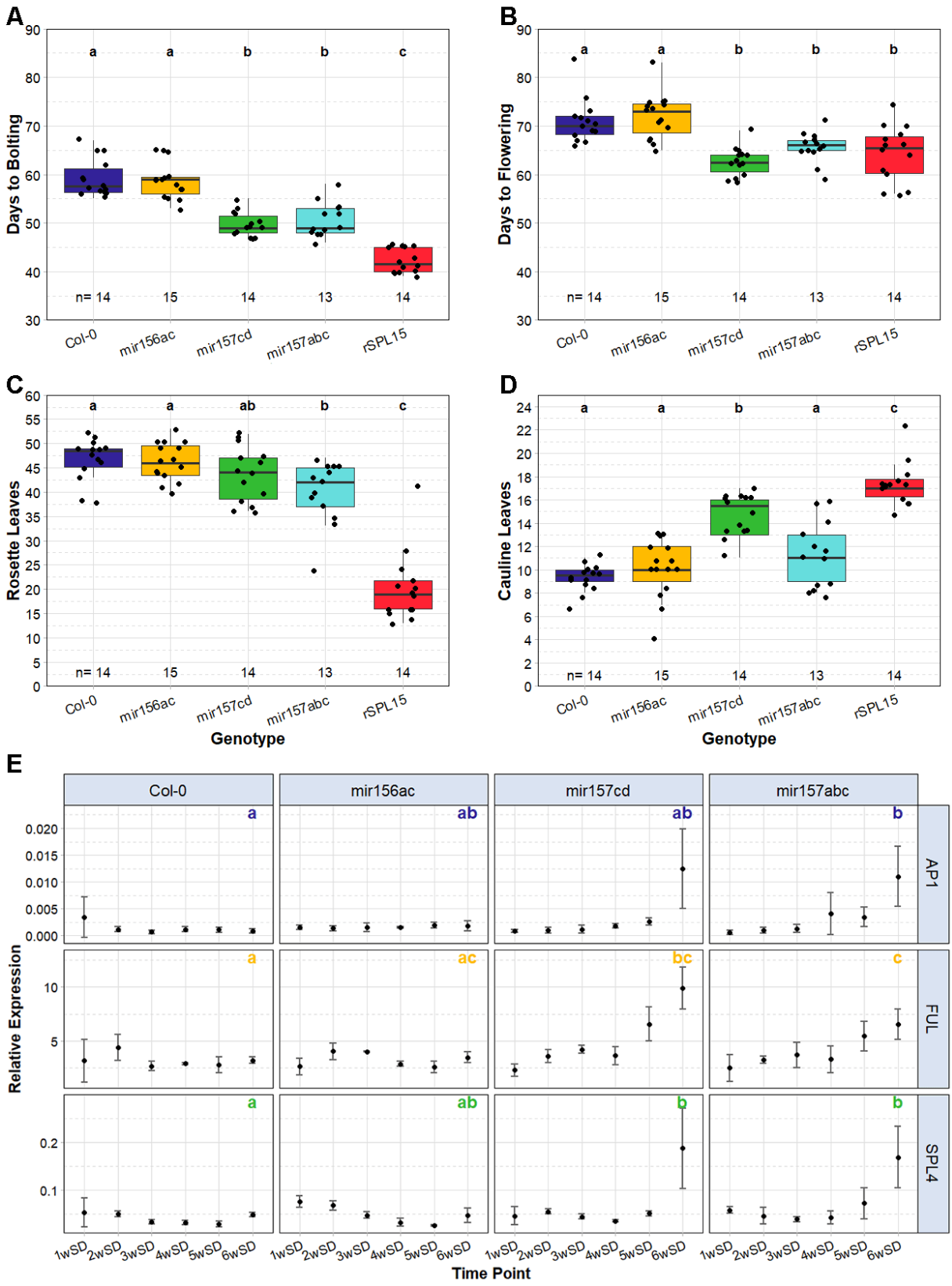

Figure 4.5. Flowering time and expression levels of floral meristem identity genes in *mir156ac* and *mir157cd* mutants in short days. Flowering time was measured as A) days to bolting; B) days to flowering. C); number of rosette leaves and D) number of cauline leaves. The sample size (n) is shown for each panel. E) qRT-PCR analysis of *APETALA1* (*AP1*), *FRUITFULL* (*FUL*) and *SQUAMOSA PROMOTER BINDING PROTEIN-LIKE 4* (*SPL4*) genes. The expression values are relative to that of *PEROXIN4* and represent means and standard deviations for three replicates. Significant differences were determined by ANOVA with genotype and time point as factors, followed by Tukey's HSD pairwise comparisons. Different letters indicate statistically significant differences among genotypes at $p < 0.05$.

Floral transition is associated with changes in meristem morphology (Kinoshita et al., 2020; Tal et al., 2017). To compare floral transition in short days between the early bolting *mir157cd* mutant and Col-0 at the meristem level, the *pWUSCHEL:3xVENUS-NLS pCLAVATA3::mCHERRY-NLS* (*pWUS::VENUS pCLV3::mCHERRY*) double reporter line (Pfeiffer et al., 2016) was introduced into the *mir157cd* background.

The double reporter line reports the promoter activities of *WUS* and *CLV3,* which engage in a negative feedback loop to regulate stem cell homeostasis at the SAM (Fuchs and Lohmann, 2020). Expression of *CLV3* defines the central zone, whereas *WUS* is expressed in the organising centre. The expression patterns were analysed over a time course in short days from 1wSD to 7wSD (Figure 4.6).

The SAM of one-week-old Col-0 and *mir157cd* seedlings was small and flat. Both genotypes expressed the *pCLV3::mCHERRY* reporter in L1 and L2 cells of the meristem and in a few underlying cells, where expression overlapped with that of *pWUS::VENUS* in the organising centre (yellow signal in Figure 4.6). As expected, both double reporter constructs were not expressed in leaves or the hypocotyl. The size of the SAM of *mir157cd* and wild-type apices increased continuously from 1wSD to 5wSD. Expansion of the organising centre led to a rounder shape of the meristem surface and a broader *pWUS::VENUS* expression domain. The number of cell layers in the distal meristem region increased from two at 1wSD to five at 5wSD. These layers formed part of the *pCLV3::mCHERRY* expression domain, whereas only the adjacent cells below expressed *pWUS::VENUS*. This was the case for both *mir157cd* and wild type. An expansion in the degree of overlap between *pWUS::VENUS* and *pCLV3::mCHERRY* domains was observed at 5wSD. At this time point, strong expression of *pWUS::VENUS* also spread to the meristem base, and this expression was more pronounced in apices of *mir157cd* than in those of wild type. The difference

in expression was greatest at 6wSD, when *mir157cd* apices started to elongate. By 7wSD, floral primordia that express *pWUS::VENUS* appeared at the flanks of *mir157cd* apices and the rib zone continued to elongate. By contrast, wild type apices were less elongated and floral transition was still ongoing.

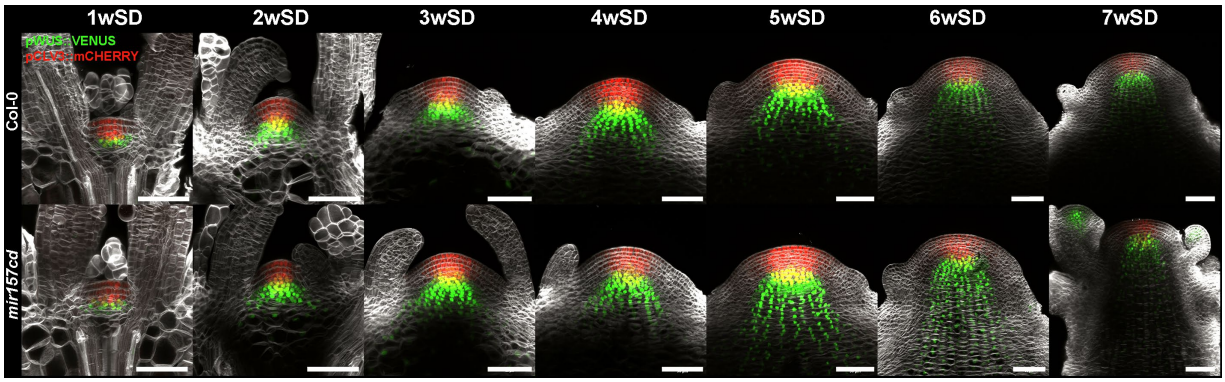

Figure 4.6. Comparison of the expression patterns of the *pWUSCHEL:3xVENUS-NLS* (*pWUS::VENUS*, green) *pCLAVATA3::mCHERRY-NLS* (*pCLV3::mCHERRY,* red) reporters in wild type (Col-0, first row) and *mir157cd* (second row) grown in short days. Nuclei that co-express *pWUS::VENUS* and *pCLV3::mCHERRY* appear in yellow. The *pWUS::VENUS pCLV3::mCHERRY* double reporter line was published in Pfeiffer et al. (2016). SCRI Renaissance 2200 cell-wall stain is shown in grey. The scale bar represents 50 µm in all panels.

4.5. SPL15 expression pattern in short-day conditions

Following the observation that *mir157cd* mutants bolted early under short days, I investigated the accumulation of SPL15 protein at the SAM of *mir156* and *mir157* mutants. For this, I introduced the *pSPL15::9AV:SPL15* (*pSPL15*) reporter into the *mir156ac* and *mir157cd* genotypes. The reporter transgene consisted of a translational fusion between SPL15 and the VENUS fluorophore under the control of native *SPL15* promoter sequences (Hyun et al., 2016). The *pSPL15* expression pattern in *mir156ac* and *mir157cd* was imaged by confocal microscopy in separate time courses, in both cases with *pSPL15* in the Col-0 background as a control (Figure 4.7). In addition, the expression of the miR156/mir157-resistant *pSPL15::9AV:rSPL15* (*rSPL15*) reporter variant was analysed (Figure 4.7A). Apices from two- to six-week-old plants (2wSD to 6wSD) were dissected and imaged. These time points were chosen to capture meristems that were undergoing floral transition in controlled short-day conditions. The *pSPL15* reporters were not complementation lines, but contained wild-type alleles of the endogenous *SPL15* locus. Thus, the homozygous transgene provided two

additional copies of functional *SPL15,* which might result in mild overexpression compared with expression in non-transgenic Col-0 plants. The same growth conditions were used to compare the reporter activity among genotypes.

At 2wSD, fluorescence signal resulting from *pSPL15* expression in Col-0 was either extremely weak or was absent from the SAM, depending on the time course (Figure 4.7A, B). The VENUS signal at the SAM of *mir156ac* mutants was stronger than that in wild type apices (Figure 4.7A). At this time point, no expression was detectable outside of the apical meristem. This was different from the miR156/mir157-insensitive *rSPL15* construct, the expression domain of which extended into vascular tissue. The *rSPL15* construct was highly expressed, which necessitated reducing the laser power to prevent damaging the detector of the microscope. Thus, tissues expressing *rSPL15* were imaged with different settings from those used to image *pSPL15* and these settings were used consistently throughout the time course.

The spatial expression patterns of *pSPL15* and *rSPL15* in the wild-type SAM were similar and were consistent with reports in the literature (Hyun et al., 2016), and any differences in expression were temporal or quantitative. Shoots of *rSPL15* apices rapidly underwent floral transition. At 2wSD, the SAM of *rSPL15* plants was rounder than that of other genotypes and cauline leaves were formed by 4wSD. At 5wSD, axillary meristems subtended by cauline leaves emerged from *rSPL15* apices. In apical and axillary meristems, *rSPL15* was expressed in analogous domains.

The expression domain of *pSPL15* in *mir156ac* and Col-0 expanded at 3wSD and became more similar to that of *rSPL15*. At subsequent time points, *pSPL15* activity increased in intensity. Strongest expression was present at the SAM and in narrow domains extending from the rib meristem into the shoot. These cells probably correspond to differentiating vasculature and might be associated with bolting. At later time points, strong and focussed VENUS signal appeared in single continuous cell files that connected the main stem with cauline leaves and axillary meristems. This was observed in all genotypes, but was most apparent in *rSPL15* plants.

At 5wSD, the pattern of *pSPL15* expression in *mir156ac* was different to that in Col-0 and the shoot morphology of *mir156ac* mutants was developmentally more advanced than that of Col-0. The *mir156ac* meristem was flatter and *pSPL15* expression

extended further down the shoot than in Col-0. However, at 6wSD, the morphology of Col-0 and *mir156ac* plants was very similar and cauline leaves were present in both genotypes.

Although *pSPL15* and *rSPL15* were expressed consistently in adaxial and basal regions of older leaf primordia, VENUS signal was always absent from young and incipient primordia. Within the SAM, expression of both reporters was weaker in the L1 layer.

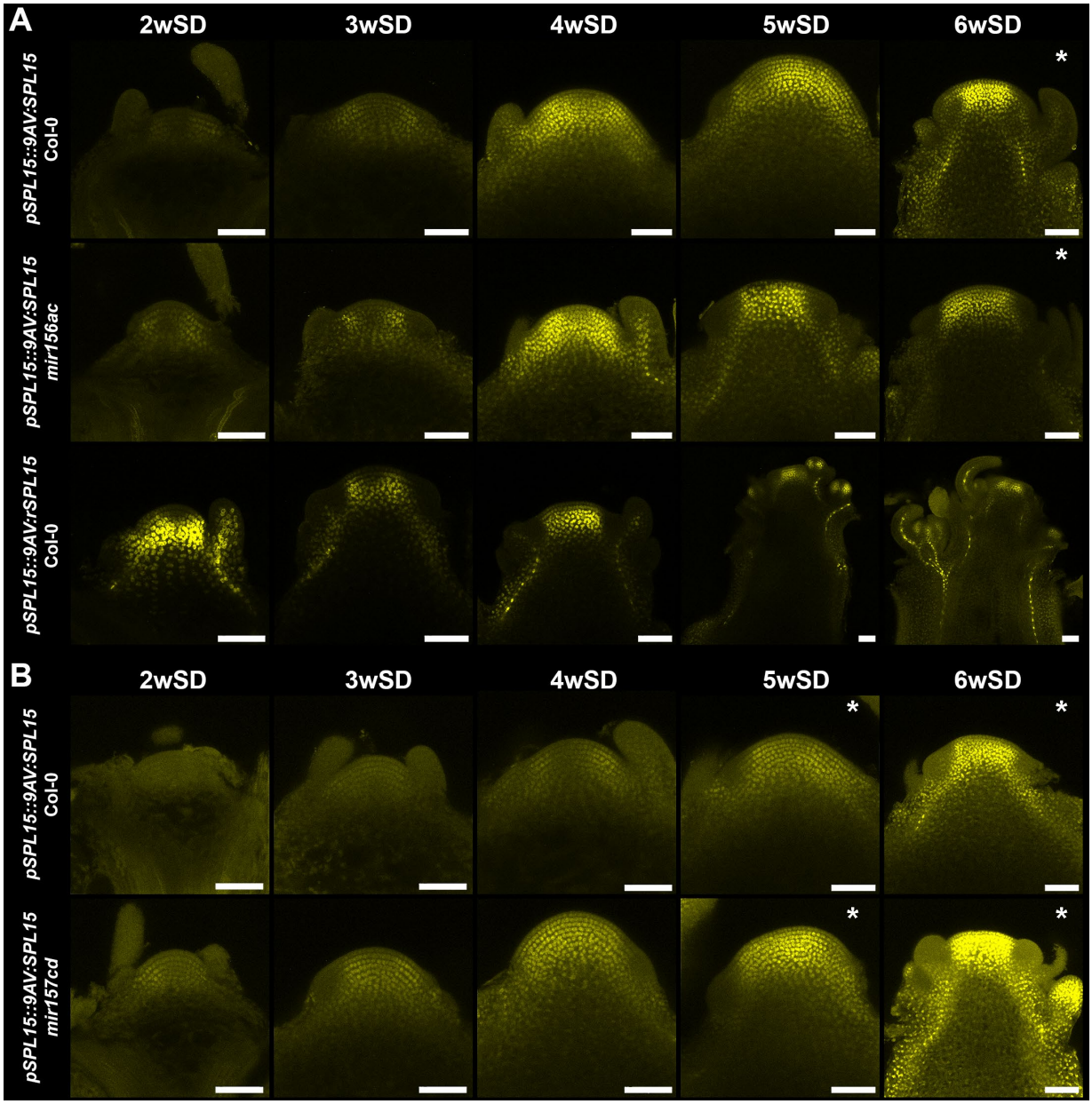

Figure 4.7. Expression of *pSPL15::9AV:SPL15* in Col-0 and in *mir156ac* and *mir157cd* mutants grown in short days, with the miR156/mir157-resistant *pSPL15::9AV:rSPL15* (*rSPL15*) variant as a reference. A) Due to differences in signal intensity, plants expressing *rSPL15* were imaged with

different settings to the other genotypes. Similarly, laser intensity was reduced for *pSPL15::9AV:SPL15* at 6wSD. B) An independent time course compared the expression of *pSPL15::9AV:SPL15* in Col-0 and in *mir157cd* backgrounds. The laser intensity for VENUS excitation was lowered to image both genotypes at 5wSD, to protect the HyD detectors. Representative images of at least five samples are shown. The scale bar represents 50 µm in all panels.

The spatial expression of *pSPL15* was also consistent with that observed in the independent experiment that compared *pSPL15* activity between *mir157cd* and Col-0 over time (Figure 4.7B). At 2wSD, the signal intensity of *pSPL15* was stronger in *mir157cd* and the meristem had a more rounded shape than in Col-0. These differences were observed throughout the time course. At 4wSD, the SAM of *mir157cd* reached its maximum domed state, before adopting a flatter morphology. Floral transition was advanced at 6wSD, when cauline leaves were present at the *mir157cd* apex. Wild-type apices were delayed in development by approximately one week compared with *mir157cd* apices.

To further investigate bolting in *mir157* mutants, the *pFUL::9AV:FUL ful-2 (pFUL)* reporter line was introduced into the *mir157c* single mutant. The expression pattern of this translational reporter line was then analysed in another short-day time course (Figure 4.8).

No *pFUL* expression was detected in wild-type and *mir157c* SAMs early in development (1wSD to 3wSD, Figure 4.8). However, VENUS signal was present in stipules in both genotypes at 1wSD. This is consistent with the published *FUL* expression pattern (Gu et al., 1998). At 4wSD, *pFUL* expression appeared in nuclei speckled throughout the SAM. There were no differences between *pFUL* expression in either genotype at this time point, nor at 5wSD, when the expression domain expanded slightly. After 6 weeks of growth, the *pFUL* expression domain in apices increased in intensity and expanded, which occurred to a considerably greater extent in *mir157c* mutants than in control plants, and the signal then covered the entire central and peripheral zones. The increase in *pFUL* expression also correlated with a change in SAM morphology. The presence of spherical primordia in the peripheral zone and cauline leaves indicated that meristems had undergone floral transition.

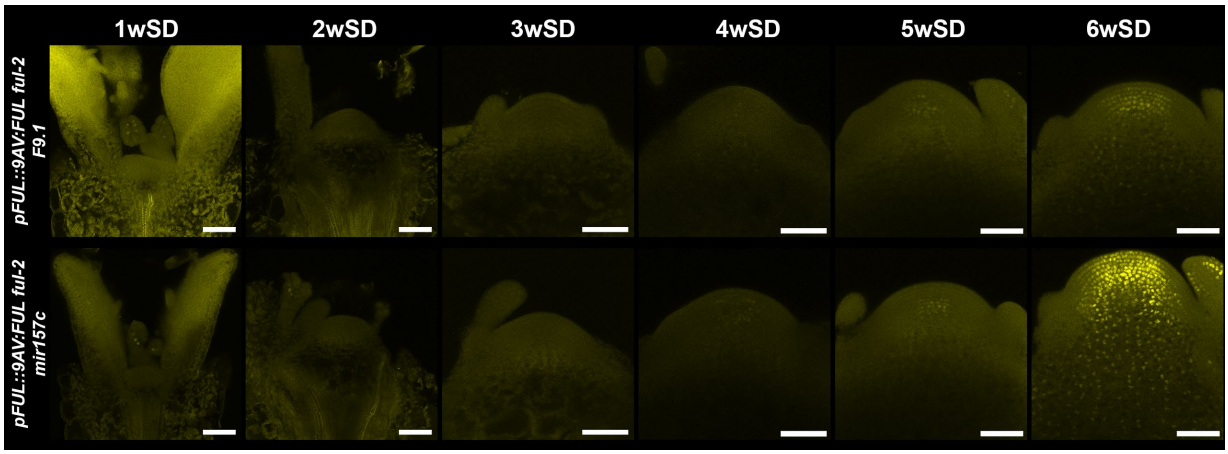

Figure 4.8. The pattern of FRUITFULL (FUL) protein accumulation reported by *pFUL::9AV:FUL* in *ful-2* and *mir157c ful-2* mutant backgrounds. The same confocal imaging settings were used for both genotypes and at all sampling time points. For clarity, only the VENUS channel is shown. The scale bar represents 50 µm in all panels.

4.6. Response of *MIR156* and *MIR157* precursors to cold treatment

The contribution of miR156 to the response to various stresses has been well described in the literature (Cui et al., 2014; Stief et al., 2014; Visentin et al., 2020). For example, *MIR156* precursors are upregulated during cold, which is a mechanism that is particularly important to the life strategies of winter annuals and perennials (Bergonzi et al., 2013; Hyun et al., 2019; Park et al., 2017; Zhou et al., 2013a). To test whether *MIR156* reporter lines responded to this cold stress, apices of *MIR156A::GFP A1-1* and *MIR156C::VENUS:GUS C5-2* and *C10-1* reporter lines were sampled for a quantitative real-time PCR experiment. Plants were grown at 21°C for two weeks in short-day conditions and where then transferred to 4°C cabinets in short day conditions for four additional weeks. Control plants were grown continuously at 21°C. The three biological replicates that were harvested before treatment (at 2wSD) serve as common point of reference. They contained apices randomly sampled from both treatment groups.

The expression of endogenous *MIR156A*, *MIR156C*, *MIR157A* and *MIR157C* was tested first (Figure 4.9B). The three transgenic lines were comparable in terms of *MIR* gene expression pattern and stress response, indicating that the transgene insertions did not interfere with expression of the tested genes. In the control group, the expression of *MIR156A*, *MIR156C* and *MIR157A* was highest at 2wSD and gradually

decreased during the time course. The expression of *MIR157C* was more variable and did not show a strong trend over time. Physiologically, the cold treatment strongly delayed growth and only a few leaves appeared during treatment (Figure 4.9A).

Cold treatment strongly affected the expression levels of *MIR156A* and *MIR157A* (Figure 4.9B). In the first week of treatment (2+1w), the abundance of transcripts of both genes decreased. However, at subsequent time points, *MIR156A* and *MIR157A* expression remained constant in the treatment group, but was continuously downregulated in the control group. Fitting generalised additive models revealed a significant effect of cold treatment on the temporal expression of endogenous *MIR156A* and *MIR157A* precursors (Figure 4.9).

The response of *MIR156C* to cold differed from that of *MIR156A* and *MIR157A.* During the first week, the level of *MIR156C* transcripts in the treatment group decreased to a lower level than in the control group. Notably, during the next two weeks of treatment, expression of *MIR156C* increased to a level greater than that in the control group. However, this increase was transient, and after four weeks of treatment (2+4w, Figure 4.9B), no differences in *MIR156C* expression among treatment and control groups were observed. Quantification of *MIR157C* expression did not reveal any specific response to cold.

Next, the expression level of *MIR156A::GFP* and *MIR156C::VENUS:GUS* reporter transgenes was quantified using primers specific to *VENUS/GFP* reporter genes (Figure 4.9C). In warm conditions, *MIR156C::VENUS:GUS* transcript abundance decreased over time. During the experiment, the mean *MIR156C::VENUS:GUS* expression level in both C5-2 and C10-1 lines decreased almost four fold. Compared with endogenous *MIR156C* expression, the decrease in *MIR156C::VENUS:GUS* expression occurred more gradually over time and no significant difference was observed among treatments.

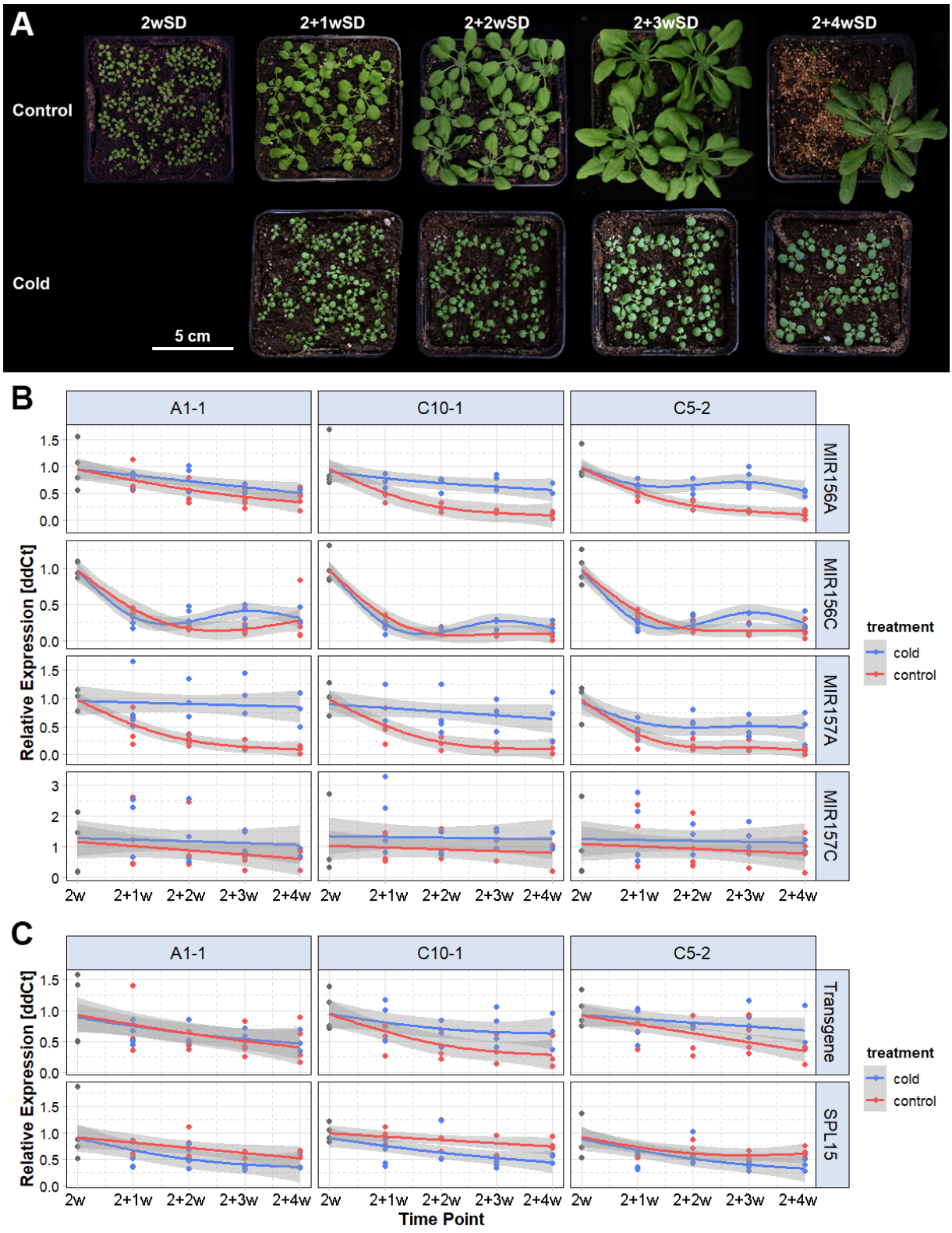

Figure 4.9. Transcriptional response of *MIR156/MIR157* precursors and *MIR156* reporters to cold treatment in apices of *MIR156A::GFP* A1-1, *MIR156C::VENUS:GUS* C10-1 and *MIR156C::VENUS:GUS* C5-2 reporter lines as determined by qRT-PCR. A) Representative plants of control and treatment groups, B) Relative expression of *MIR156/MIR157* precursors and C) transgenes and *SQUAMOSA PROMOTER BINDING PROTEIN-LIKE 15* (*SPL15*) normalised to expression levels of *PROTEIN PHOSPHATASE 2A* and *PEROXINX4* reference genes and to the 2wSD time point.

Generalised additive models were fitted to the expression of four biological replicates. The 95% percent confidence intervals are plotted in grey. Transgene refers to transcripts of *MIR156A::GFP* or *MIR156C::VNG* detected by primers that bind to both *GFP* and *VENUS.*

The qRT-PCR expression analysis showed that cold-treated plants maintained higher levels of *MIR156A, MIR156C* and *MIR157A* transcripts and that this correlated with a reduction in *SPL15* expression. In two subsequent experiments, how this transcriptional response related to the regulation of flowering time was analysed (Figure 4.10). For this, plants were grown for either two or four weeks at 21°C in short-day conditions, and were then subjected to two-weeks at 4°C in short days before they were returned to 21°C until flowering. Wild-type and *mir157cd* plants were subjected to two or four weeks at 21°C before cold treatments, but *mir156ac* plants were grown for two weeks at 21°C and *mir157abc* plants were grown for four weeks at 21°C before cold treatment.

To assess the effect of cold on plant growth, the number of rosette leaves produced during the two weeks of treatment after growth for two or four weeks at 21°C was recorded (Figure 4.10D). The control groups of wild type and *mir157cd* plants both produced approximately twice as many rosette leaves after four weeks of growth as after two weeks of growth. There were no significant differences in rosette leaf number between control groups of wild type and *mir157cd* mutants. The control group of *mir157abc* plants produced fewer leaves than both wild type and *mir157cd*. The number of rosette leaves produced by plants subjected to cold treatments was extremely low. When the treatment started after two weeks, most plants produced only one additional leaf over the two subsequent weeks. In plants treated after four weeks of growth at 21°C, a median of five rosette leaves were formed during treatment. There were no differences among treatment groups of all genotypes. Therefore, a cold treatment of 4°C strongly delayed plant growth, but older plants maintained a higher rate of leaf initiation.

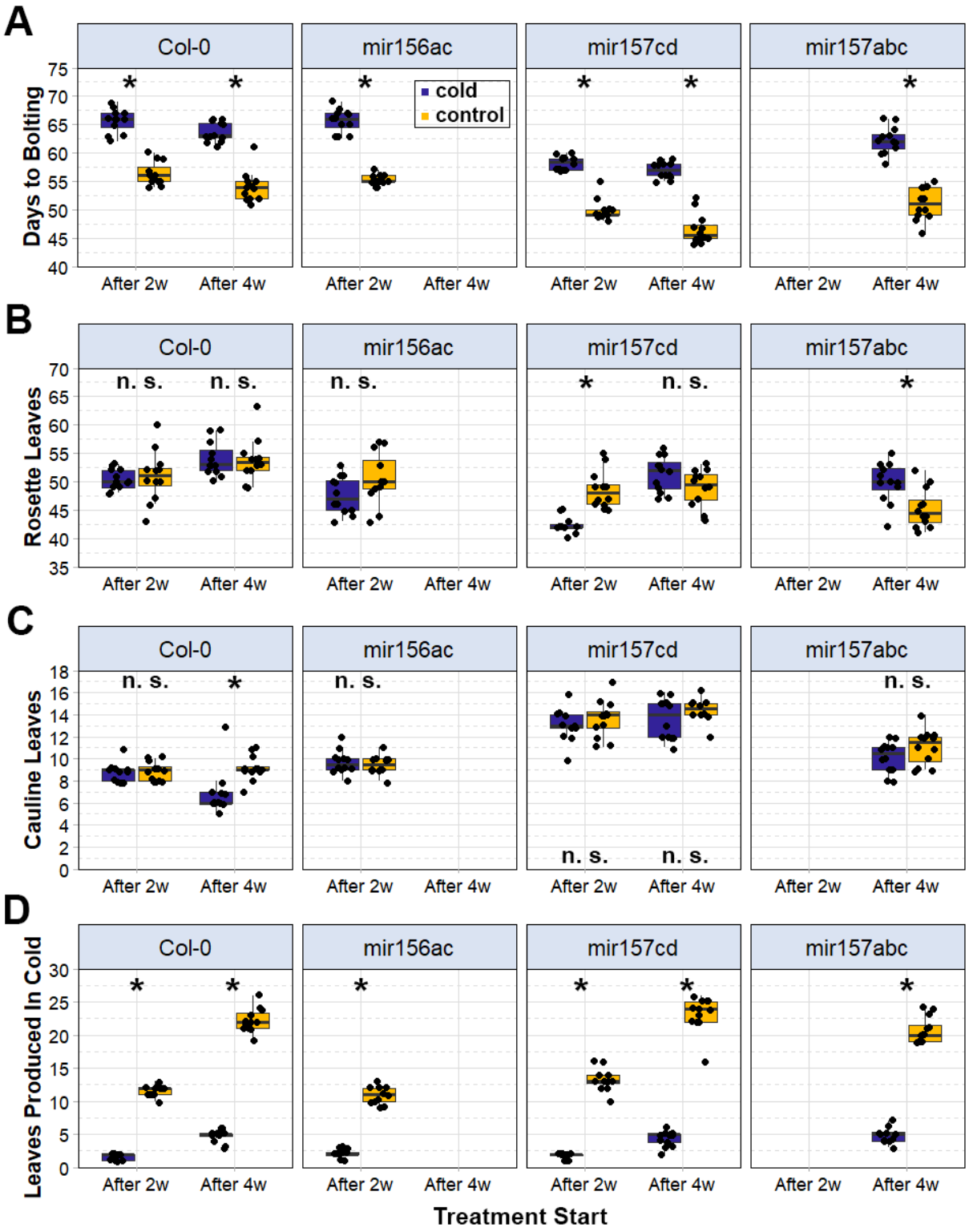

Figure 4.10. Flowering-time data to analyse the effect of a temporary shift from 21°C to 4°C on the flowering of *mir156* and *mir157* mutants. In independent experiments, plants were grown for either two (After 2w) or four weeks (After 4w) in 21°C in short-day conditions, and were then subjected to two-week-treatments at 4°C in short days before they were returned to 21°C until flowering occurred. Wild-type (Col-0) and *mir157cd* genotypes were subjected to two or four weeks at 21°C in short days before cold treatment, whereas *mir156ac* and *mir157abc* mutants were subjected to cold treatment after two or four weeks of growth at 21°C in short days, respectively. A) The number of days to bolting. Three-factor ANOVA found significant effects for treatment start, genotype and treatment group but did not

identify any significant interaction effects among these factors at $p < 0.05$. B) The final number of rosette leaves produced, C) The number of cauline leaves; D) The number of rosette leaves produced during cold treatments. Asterisks denote significant differences between treatment and control groups of each genotype and per experiment as determined by ANOVA followed by post-hoc Tukey's HSD tests, $p < 0.05$., n. s. = not significant.

In both experiments, cold treatment clearly affected bolting time, delaying it for 9 to 11 days in all genotypes (Figure 4.10A). The extent of the delay was independent of the type of treatment. Accordingly, *mir157cd* mutants bolted consistently earlier than wild-type plants in similar conditions. The bolting time of *mir156ac* treated after two weeks of growth was similar to that of wild-type plants. Similarly*, mir157abc* mutants subjected to cold after four weeks of growth bolted earlier that wild-type plants, although both *mir157abc* treatment and control groups bolted later than *mir157cd* mutants.

The number of rosette leaves of control and treatment groups of wild-type plants was similar, irrespective of the start of treatment (Figure 4.10B). For *mir157cd* mutants, the response to cold treatment differed from that of wild type and was experiment dependent. When cold treatment was performed after two weeks of growth at 21°C in short days, *mir157cd* plants in the treatment group had significantly fewer rosette leaves than those in the control group. A similar trend was observed for the *mir156ac*, but the difference was not significant. However, when treatment occurred after four weeks of growth at 21°C in short days, the number of rosette leaves in control and treatment groups of *mir157cd* did not differ significantly. Strikingly, cold-treated *mir157abc* triple mutants produced significantly more rosette leaves than untreated *mir157abc* mutants. Untreated but not cold-treated *mir157abc* mutants produced fewer leaves than *mir157cd* mutants.

The number of cauline leaves produced by *mir156ac*, *mir157cd* and *mir157abc* mutants was not affected by cold treatments and for *mir157cd* mutants the cauline leaf number was similar across experiments (Figure 4.10C). Although cold treatment after two weeks did not affect the number of cauline leaves in wild-type plants, cold treatment after four weeks caused a reduction from a median of nine cauline leaves in the control group and six in the treatment group.

4.7. Conclusion

Targeted genome editing by CRISPR/Cas9-induced deletions in hairpin sequences of *MIR156* and *MIR157* genes. Quantification through sRNA-sequencing showed that these mutations were effective in reducing mature miR156 and miR157 levels in a family-specific manner. The *MIR156A* and *MIR156C* genes accounted for about half of the total abundance of miR156 in short-day-grown apices. Similarly, the majority of miR157 was derived from *MIR157C,* followed by the combined output of *MIR157A* and *MIR157B*. The miR157 level in *mir157abc* mutants revealed, that *MIR157D* was expressed at a very low levels in apices. This was consistent with *MIR157D::VNG* reporter activity, which was localized to leaf veins in the distal parts of expanding leaves, but was not detected at the SAM or in young leaf primordia from 1wSD to 6wSD.

The phenotypes of *mir156ac*, *mir157cd* and *mir157abc* mutant combinations were analysed in detail. The *mir156ac* mutant expressed a stronger vegetative phenotype than *mir157* mutants in terms of both phyllotaxis and leaf morphology. The flowering time of *mir156ac* was earlier than that of wild type in long days, but similar to that of wild type in short days. By contrast, *mir157* mutations accelerated flowering in short days, but not in long days. These contrasting *mir156* and *mir157* phenotypes were consistent with the different expression dynamics of miR156 and miR157 and correlated with the temporal changes in expression of *AP1*, *FUL* and *SPL4*. The level of *SPL15* transcription was not altered in *mir156* and *mir157* mutants. Nevertheless, SPL15 and FUL proteins rapidly accumulated in short days in meristems of *mir157cd* and *mir157c* mutants, respectively. Early bolting in these genotypes was also associated with accelerated changes in SAM organisation as monitored by *WUS* and *CLV3* reporters.

Apices of plants that were cold treated at 4°C maintained higher expression levels of *MIR156* and *MIR157* genes than plants continuously grown at 21°C., *MIR156A* and *MIR157A* showed the strongest cold response of the *MIR* genes tested. Both genes were expressed in vasculature and surrounding tissues, which might contribute to cold acclimation. Cold treatment also strongly delayed plant growth, both in rosette size and number of leaves produced during treatment. However, the response of *mir156* and *mir157* mutants to cold treatment during vegetative growth did not differ from that of wild-type plants in terms of time to bolting. This suggests that either the elevated

MIR156 and *MIR157* expression levels were insufficient to delay flowering, or that the increases in expression did not occur in the SAM. The second explanation is consistent with the spatial expression pattern observed for *MIR156A* and *MIR156C* reporters. Irrespective of the cold treatment, the number of rosette leaves produced by wild-type plants was similar. By contrast, the cold response of *mir157* mutants differed depending on the plant age at treatment. This suggests a dynamic cold response that might balance short- and long-term cold acclimation with plant age.

After bolting, *mir157cd* and *mir157abc* mutants produced more cauline leaves than wild type, irrespective of photoperiod. The phenotype was also unaffected in *mir157cd* and *mir157abc* mutants subjected to cold treatments during vegetative growth. The higher number of cauline leaves in *mir157cd* and *mir157abc* mutants was similar to the *rSPL15* phenotype. Despite flowering early in long days, the number of cauline leaves produced by *mir156ac* mutants did not differ from that of wild type plants in both long and short days. Notably, the *mir157abc* triple mutant produced fewer cauline leaves than the *mir157cd* double mutant, which suggests that *MIR157D* might also regulate inflorescence development. During vegetative growth, *MIR157D* expression was not detected at the SAM. After floral transition, *MIR157D* expression appeared in a domain at the boundary between cauline leaves and axillary meristems, which expanded in older cauline leaves. Additional expression emerged in boundary regions of stage seven floral primordia. This suggests that the spatial expression pattern might be relevant for cauline leaf specification. Taken together, these observations indicate that *MIR156* and *MIR157* genes are functionally different. *MIR156* genes were more relevant for vegetative phenotypes, whereas *MIR157* genes affected inflorescence development. The *rSPL15* phenotype then represents the combined loss-of-function phenotypes of both gene families.

5. Genetic dissection of flowering behaviour under non-inductive short days

5.1. Introduction

The targets of miR156- and miR157-mediated repression are genes encoding SPL transcription factors, which possess complementary miR156/miR157-binding sites within their transcripts (Gandikota et al., 2007; Preston and Hileman, 2013). Constitutive overexpression of miR156 leads to late flowering, a phenotype that is stronger under non-inductive short days than in long days (Schwab et al., 2005; Wang et al., 2009; Wu and Poethig, 2006). Similarly, transgenic plants carrying a miR156/7-resistant version of *SPL15* (*rSPL15*) express the transcription factor early in development, which leads to earlier bolting in long and short days (Hyun et al., 2016). Mutations in *SPL15* cause a slight delay in flowering under long-day conditions and a marked delay in non-inductive short days (Hyun et al., 2016, 2019). Mutant alleles of *SPL9*, the closest paralogue to *SPL15*, only slightly enhance the *spl15-1* phenotype, suggesting that both genes show some redundancy in regulating floral transition (Hyun et al., 2016).

Both *FUL* and *MIR172B* are direct targets of *SPL15* (Hyun et al., 2016). Recently, *SPL4* was shown in our group to be differentially expressed between *rSPL15* plants and Col-0 in long days and between *spl15-1* and Col-0 in short days (PhD thesis, Annabel van Driel, 2021). A CRISPR/Cas9-induced *spl4* mutation (Hyun et al., 2015) was introduced into *spl15-1* mutants and plants carrying *rSPL15* to study the genetic relationship between *SPL4* and *SPL15* in regulating flowering time.

In long days, the photoperiodic pathway strongly promotes floral transition and five long days are sufficient (Torti et al., 2012). The photoperiodic pathway is not active under short days, but constitutive overexpression of *FT* promotes flowering irrespective of day length (Yamaguchi et al., 2005). To test whether *rSPL15* causes ectopic activation of *FT/TSF* prior to bolting under short days, the *rSPL15* transgene was introduced into the *ft-10 tsf-1* double mutant background.

The genetic basis for early bolting of *mir157* mutants in short days was analysed by combining them with mutants of their target genes *spl15* and *spl4* and also *ful* loss-of-function mutants.

5.2. Genetic characterisation of bolting in *rSPL15*.

A flowering-time experiment tested whether the early bolting of *rSPL15* plants grown in long days was dependent on functional FT/TSF (Figure 5.1). In this experiment, *rSPL15* plants bolted after a median of 24 days, which was three days earlier than Col-0 (Figure 5.1A). The photoperiod-insensitive *ft-10 tsf-1* mutant bolted with a median of 43 days, which was approximately double the time taken for *rSPL15* plants to bolt. Therefore, the effect of rSPL15 on bolting was very mild in plants with an active photoperiodic pathway.

The combination of *ft-10 tsf-1* and *rSPL15* led to a bolting phenotype that was intermediate between that of *rSPL15* and *ft-10 tsf-1*, and *rSPL15 ft-10 tsf-1* plants bolted after 30 days. This delay in bolting of *rSPL15 ft-10 tsf-1* compared with wild type was also associated with an increase in rosette leaf number (Figure 5.1D). Therefore, early bolting caused by *rSPL15* in long days was partially depend on FT/TSF function. However, *rSPL15* can cause early flowering via an FT/TSF-independent mechanism. The effect of *rSPL15* on bolting in the *ft-10 tsf-1* background was much stronger than that on flowering time (Figure 5.1B).

The number of cauline leaves and bracts and the height of the I1 zone of *rSPL15 ft-10 tsf-1* plants were not intermediate between those of the *rSPL15* or *ft-10 tsf-1* genotypes (Figure 5.1C, E and F). Instead, these phenotypes in *rSPL15 ft-10 tsf-1* plants were additive or even synergistic compared with those of *rSPL15* or *ft-10 tsf-1*. The shortest I1 zones were shown by wild type, followed by *rSPL15*, *ft-10 tsf-1* and *rSPL15 ft-10 tsf-1* plants. The differences in height of the I1 zone were statistically significantly different among all genotypes. The differences in I1 height were associated with differences in cauline leaf number, although the effect of *rSPL15* on cauline leaf number relative to wild type was not as great as that on height (Figure 5.1E).

The outgrowth of bracts is not characteristic for wild-type plants and indicates an impairment in floral meristem identity (Chandler, 2012). In this experiment, *rSPL15* plants did not develop visible bracts, whereas *ft-10 tsf-1* occasionally produced one or two flowers with bracts. The combination of *rSPL15* with *ft-10 tsf-1* increased both the number of bracts and the number of plants carrying bracts. Bracts were observed for

half of the phenotyped *rSPL15 ft-10 tsf-1* population. The other half showed complete suppression of bract outgrowth.

Taken together, the data show that the effect of *rSPL15* on bolting and flowering time in long days is partially dependent on FT/TSF functions, but during inflorescence development, *rSPL15 ft-10 tsf-1* plants show FT/TSF-independent functions that also lead to additive or synergistic phenotypes.

After demonstrating that *rSPL15* and *ft-10 tsf-1* interactively influence flowering under long days, a follow-up experiment focused on the functional relationship between *rSPL15* and *ft-10 tsf-1* in regulating flowering time under short days (Figure 5.2). The experiment also included plants carrying the *rSPL15* transgene in the *spl4* loss-of-function mutant background. A previous transcriptome analysis identified *SPL4* as one of the earliest upregulated and strongest differentially expressed genes between wild type and *rSPL15* plants in a long-day time course (PhD thesis, Annabel van Driel, 2021). Therefore, the aim of this experiment was to test whether *rSPL15* promoted floral transition via activating *SPL4*.

The median bolting time of wild-type plants was 60 days, which was not significantly different from that of *ft-10 tsf-1* (Figure 5.2A). Thus, as expected, bolting of wild-type plants in short days did not depend on the photoperiodic pathway. The median bolting time of *rSPL15* plants was 45 days, which represented an earlier floral transition than wild-type plants. However, the time when the first flower opened was the same as that of wild type. Both *rSPL15* plants and wild type flowered significantly earlier than *ft-10 tsf-1,* but *ft-10 tsf-1* plants that also carried the *rSPL15* transgene did not flower later than *ft-10 tsf-1*. Notably, *ft-10 tsf-1 rSPL15* plants bolted at the same time as *rSPL15* plants, but with significantly more rosette leaves (Figure 5.2D). This suggests that the promotion of bolting by rSPL15 in short days is independent of FT/TSF and mechanistically different from that in long days.

The number of cauline leaves was affected by the combination of *ft-10 tsf-1* and *rSPL15*. Although *ft-10 tsf-1* plants did not bolt later than wild type plants under short days, they produced significantly more cauline leaves than Col-0 and a comparable number to *rSPL15* plants (Figure 5.2E). The median number of cauline leaves of *ft-10*

tsf-1 rSPL15 plants was 25*,* which was significantly more than the median number of *ft-10 tsf-1* or *rSPL15* plants.

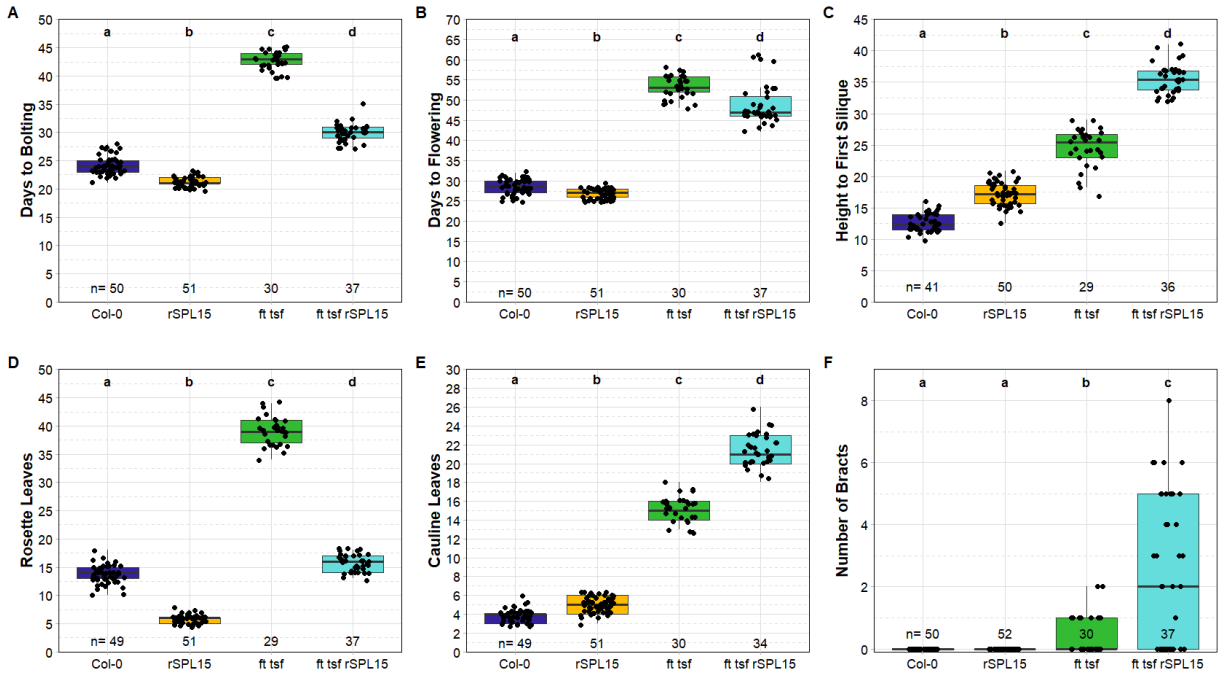

Figure 5.1. *rSPL15* causes early bolting of *ft-10 tsf-1* mutants in long days. A) Days to bolting B) days to first open flower; C) height of the I1 zone measured from the soil surface to the first silique; D, E) number of rosette and cauline leaves, respectively, at flowering. F) Number of bracts that subtended a flower. The sample size (n) is given for each panel. A–E) Significance levels calculated by one-factor ANOVA followed by Tukey's HSD post-hoc comparison. F) Significance levels were calculated by the non-parametric Kruskal-Wallis test followed by Dunn all-pairs post-hoc comparison.

The *spl4* mutant bolted and flowered later than wild type in short days (Figure 5.2A and B) and also produced more rosette leaves, which was proportional to the delay in bolting compared with wild type (Figure 5.2D). The s*pl4* mutant also produced more cauline leaves than wild type (Figure 5.2E). *spl4 rSPL15* plants bolted later than *rSPL15* plants but earlier than *spl4*, and significantly earlier than wild type. The same relationships were observed for rosette leaf number (Figure 5.2D). Notably, the number of days to flower for *spl4 rSPL15* plants was indistinguishable from that of *spl4* and was similar to that for *ft-10 tsf-1* and *ft-10 tsf-1 rSPL15* plants*,* but later than that for wild-type plants. The *spl4* mutation enhanced the cauline leaf phenotype of *rSPL15* and *spl4 rSPL15* plants initiated a median of 22 cauline leaves, but the effect remained weaker than the increase in cauline leaf number of *ft-10 tsf-1 rSPL15.*

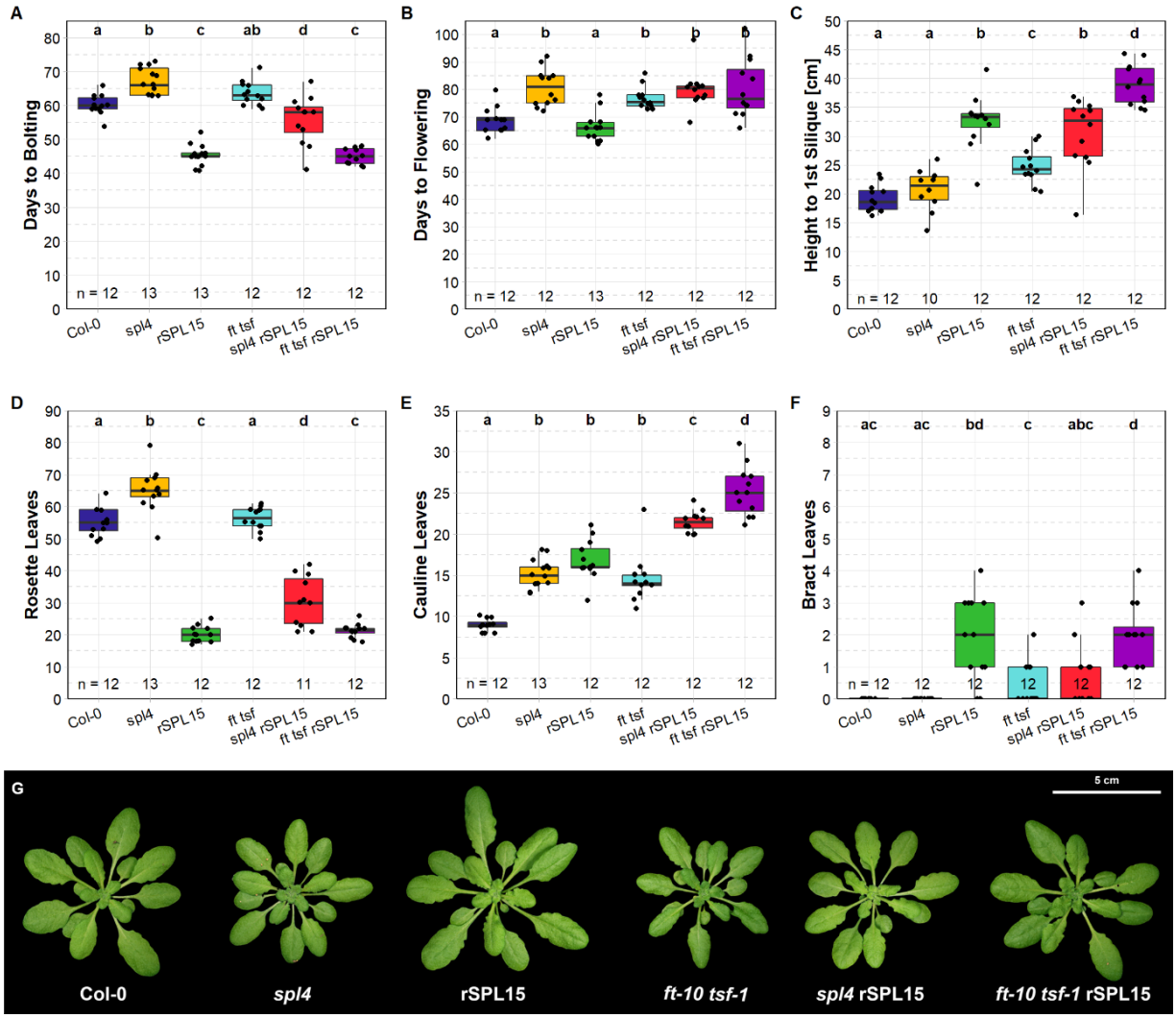

Figure 5.2. Genetic interactions of *rSPL15* with *spl4* and *ft-10 tsf-1* in short days. A) Days to bolting; B) days to first open flower; C) height of the I1 zone measured from the soil surface to the first silique; D, E) number of rosette and cauline leaves, respectively, at flowering; F) number of flowers subtended by bracts; G) rosette phenotypes after 4 weeks in short days. The sample size (n) is given for each plot. A–E) The significance levels were calculated by one-factor ANOVA followed by Tukey's HSD post-hoc comparison. The significance levels in F) were calculated by the non-parametric Kruskal-Wallis test followed by Dunn all-pairs post-hoc comparison, with $p < 0.05$.

The influence of genotypes on bract formation in short days was not consistent with results from the long-day experiment (Figure 5.2F). No bracts developed on wild type and *spl4* plants. The *rSPL15* and *ft-10 tsf-1 rSPL15* plants developed bracts, but these only developed on one-quarter of the *ft-10 tsf-1* population. The combination of *spl4* with *rSPL15* led to fewer bracts than for *rSPL15* plants.

5.3. Genetic interactions between *mir157c* and target genes encoding transcription factors

Following the demonstration that *SPL4* contributes to the early bolting of *rSPL15* plants, the focus shifted to whether this was also the case in plants with reduced levels of miR157, which should lead to the derepression of several *SPL* target genes, including *SPL4* and *SPL15*. To study bolting under these conditions, *mir157c spl4* and *mir157c spl15-1* mutant combinations were generated. The genotypes were then analysed in short days in a flowering-time experiment that also included the *spl4 spl15-1* and *mir157cd* double mutants (Figure 5.3).

Consistent with the results of the previous experiment, the *spl4* mutant bolted and flowered later than wild type. The *spl15-1* mutant caused delayed bolting and flowering compared with wild type and *spl4*, but the strongest delay in bolting and flowering was observed for plants carrying both *spl4* and *spl15-1* mutations. In several cases, secondary inflorescences grew out from the rosette whilst the shoot apex continued to grow vegetatively (this was observed qualitatively and was not quantified). By the end of the experiment, three *spl4 spl15-1* plants had only produced leaves. A considerable amount of variation in days to bolting was shown by the late-flowering *spl15-1* and *spl4 spl15-1* genotypes.

The majority of *spl15-1* and all of the *spl4 spl15-1* mutants initiated flowering from secondary inflorescences from the rosette leaf axils (Figure 5.3B). Therefore, open flowers on side shoots were also scored when flowering time was quantified. The onset of anthesis in *spl4 spl15-1* was not significantly different from that in *spl15-1*. A subset of *spl4 spl15-1* plants flowered as early as *spl4* mutants. Given the strong phenotypes observed on the main shoot, *SPL4* and *SPL15* might differentially regulate flowering from primary and secondary inflorescences.

The *mir157c* single mutant bolted and flowered at the same time as *mir157cd.* The small differences in the flowering-time of these genotypes compared with that of wild-type plants were not statistically significant. The *spl4* mutation was unable to delay *mir157c* plants in terms of bolting and flowering. However, *mir157c spl4* produced significantly more cauline leaves than *mir157c* and a similar number to that of *spl4*

(Figure 5.3B). *mir157c* single mutants produced a similar number of cauline leaves as wild-type plants, but fewer than *mir157cd* mutants.

Because *spl15-1* and *spl4 spl15-1* plants prematurely produced secondary inflorescences from the rosettes, the number of rosette leaves could not be accurately determined (Figure 5.3C). The late-flowering *spl4* mutant initiated significantly more leaves than Col-0, *mir157c* and *mir157cd.* The number of rosette leaves of *mir157c spl4* showed large variation, but was significantly lower than that of *spl4* single mutants.

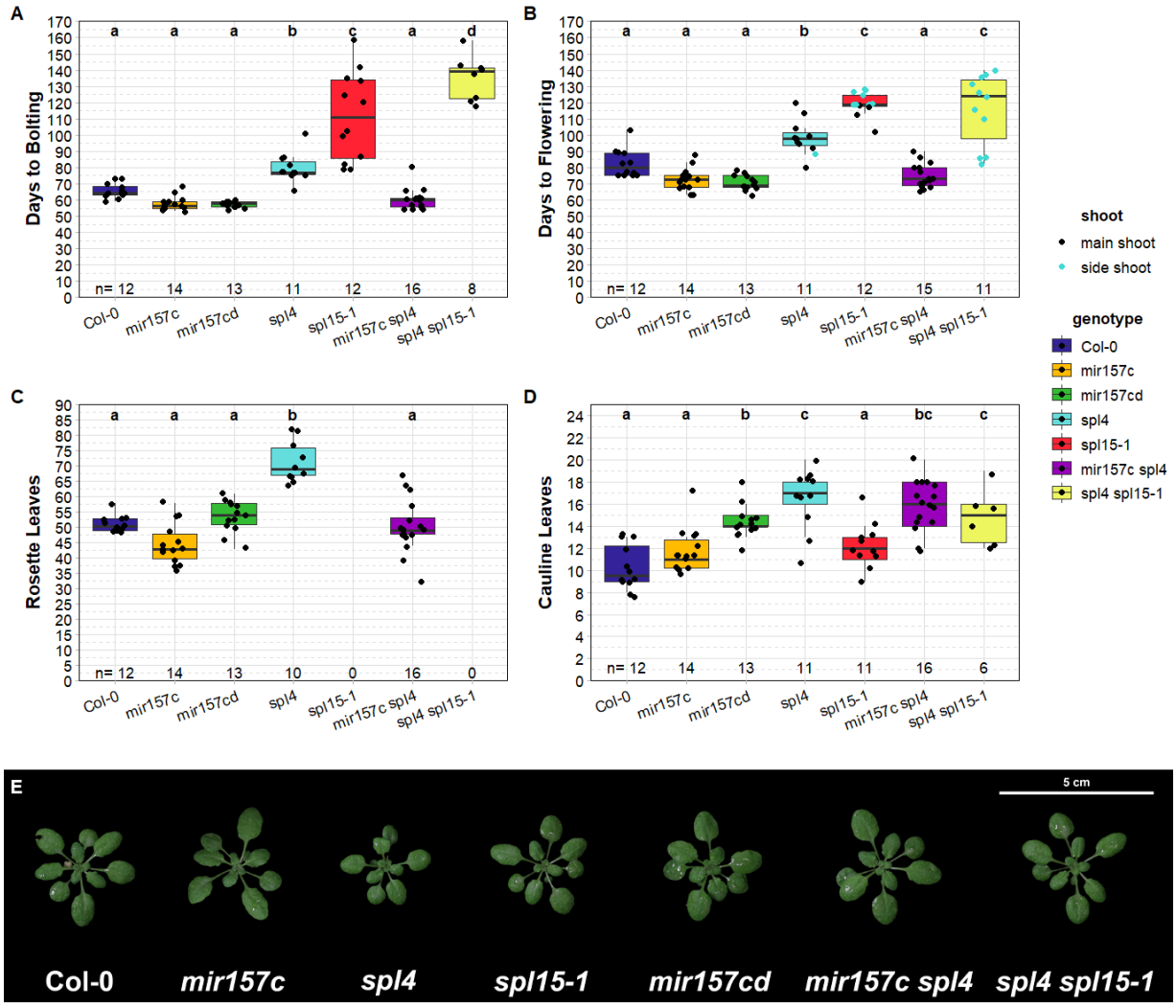

Figure 5.3. Experiment to study the genetic interactions between *spl4* and *spl15-1* mutants in regulating flowering time in short days. Flowering time was scored as: A) The number of days to bolting; B) the number of days to flowering. Turquoise points mark plants that initiated flowering from side shoots; C) the number of rosette leaves; D) the number of cauline leaves; E) rosette phenotypes after 4 weeks in short days. The scale bar represents 5 cm. A to D) Letters correspond to significance groups as determined by one-way ANOVA combined with a post-hoc Tukey's HSD test, $p<0.05$.

In summary, the absence of *SPL4* function during the early stages of floral transition had a greater effect in *rSPL15* plants than in the *mir157c* genetic background. *spl4* was epistatic to *mir157c* in the regulation of cauline leaf number*,* whereas *spl4* and *rSPL15* had an additive effect on cauline leaf number. The *spl4* mutant further enhanced the extremely late bolting of the *spl15-1* main shoot, which led to the outgrowth of secondary inflorescences from the rosette before bolting of the primary shoot.

Following the observation that loss of *SPL4* function during the early stages of floral transition had a greater effect in combination with *rSPL15* than with *mir157c,* the importance of SPL15 for early bolting in *mir157c* mutants was assessed. In a large flowering-time experiment in short-days, *mir157c spl4* and *mir157c spl15-1* mutants were grown alongside *spl4 rSPL15, mir156ac, mir157cd* and appropriate controls (Figure 5.4). The experiment included *mir157d* to investigate phenotypic differences between *mir157c* and *mir157cd*, that were apparent in five-week-old rosettes (Figure 5.4A). Rosettes of *mir157c* mutants were less dense than those of *mir157d* and *mir157cd* mutants. Petioles on rosette leaves of *mir157c* and *mir157cd* appeared thin and elongated. This phenotype was also observed in *mir157c spl4* and *mir157c spl15-1* mutants. By contrast, rosette leaves of *mir157d* mutants were more similar to that of wild type. The phenotypes of *spl4* and *spl15-1* rosettes were also wild-type like, but leaves of *spl4 rSPL15* plants grew more densely than in *rSPL15* plants. Cauline leaves of *mir157c*, *mir157d* and *mir157cd* mutants appeared more serrated than those of wild type and this phenotype was further enhanced in the *mir157c spl4* double mutant (Figure 5.4B). Cauline leaves of *rSPL15* plants were also more serrated, but the *spl4* mutant did not appear to enhance this phenotype further.

Consistent with results from the previous experiment, bolting of *spl4* and *spl4 rSPL15* plants was delayed (Figure 5.5A). Again, *spl4* had no significant effect on the bolting time of *mir157c.* Although the bolting time of *mir157cd* was statistically significantly different from that of wild type plants, the bolting time of *mir157c* and *mir157d* single mutants was similar to that of wild-type and *mir157cd* plants. The *mir156ac* mutant bolted at a similar time to wild type and *mir157d*, but later than *mir157c* and *mir157cd.* Therefore, the *mir157c* mutation affected bolting time, but the combination of *mir157c* with *mir157d* reduced the variation in the early-bolting phenotype.

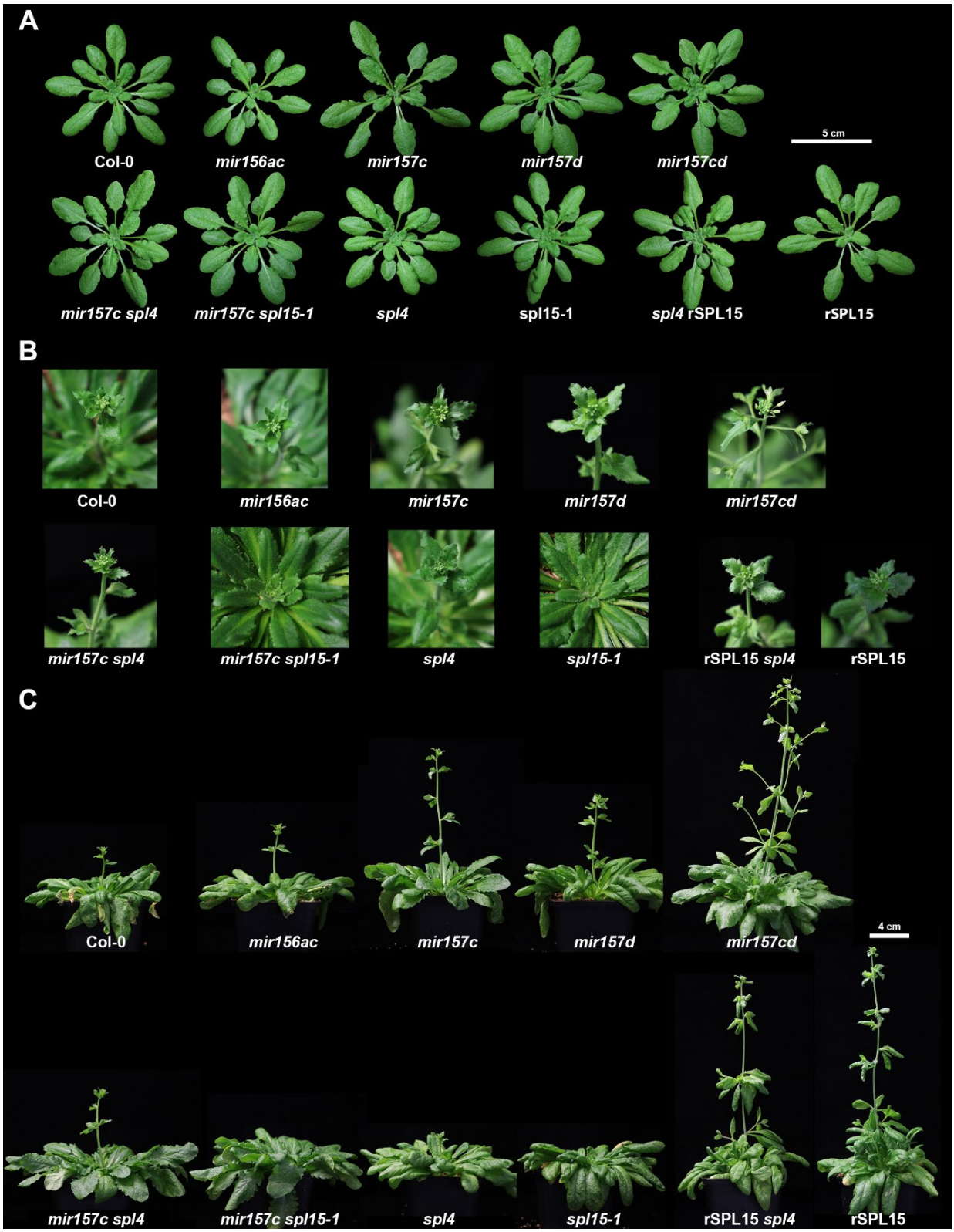

Figure 5.4. Representative images of mutant genotypes in short days. A) Rosette phenotype of wild-type and mutant plants after five weeks in short days. B, C) Representative appearance of

genotypes after nine weeks of growth in short days. b) Close-up view of plant apices shown in B, not to scale. C) Rosettes and inflorescence shoots after growth for 9 weeks in short days, to scale.

The *spl15-1* mutation greatly delayed bolting time (Figure 5.5A): *spl15-1* plants started to bolt after 80 days, which was 30 days later than the earliest wild-type plants. The bolting time phenotype of *mir157c spl15-1* double mutant plants was intermediate between that of *mir157c* and *spl15-1* and was significantly later than that of *spl4* mutants.

In this experiment, the number of days to flowering of only a few genotypes significantly differed from that of wild type (Figure 5.5B). Among these genotypes, *mir157c*, *mir157cd* and *mir157c spl4* started to flower significantly earlier than *mir156ac*. The *spl4* mutant flowered significantly later than wild type, but *mir157c spl4* double mutants flowered at the same time as wild-type and *mir157c* plants. The increased activity of other SPL genes might mask the effect of *spl4* loss of function in the *mir157c* mutant background. By contrast, loss of *SPL15* function in combination with *mir157c* notably delayed bolting and flowering time: The flowering time of *mir157c spl15-1* was similar to that of *spl4,* and was later than that of both *mir157c* and wild type.

An unexpected difference in the number of rosette leaves was observed between *mir157c* and *mir157d* single mutants (Figure 5.5C). Similar to in previous experiments, the *mir157cd* double mutant initiated a similar number of rosette leaves as wild type. The expectation therefore, was that the number of rosette leaves was not significantly affected in either single mutant. In the short-day experiment described above, the slightly lower number of rosette leaves of *mir157c* mutants was not statistically significant, in part to a high degree of variation (Figure 5.3C). In this experiment, a significant reduction in the number of leaves of *mir157c* compared with that of both wild type and *mir157cd* was observed (Figure 5.5C). Notably, the *mir157d* single mutant produced significantly more rosette leaves than *mir157cd*. Hence, the number of rosette leaves of *mir157cd* was intermediate between that of the single mutants from which it was derived. The median and range of rosette leaf number of *mir156ac* and wild type were.

The *spl15-1* plants produced the most rosette leaves, and significantly more than all other genotypes. By contrast, *rSPL15* plants produced the fewest rosette leaves. Combination of *spl4* with *rSPL15* led to an increase in leaf number, but the leaf number

of the *mir157c spl4* double mutant did not differ significantly from that of *mir157c*, which was similar to the relationship in bolting time between these genotypes. The leaf number of *mir157c spl15-1* was intermediate between that of *mir157c* and *spl15-1.*

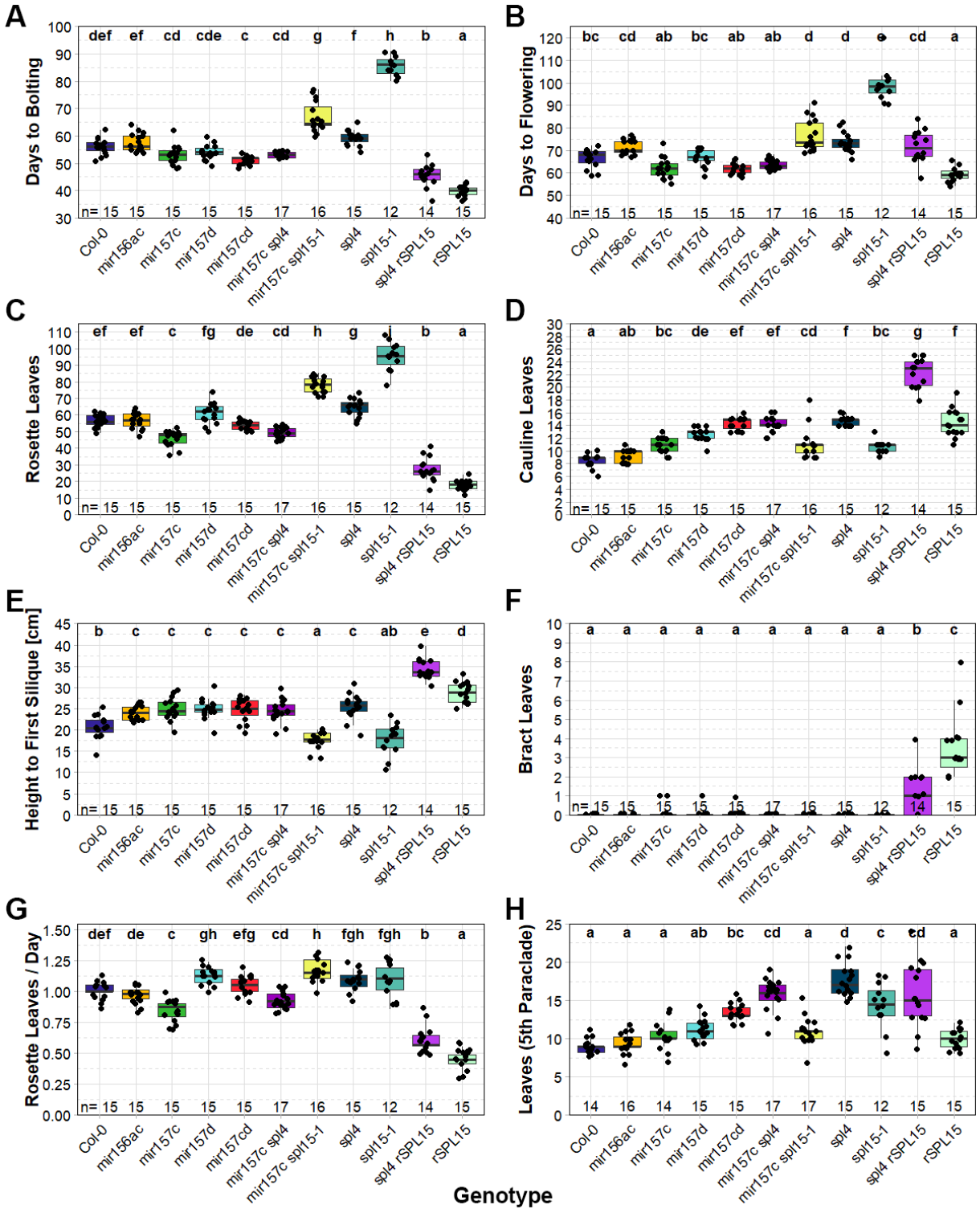

Figure 5.5. Flowering-time of *mir157* mutants and combinations between *mir157c* and *spl4, spl15-1* mutants or *rSPL15* plants grown in short days. A) Days to bolting; B) number of days to first

open flower; C) number of rosette leaves produced; D) number of cauline leaves produced by the inflorescence; E) height of the inflorescence I1 zone; F) number of bracts that subtended a flower. Bracts were present in genotypes carrying the *rSPL15* transgene; G) leaf initiation rate estimated by the number of rosette leaves divided by days to bolting; H) number of leaves formed by the fifth paraclade. The *spl4* mutation significantly reduced the number of bracts. Bracts were largely absent in other genotypes. Letters correspond to significance groups as determined by one-way ANOVA combined with a post-hoc Tukey's HSD test, $p < 0.05$.

In the previous chapter, *mir157cd* produced more cauline leaves than wild type in long-day and short-day conditions. In this experiment, *mir157cd* mutants produced a median of 15 cauline leaves, which was 6 more than the median of 9 cauline leaves produced by wild-type plants (Figure 5.5D). The cauline leaf numbers of *mir157c* and *mir157d* were also significantly different from wild type, and had a median of 11 and 13, respectively. Thus, the supernumerary cauline leaves of *mir157cd* resulted from additive effects of *mir157c* and *mir157d* phenotypes.

The median number of cauline leaves of *spl4* was 15, which was significantly greater than that of wild type or *spl15-1*, but similar to that of *mir157cd*. It was also similar to the number of cauline leaves of *mir157c spl4*, suggesting that the *spl4* mutation was epistatic to *mir157c* in determining this phenotype. Similarly, the combination of *mir157c* with *spl15-1* did not result in additive phenotypes apart from two outliers.

In addition to counting the number of cauline leaves at the main shoot, the number of leaves was also recorded on the fifth paraclade (Figure 5.5H). The relationship among *mir156* and *mir157* mutants for this phenotype was largely similar to that for the number of cauline leaves. For example, the *mir157cd* double mutant had more paraclade leaves than either parental line. Combination of *spl4* with *rSPL15* also enhanced this phenotype of *rSPL15* plants.

In contrast to the number of cauline leaves, paraclades of spl4 mutants formed significantly more leaves than those of *mir157cd* mutants. Moreover, paraclades of *spl15-1* mutants had significantly more leaves than paraclades of *mir157c* mutants. Strikingly, paraclades of *mir157c spl15-1* mutants carried significantly fewer leaves than those of *spl15-1* and were more similar to those of *mir157c* mutants. Therefore, the epistasis between *mir157c* and *spl15-1* in paraclade leaf initiation was the opposite to that between *mir157c* and *spl4.*

Inflorescence height, measured as the height to the first silique, was greater in all *mir156* and *mir157* single or double mutants than that of wild-type plants (Figure 5.5E). Late-flowering *spl15-1* mutants had a similar I1 zone height to wild-type plants and the phenotype was also epistatic to that of *mir157c* mutants. Although *spl4* had a significantly elongated inflorescence and led to an increase in the height of *rSPL15* plants, the height of *mir157c spl4* plants did not differ from that of *mir157c* or *spl4.*

The mutants analysed in this experiment developed few bracts and the *rSPL15* genotype was the only genotype for which all plants produced bracts. The combination of *spl4* and *rSPL15* significantly reduced the number of visible bracts.

The number of rosette leaves correlates with the timing of the floral transition, after which plants produce flowers. The time interval between the initiation of two successive primordia is known as the plastochron and represents the inverse of the rate of leaf initiation (McMaster, 2005; Meicenheimer, 2014). The plastochron is negatively regulated by *SPL15* (Hyun et al., 2016; Schwarz et al., 2008; Wang et al., 2008). To analyse differences in leaf initiation rate among genotypes, the mean leaf initiation rate was estimated by normalising the number of rosette leaves by bolting time (Figure 5.5G). According to this parameter, wild-type plants produced approximately one leaf per day before bolting, which was a similar rate to that of *mir156ac* and *spl4* mutants. The slowest leaf initiation rate was shown by *rSPL15* plants, which on average initiated one rosette leaf approximately every two days. Although *spl4* did not significantly affect the number of leaves produced, it significantly accelerated the rate of leaf production of *rSPL15* plants. It also slightly accelerated the rate of leaf production of the *mir157c* single mutant, which initiated leaves slower than wild type. The rate of leaf production of *mir157c spl4* was similar to that of *mir157c* and wild-type plants.

In contrast to the rate of leaf production of *mir157c*, that of *mir157d* was faster than that of wild type and the leaf initiation rate of *mir157cd* was intermediate between that of *mir157c* and *mir157d*. The leaf initiation rate of *spl15-1* varied considerably and therefore did not significantly differ from that of wild type. Notably, the leaf initiation rate of *mir157c spl15-1* plants was very similar to that of *spl15-1* and significantly more rapid than that of *mir157c*.

5.4. Genetic interaction between *mir157* mutants and *ful-2* in inflorescence development

The AGAMOUS-like transcription factor FUL promotes flowering in parallel with miR172 and both regulators remove the inhibitory effect of AP2-like repressor proteins on flowering (Balanzà et al., 2018; Ó'Maoiléidigh et al., 2021). The functions of several miR156-targeted *SPL* genes converges on *FUL*. Direct binding to the *FUL* promoter has been reported for SPL15 (Hyun et al., 2016), SPL3, SPL4 and SPL5 (Wang et al., 2009; Xie et al., 2020a; Yamaguchi et al., 2009). Therefore, *FUL* represents a convergence point in the age-pathway of flowering and also inflorescence development (Ferrandiz et al., 2000; Jiang et al., 2022).

The *ful-2* mutant was combined with *mir157c*, *mir157d* and *mir157cd* to analyse their genetic interactions in regulating flowering time and inflorescence phenotypes (Figure 5.6). In short-day conditions, the *ful-2* single mutant was later bolting and later flowering than wild-type plants. The median bolting time of *mir157c* and *mir157cd* mutants (54.5 and 55 days) was lower than that of wild type plants (59 days, Figure 5.6A), which was consistent with the findings of previous experiments. However, the difference was not statistically significant, probably due to the inclusion of extremely late-bolting *ful-2* mutants (a median of 69.5 days to bolting). Bolting time of *mir157d* was 57 days, which was more similar to that of wild type than that of *mir157c* and *mir157cd*. The relationships among these genotypes were similar for flowering time.

All combinations of *mir157c*, *mir157d* and *mir157cd* with *ful-2* bolted and flowered at a similar time to *ful-2* single mutants. Therefore, the function of *FUL* in promoting bolting could not be compensated through higher *SPL* activity in *mir157* mutants.

The *mir157d* mutant produced significantly more rosette leaves than wild type, *mir157c* and *mir157cd*, which was consistent with the observations of the previous experiment (Figure 5.6C). The number of rosette leaves in late-flowering mutants showed a high amount of variation, but normalisation of the number of rosette leaves against days to bolting to approximate the leaf initiation rate reduced this variation (Figure 5.6E). The estimated leaf initiation rate of *ful-2* was not significantly different from that of Col-0, but had a lower median. Introduction of the *ful-2* mutation into *mir157* mutant backgrounds led to varied results. The number of rosette leaves initiated per day by

mir157c ful-2 mutants was significantly fewer than that of *mir157c* and wild type but was not statistically different from that of *ful-2.* Similarly, the *mir157d ful-2* double mutant initiated leaves more slowly than the *mir157d* single mutant. By contrast, the leaf initiation rate of *mir157cd ful-2* was comparable to that of *mir157cd* mutants and wild type plants. Both *mir157d ful-2* and *mir157cd ful-2* initiated leaves significantly faster than *ful-2*.

All three *mir157* mutants analysed produced more cauline leaves than wild type plants . Combination of *mir157c* and *mir157d* resulted in an additive phenotype (Figure 5.6D). The *ful-2* mutant produced significantly more cauline leaves than *mir157* mutants. The cauline leaf number of *mir157* and *ful-2* mutants was additive compared with the number of cauline leaves of each single mutant. The greatest number of cauline leaves was shown by *mir157cd ful-2* mutants, which had a median of 34 cauline leaves.

The number of cauline leaves was partially correlated with the height of the I1 zone (Figure 5.6D). The height of the I1 zone was greatest for *mir157cd ful-2,* followed by *mir157c ful-2* and *mir157d ful-2*, which had similar values to each other. Except for *mir157c* and *ful-2* single mutants, most genotypes had significantly taller inflorescences than wild type.

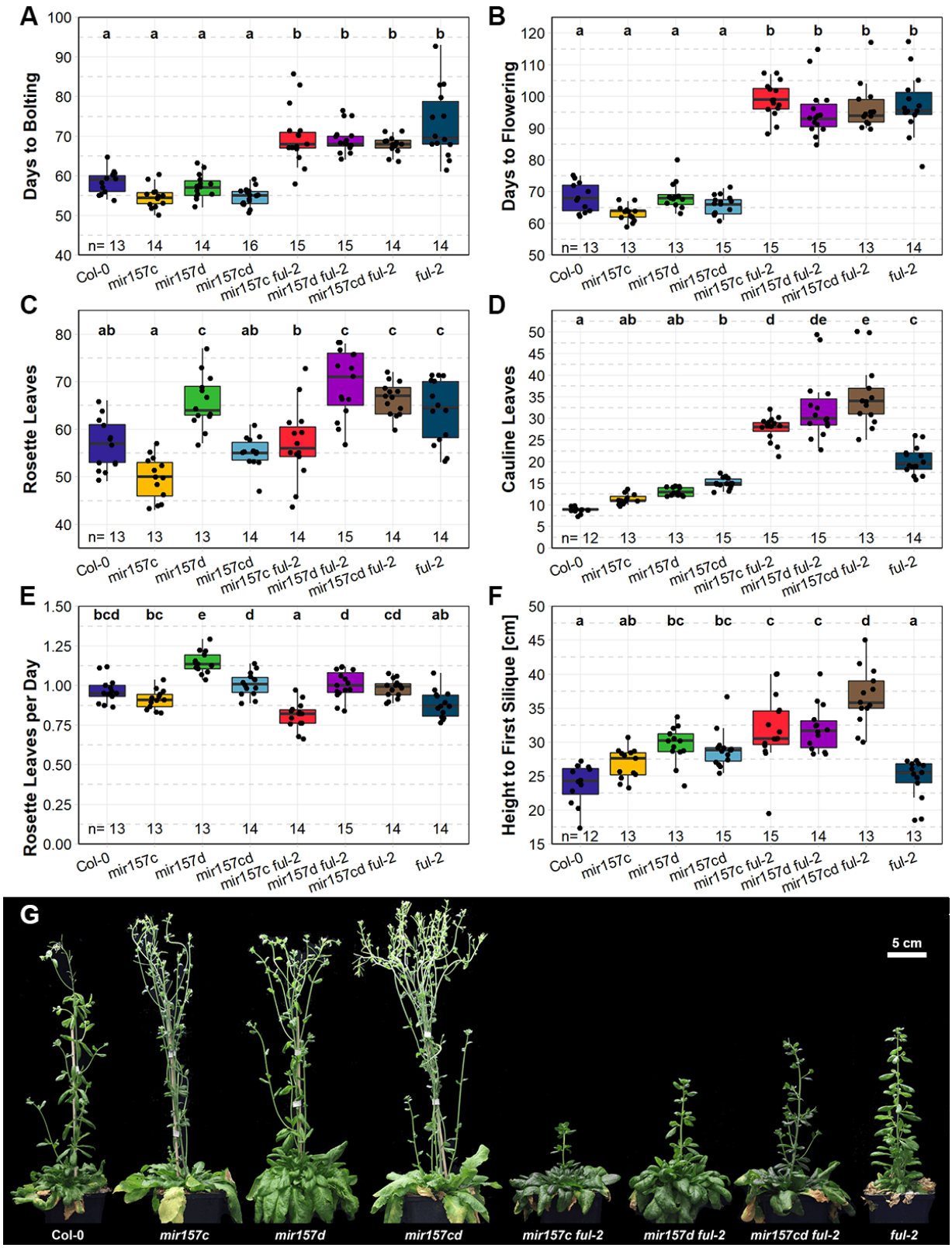

Figure 5.6. Flowering time of different *mir157* genotypes to analyse the genetic relationship among them and the *FRUITFULL* loss-of-function (*ful-2*) mutant. Flowering time is shown as A) the number of days to bolting and B) the number of days to flowering; C) number of rosette leaves and D) number of cauline leaves produced; E) leaf initiation rate estimated by dividing the number of rosette leaves by the number of days to bolting. F) Inflorescence height measured as the height to the first silique. G) Plant phenotypes after growth in short days for 12 weeks. Significant differences were

determined by ANOVA analysis with genotype and time point as factors, followed by Tukey's HSD pairwise comparisons. Different letters indicate statistically significant differences among genotypes at $p < 0.05$.

5.5. Conclusions

Collectively, these results indicate that bolting of *rSPL15* in long days was partially dependent on *FT/TSF* function, but *rSPL15* plants bolted independently of *FT/TSF* in short-days. In both inductive and non-inductive conditions, functional *FT/TSF* was required for the timely flower development and inflorescence phenotypes of *rSPL15* plants, and *rSPL15* and *ft-10 tsf-1* interacted with each other, for example in determining the number of cauline leaves. A genetic interaction between *ft-10 tsf-1* and *rSPL15* in bract outgrowth was observed exclusively under long days. The exceptionally early bolting of *rSPL15* plants was significantly delayed by combining *rSPL15* with *spl4,* suggesting that *SPL4* is a major downstream component in regulating bolting. Consistent with this, *spl4 spl15-1* double mutants flowered extremely late.

The *mir157c* single mutant bolted earlier than wild type. The bolting time of *mir157d* single mutants was not significantly different from that of wild type, but combination of *mir157d* with *mir157c* reduced the variation in the bolting phenotype of *mir157c*. In contrast to when *spl4* was combined with *rSPL15*, the *spl4* mutation did not delay bolting of *mir157c* mutants, which might be due to redundant functions between *SPL4* and *SPL3* or *SPL5.* The *spl15-1* mutation delayed bolting of *mir157c,* but *mir157c spl15-1* double mutants bolted earlier than the *spl15-1* single mutant, which highlights the importance of the activities of other SPL transcription factors in determining bolting time.

The *mir157cd* double mutant produced significantly more cauline leaves than both *mir157c* and *mir157d* single mutants and wild type. The number of cauline leaves of *mir157cd* was additive compared with the number produced by *mir157c* and *mir157d*. Strikingly, the increased cauline leaf number phenotype was stronger in *mir157d* compared with *mir157c*, which contrasted with their flowering-time phenotypes.

The increased number of cauline leaves shown by *mir157c* and *mir157d* is similar to the *rSPL15* phenotype. The number of cauline leaves in the I1 zone of *rSPL15* plants was enhanced when *rSPL15* was combined with *spl4* or *ft-10 tsf-1* mutants. The combination of *rSPL15* and *ft-10 tsf-1* also strongly increased the number of bracts in the I2 zone by comparison with wild-type plants and *mir157* mutants, which developed bracts only occasionally.

The number of cauline leaves of *mir157* mutants and *ful-2* mutants was additive when the mutants were combined. However, combinations of *spl4* or *spl15-1* with *mir157c* did not increase the number of cauline leaves and the resulting double mutant phenotype was similar to that of *spl4* or both *spl15-1* and *mir157c* single mutants. Although the number of leaves on paraclades of *mir157c spl4* was similar to that of *spl4*, the phenotype of *mir157c spl15-1* was more comparable to that of *mir157c* than to that of *spl15-1*. On the basis of the findings in this chapter, *SPL4* and *SPL15* have differing roles in inflorescence development.

The *rSPL15* plants had a drastically reduced rate of leaf initiation and produced on average less than one leaf every two days. Consistently in different experiments, *mir157c* and *mir157d* expressed contrasting phenotypes in terms of rosette leaf number and initiation rate. This finding was supported by the phenotype of *mir157cd* double mutants, which was intermediate to that of *mir157c* and *mir157d*. This suggests that the plastochron in not only regulated by the strength of miR157 expression, but also by its spatial pattern, which was previously suggested in *MIR156* overexpression studies (Wang et al., 2008).

6. Discussion

6.1. Differences in miR156 and miR157 expression dynamics in apices correlate with flowering-time phenotypes of *mir156* and *mir157* mutants

The abundance of miR156 and miR157 was directly quantified by sRNA sequencing in apices of plants grown in long or short days for different lengths of time. In general, miR156/miR157 levels decreased more rapidly in long days than in short days, but the analysis revealed differences in the dynamics of the decline in miR156 and miR157 levels. In both growth conditions, the decrease in the level of miR156 was more extreme than that of miR157. This resulted in changes in the relative abundance of miR156 and miR157 over time. The level of miR156 was higher than that of miR157 in young apices, but, as miR156 decreased rapidly, miR157 became the more abundant form in older apices and inflorescences. At the time plants grown in long days transitioned to flowering, the levels of miR156 and miR157 were similar. However, in short days, plants are older when they undergo floral transition. Here, the change in the relative abundance of both miRNAs occurred during vegetative growth, so that miR157 was more abundant than miR156 in apices that transitioned to flowering.

The expression dynamics of miR156 and miR157 during development was reflected in the phenotypes of *mir156* and *mir157* mutants and is therefore likely to be functionally relevant. The morphology of cotyledons and the first true leaves, as well as the robustness of phyllotaxis during vegetative growth was strongly affected in the *mir156ac* mutatant. This is consistent with miR156 functioning as a master regulator of vegetative phase change when it is highly expressed early in plant development (He et al., 2018; Wu et al., 2009). By contrast, the cotyledons and young leaves of *mir157* mutants were similar in shape to those of wild-type plants, consistent with miR157 being relatively lowly expressed at these stages. Strikingly, *mir156ac* but not *mir157cd* mutants were early flowering in long days, again consistent with the higher level of expression of miR156 at this stage. These observations are consistent with miR156 being functionally more important in young plants, in which its level is highest.

Flowering in long days is rapidly induced by the photoperiodic pathway (Abe et al., 2005; Corbesier et al., 2007; Jaeger and Wigge, 2007) and after five consecutive long days, Arabidopsis shoots are fully committed to flowering (Torti et al., 2012). According

to the sRNA-sequencing time course, the abundance of miR156 was significantly higher than that of miR157 when plants undergo floral induction under long days. Under these conditions, the miR156–SPL pathway acts downstream of FT/TSF, the main effectors of the photoperiodic pathway, and the expression of *SPL3, SPL4* and *SPL5* is directly activated by FD/FT (Jung et al., 2016) during floral induction. Therefore, a reduction in miR156 or miR157 expression is likely to occur early in development to allow high *SPL* gene expression during the early flowering response that occurs under long days. Conversely, the high abundance of miR156 in very young plants prevents early flowering and is sufficient to prevent flowering even in *mir157* mutants.

The photoperiodic pathway does not contribute to the induction of flowering in short days, which occurs later than in long days. The significant reduction in the level of miR156 in apices of *mir156ac* mutants compared with wild-type apices was strongest after one week in short days. However, this had no measurable effect on flowering time. Thus, the early-flowering *mir156ac* phenotype is dependent on FT/TSF. The reduction in miR156 levels in the mutants was not sufficient to accelerate flowering in short days, probably because of the absence of a floral induction signal that activates downstream gene transcription.

Gibberellin is absolutely required for flowering in short days (Wilson et al., 1992) and levels of bioactive gibberellins rapidly increase before floral transition but after the steep decline in miR156 levels in short-day grown plants (Eriksson et al., 2006). Therefore, miR156 mutants might not be early flowering because the reduction in miR156 levels occurs before the inductive GA signal is expressed. Elevated gibberellin levels induce the degradation of DELLA proteins to enable downstream signalling (Galvão et al., 2012). The gibberellin and miR156/miR157 signalling pathways converge at SPL and SOC1 function. DELLA proteins physically interact with SPL9 and SPL15 proteins and inhibit the transactivation of target genes (Galvão et al., 2012; Hyun et al., 2016; Yu et al., 2012). Plants that express gibberellin-insensitive DELLA proteins at the meristem show late bolting and a significant reduction in the levels of *SPL3, SPL4* and *SPL5* in apices compared with wild type (Andrés et al., 2014; Galvão et al., 2012). Additionally, the *spl15* mutant shows a reduced sensitivity to the exogenous application of gibberellins (Hyun et al., 2016).

In contrast to *mir156ac* mutants, several *mir157* mutants were early flowering in short days. The abundance of miR157 in short days therefore appears to be more relevant for flowering than that of miR156, which is consistent with higher relative levels of miR157 when flowering occurs under short days. The spatial domains of *MIR156* and *MIR157* gene expression might also be relevant. The spatial expression patterns of *MIR156A* and *MIR156C* were similar in long and short days. Initially, *MIR156C* was expressed at the SAM, but during the experiment, expression disappeared from the central zone of the SAM and then gradually from the rest of the apex. Recently, it was suggested that the rate of cell division is instructive in repressing *MIR156* gene expression (Cheng et al., 2021). The spatial expression of *MIR156A* was similar to that of *MIR156C* except that *MIR156A* was immediately absent from the central zone. Therefore, local miR156 abundance within the central zone of wild-type apices might be lower than that in surrounding tissues. This might reduce the impact on flowering, which is induced at the SAM (Hyun et al., 2016).

Unexpectedly, the spatial expression and apparent level of expression of the *MIR156B* reporter remained stable in the L1 throughout the time course and until after floral transition. Consistent with this, chromatin at the *MIR156B* locus appears to be accessible throughout the Arabidopsis lifecycle (Gao et al., 2022). By contrast, chromatin at the dynamically regulated *MIR156A* and *MIR156C* loci becomes less accessible in tissues of older plants (Gao et al., 2022; Hu et al., 2022). This constant expression suggests that *MIR156B* might fulfil an alternative role to dynamically regulating *SPL* expression, and that SPL expression in the L1 does not contribute to floral transition. It is unclear whether the mature miR156 can move from the L1 into deeper layers.

The spatio-temporal expression patterns of *MIR157A* and *MIR157D* were characterised in this thesis. Although the intensity of *MIR157A* expression decreased at the SAM, its spatial expression pattern remained constant. Within the SAM, *MIR157A* expression was present in cell clusters below newly formed leaf primordia. These cells might contribute to pre-patterning the formation of vascular tissues. Consistent with this, *MIR157A* expression also localised to basal regions of older leaves that surrounded leaf veins. By contrast, *MIR157D* was not expressed at the SAM during vegetative growth. Instead, it was expressed in distal leaf veins of

expanding leaves, without an apparent change in expression intensity over time. Notably, *MIR157D* was expressed during floral transition in cells at the boundary between axillary meristems and cauline leaves. The expression pattern of *MIR157C* was not characterised, but would be of interest, particularly that at the SAM, because *MIR157C* was both the most abundantly expressed *MIR157* gene and the *mir157c* mutation showed the strongest effect on flowering time of all *mir157* mutations.

The different expression dynamics of miR156 and miR157 probably largely derive from differences in transcriptional regulation. However, the terminally branched hairpin structure of miR157c (Moro et al., 2018; Zhu et al., 2013) might also contribute to its temporal expression pattern, because it might reduce the efficiency of miRNA biogenesis and buffer changes in expression over time, thus temporally extending the availability of miR157c. The sRNA-sequencing experiment made use of the TraPR method, which enriches for sRNAs that are loaded into AGO complexes. The method thus enriches for the active portion of the sRNA pool. However, miRNAs that are not bound by AGP are also present in the cytosol (Dalmadi et al., 2019).

Recently, several small RNAs have been shown to be mobile signals that regulate plant development (Carlsbecker et al., 2010; Chitwood et al., 2009; Miyashima et al., 2011). One example is miR394, which is expressed in the protoderm and represses its target gene *LEAF CURLING RESPONSIVENESS* at the distal meristem (Knauer et al., 2013). However, evidence suggests that microRNA mobility and directionality is developmentally regulated and confined within functional domains (Skopelitis et al., 2018).

It has been proposed that sRNAs and miRNAs undergo intercellular and long-distance movement (Brosnan and Voinnet, 2011; Skopelitis et al., 2018). Many miRNAs, including miR156, are present in the phloem sap of apple (*Malus domestica*, Varkonyi-Gasic et al., 2010) and pumpkin (*Curcubita maximus*, Yoo et al., 2005). Moreover, miR156 and miR157 were also detected in phloem sap extracted from *Brassica napus* (Buhtz et al., 2008). In Arabidopsis, intercellular and vascular movement of miRNAs might involve HASTY, a plant orthologue of the animal EXPORTIN5 that is also involved in miRNA biogenesis (Brioudes et al., 2021; Cambiagno et al., 2021). Thus, mature miR156 and miR157 molecules might accumulate and function outside of the expression domains reported by *MIR156* and *MIR157* promoter fusion constructs. This

might be particularly relevant for genes that are expressed in proximity to vascular tissue, such as *MIR157A* and *MIR157D*. Additionally, miRNA movement appears to be spatially and developmentally regulated at the SAM (Skopelitis et al., 2018).

6.2. Regulation of inflorescence architecture by miR157

Floral transition in Arabidopsis is a biphasic process that starts with bolting of the main shoot and concludes with flower production. In the I1 phase, paraclades are formed from axillary meristems in the axils of cauline leaves and the expansion of these leaves is suppressed, whereas in the subsequent I2 phase the axillary meristems are floral meristems and develop as flowers, and outgrowth of the subtending bracts is entirely suppressed (Hempel, 1997; Schultz and Haughn, 1991; Suh et al., 2003). In wild-type plants, bolting, which involves internode elongation to produce a long primary stem, and flowering (transition from the I1 to the I2 phase) are coupled, but the time interval between bolting and the initiation of flowers can vary under non-optimal conditions (Pouteau and Albertini, 2009).

Several genotypes described in this thesis developed more cauline leaves than wild type. These additional cauline leaves may arise by several mechanisms. This is evident from apparently contradictory phenotypes of early-flowering *mir157* and *rSPL15* genotypes on one hand and the late-flowering *spl4*, *ful* and *ft tsf* mutants on the other. All these genotypes formed more cauline leaves than wild-type plants and additive phenotypes were observed in *mir157 ful* mutants or when *rSPL15* was combined with *spl4* or *ft tsf*.

An extended I1 phase can result in an increase in the number of cauline leaves (Figure 6.1). In *rSPL15* plants, this might be achieved through an earlier onset of the I1 phase: In several long-day and short-day experiments, *rSPL15* strongly accelerated bolting compared with wild type, but had a weak effect on the timing of flower production. This was consistent with the *rSPL15* phenotype described previously (Ó'Maoiléidigh et al., 2021), and with the inability of *rSPL15* to accelerate flowering of the late flowering *ft tsf* or *spl4* genotypes. Both *rSPL15 ft tsf* and *rSPL15 spl4* genotypes produced significantly more cauline leaves than the parental lines. Thus, although the I1 phase

began earlier in *rSPL15* plants, enhanced and precocious SPL15 activity appears not to be sufficient for transition to the I2 phase.

In addition to an earlier onset of the I1 phase, delayed transition to the I2 phase can also extend the I1 phase and thus increase the number of nodes that form cauline leaves and paraclades. This applies, for example, to late-flowering mutants such as *ful-2.* A rough approximation of the duration of the I1 phase is the flowering gap, which is the difference between the number of days to bolting and days to flowering. The number of cauline leaves produced by *mir157d ful-2* and *mir157cd ful-2* mutants correlated with the length of the flowering gap (Figure 6.1A). However, this was not the case for *mir157c ful-2,* each of the single mutants, and wild-type plants; therefore, *MIR57D* function during the I1 phase appears to be distinct from that of *MIR157C*. This is supported by the additive number of cauline leaves in *mir157cd* double mutants and the difference between the number of cauline leaves of *mir157c ful-2* and *mir157d ful-2.* Although *MIR157C* might reduce cauline leaf production in a *FUL*-dependent manner, the synergistic interactions between *mir157d* and *ful-2* suggest that the *MIR57D*-mediated regulation of SPL activity has a component that is independent of *FUL*. The spatial expression patterns of *MIR157C* and *MIR157D* most likely contribute to this difference. During the I1 phase, *MIR157D* expression was detected at the boundaries between axillary meristems and cauline leaves and was absent from the SAM. The spatial expression pattern of *MIR157C* remains to be characterised. However, if *MIR157C* expression is dependent on FUL activity, which is consistent with the genetic interactions, then *MIR157C* might be expressed in similar domains to FUL, such as the SAM.

The number of cauline leaves can also vary independently from the length of the I1 phase. This occurs in plants with an enlarged SAM, such as *clavata* mutants or plants with exogenous AP2 activity (Clark et al., 1995; Fletcher et al., 1999; Sang et al., 2022). Meristem size correlates with the rate of leaf initiation among Arabidopsis accessions (Landrein et al., 2015; Mirabet et al., 2012). Independently, the rate of leaf initiation also correlates with the rate of cell division at the meristem (Cockcroft et al., 2000; Kawakatsu et al., 2006). In the SAM, both the size of cells and the rate of cell division increase dynamically during floral transition (Kinoshita et al., 2020; Kwiatkowska, 2008). Evidence suggests that SPL9 and SPL15 influence cell division rates; thus, a

hypothetical role for miR157-regulated SPL transcription factors in regulating cell division during floral transition is possible.

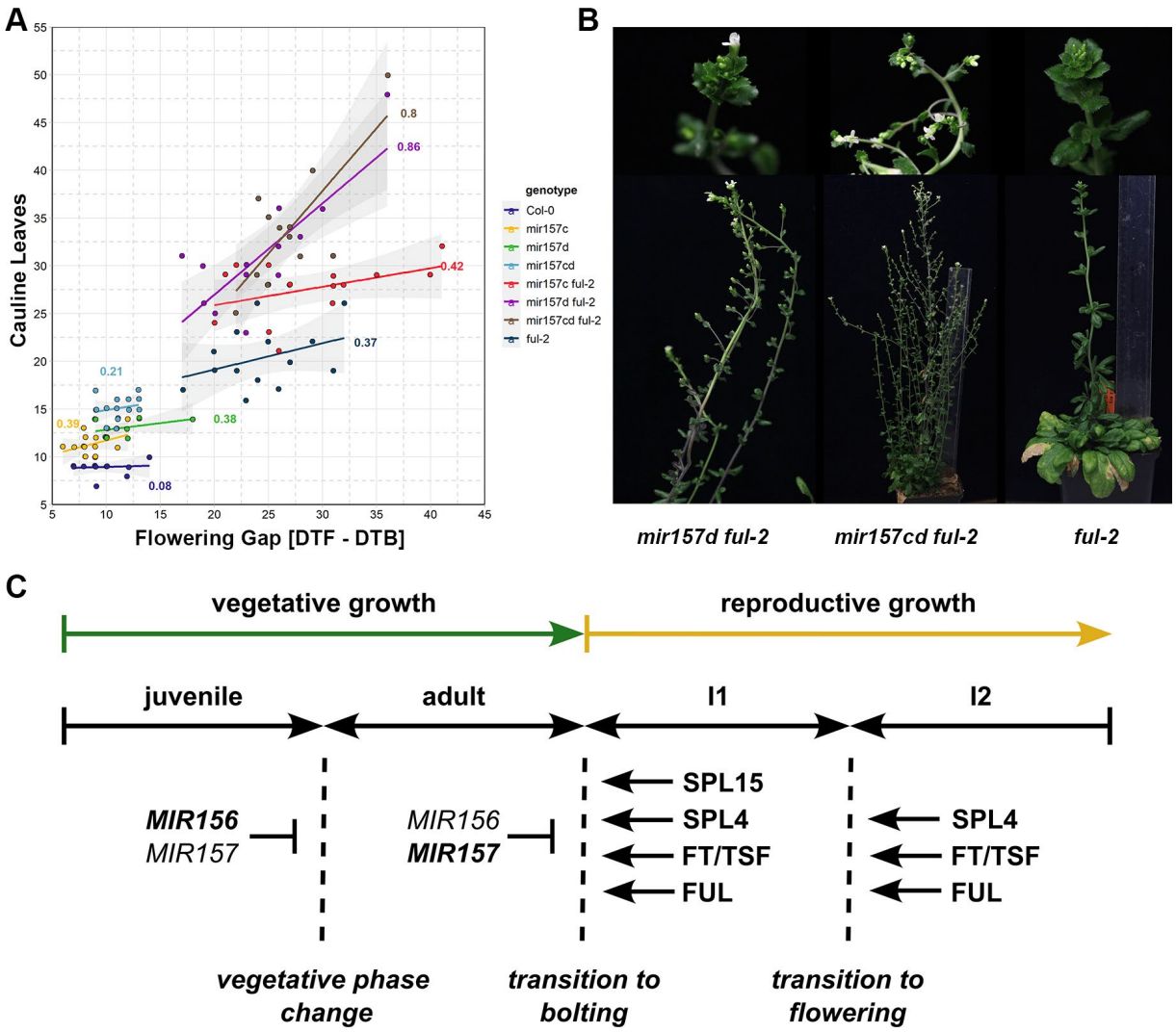

Figure 6.1. The number of cauline leaves can be increased by an extended I1 phase. A) A scatterplot comparing the number of cauline leaves to the flowering gap, which is defined as the difference between days to flowering (DTF) and days to bolting (DTB). The flowering gap serves as an approximation of I1 phase duration. The Pearson correlation coefficient is given for each regression line. The confidence interval is plotted in grey. B) Examples of *mir157d ful-2* and *mir157cd ful-2* inflorescences with an extended I1 zone. C) A model for how factors analysed in this project influence key developmental transitions.

Transgenic plants that express *rSPL9* from its native promoter sequences show a slower rate of leaf initiation that correlates with decreased meristem size and cell-division rate (Wang et al., 2008). The *more and smaller cells 1-D* (*msc1-D*) mutation was isolated in a screen for mutants with altered leaf development (Usami et al., 2009).

The *msc1-D* mutant carries a point mutation in *SPL15* that renders it less sensitive to negative regulation by miR156/miR157 and therefore expresses it at elevated levels. The *mir157d* single mutant produced more cauline leaves than wild type, and *mir157abc* triple mutants had fewer cauline leaves that *mir157cd*. After floral transition, *MIR157D* expression appeared in the boundary region between cauline leaves and axillary meristems. Boundaries are regions of reduced cell division (Breuil-Broyer et al., 2004; Žádníková and Simon, 2014). Therefore, it would be of interest to analyse the role of SPL proteins in regulating cell division in a spatial context.

A recent report suggests that a negative feed-back loop exists between *WUS* and *SPL4* during floral transition (Musialak-Lange et al., 2021). According to the model, SPL4 binds *WUS* and represses its expression, which in turn, leads to an increase in *SPL4* expression. Therefore, loss of SPL4 function should lead to higher WUS expression and an enlarged meristem, which might then produce more cauline leaves.

The greater number of cauline leaves produced by *mir157* mutants compared with wild type might arise from several mechanisms. In several genotypes, duration of the I1 phase was similar to that of wild-type plants. For example, long-day-grown *mir157cd* mutants bolted and flowered at a similar time to wild-type plants, but formed significantly more cauline leaves in both long- and short-day conditions. Similarly, the *mir157d* mutation weakly promoted flowering, but led to the production of significantly more cauline leaves than wild type. The effect of *mir157d* on cauline leaf number was additive with that of *mir157c*, which might reflect an accelerated rate of leaf initiation during the I1 phase. During vegetative growth, the leaf initiation rate of *mir157cd* mutants was intermediate between that of *mir157c* and *mir157d* mutants, not additive. It has yet to be determined, whether the rate cell of division or the size of the meristem of *mir157* mutants differs from that of wild-type plants during floral transition.

Meristem size also correlates negatively with the robustness of phyllotaxis (Landrein et al., 2015; Mirabet et al., 2012). An enlarged meristem is more likely to co-initiate primordia simultaneously, which leads to permutations in the spiral phyllotaxis. Phyllotaxis was analysed during vegetative growth, which is when *mir156ac* mutants showed the strongest defects in phyllotaxis compared with wild-type plants.

6.3. Molecular mechanisms that regulate inflorescence architecture

Plant architecture is determined by the activities and identities of apical and axillary meristems. The balance between determinate and indeterminate growth habits involves antagonistic FT/TSF and TFL1 functions (Moraes et al., 2019; Zhu et al., 2020). *TFL1* is strongly expressed in axillary meristems (Conti and Bradley, 2007) that in Arabidopsis undergo a brief vegetative phase before transitioning to flowering. The outgrowth of axillary shoots is mediated by FT/TSF in a photoperiod-independent manner (Hiraoka et al., 2013; Lee et al., 2019; Liu et al., 2014). To determine whether floral transition in the paraclades of mutant genotypes was altered, the number of cauline leaves on secondary inflorescences was counted. The *mir157cd*, *spl4* and *spl15-1* mutants produced more cauline leaves on secondary inflorescences and on the main shoot than wild-type plants. Moreover, the *spl4* cauline phenotype on paraclades was similar to that of both *rSPL15 spl4* and *mir157c spl4*, suggesting that *SPL4* is epistatic to *rSPL15* and *mir157c* and modulates floral transition in axillary meristems downstream from them. This is not surprising for *mir157c*, because *SPL4* is a direct target of miR157, but implies that SPL4 plays a greater role in this secondary inflorescence phenotype than its paralogues. The expression of *SPL4* in axillary meristems appears after floral transition (Olas et al., 2019).

In addition to their functions in regulating shoot branching, SPL3, SPL4 and SPL5 have been proposed to accelerate flowering in response to shade. The three transcription factors bind and activate *LFY, FUL* and *MIR172C* genes, and under non-shade conditions are inhibited by protein–protein interactions with FAR-RED ELONGATED HYPOCOTYL3 (FHY3) and FAR-RED IMPAIRED RESPONSE 1 (FAR1) (Xie et al., 2020a). FHY3 and FAR1 act downstream of the phytochrome A signalling pathway and are degraded during the shade response, which releases SPL3, SPL4 and SPL5 from functional inhibition.

The branching integrator BRANCHED1 (BRC1) inhibits premature outgrowth of axillary buds and delays their floral transition by interacting with FT (Aguilar-Martínez et al., 2007; Niwa et al., 2013). The interaction between BRC1 and FT affects the floral transition of axillary meristems from both rosette leaf and cauline leaf axils (Niwa et al., 2013). Although the role of SPL4 in this context is unknown, SPL9 and SPL15 repress branching by activating *BRC1* expression (Xie et al., 2020b). The *spl9 spl15* double

mutant exhibits enhanced outgrowth of rosette branches (Schwarz et al., 2008; Wang et al., 2008; Xie et al., 2020b). The *spl4 spl15* double mutant described in this thesis also showed reduced apical dominance in short days and often flowered from rosette branches before the main shoot bolted. The strigolactone (SL) pathway is involved in the regulation of branching and might integrate with SPL9 and SPL15 functions. Three key repressors of SL signalling, SUPPRESSOR OF MAX2 1-LIKE6 (SMXL6), SMXL7 and SMXL8, can directly interact with SPL9 and SPL15 and suppress the activation of *BRC1* expression (Xie et al., 2020b).

In meristems, floral meristem identity is established through synergistic interactions between *AP1* and *LFY* and both genes are activated by SOC1 and SPL3, SPL4 and SPL4 (Immink et al., 2012; Jung et al., 2012, 2016; Liu et al., 2008). Moreover, SPL9 activates *AP1* at the SAM periphery (Hyun et al., 2016; Wang et al., 2009; Yamaguchi et al., 2014). Although many interactions among flowering-time genes and floral meristem identity genes are known, their relative temporal expression patterns are less well elucidated.

The earliest flowering-time gene to be upregulated at the shoot meristem in response to long days is SOC1, which integrates signalling from the photoperiodic and gibberellin pathways (Borner et al., 2000; Moon et al., 2003; Samach et al., 2000). *LFY* is expressed in cauline leaves and its expression therefore precedes that of *AP1,* which is restricted to floral meristems and flowers (Mandel et al., 1992; Wang et al., 2009; Weigel et al., 1992).

The *FUL* and *MIR172* genes are activated cooperatively by SOC1 and SPL (Hyun et al., 2016). Accordingly, the function of *rSPL15* is partially dependent on that of *FUL* and *MIR172* (Ó'Maoiléidigh et al., 2021). *SPL4* might also function downstream of *rSPL15*. This is supported by the finding that *SPL4* is upregulated in *rSPL15* plants (PhD thesis Annabel van Driel, 2021) and that *spl4* delays bolting of *rSPL15* plants.

The establishment of floral meristem identity also involves the repression of flowering-time genes. *SOC1* and *FUL* are repressed by AP1 (Ferrandiz et al., 2000; Liu et al., 2007) and *AGAMOUS-LIKE 24* (*AGL24*), a close homologue of *SOC1*, is repressed by LFY (Yu et al., 2004). Consistent with this, the expression domain of *SOC1* covers the entire IM, but does not extend into floral primordia (Immink et al., 2012). The

expression of miR156-susceptible and -resistant *SPL15* reporter variants is similarly absent from floral primordia (Hyun et al., 2016). Thus, their presence might interfere with the specification of floral meristem identity. Plants expressing *rSPL15* produced wild-type flowers, but the appearance of bracts subtending flowers under short days suggests that these plants had a reduced commitment to flowering.

The *rSPL15* phenotypes suggest that the role of *rSPL15* is similar to that of gibberellins during floral transition, which promote bolting but inhibit flower production (Yamaguchi et al., 2014). Bioactive gibberellins accumulate in apices shortly before floral transition (Andrés et al., 2014; Eriksson et al., 2006) and the expression of gibberellin biosynthesis genes increases transiently during doming of the SAM (Kinoshita et al., 2020). The accumulation of DELLA proteins during floral transition depends on the gibberellin-catabolising enzyme EUI-LIKE P450 A1 (ELA1), which is expressed in incipient floral primordia and reduces local gibberellin levels (Yamaguchi et al., 2014). LFY activates *ELA1* expression, which then stabilises DELLA proteins during transition to the I2 phase. In incipient floral primordia, DELLA proteins might promote flower formation by enhancing the transcriptional activation of *AP1* by SPL9 (Yamaguchi et al., 2014). Consistent with this, *ela1* mutants form more cauline leaves than wild-type plants. The interactions between miR156/miR157-regulated SPL transcription factors and gibberellin signalling during I1 to I2 transition requires further investigation.

6.4. Perspectives

In 2006, Jones-Rhodes and colleagues commented that it is unclear why a plant would need twelve genes encoding miR156 (Jones-Rhoades et al., 2006). By characterising flowering-time phenotypes of *mir156* and *mir157* mutants and by studying the spatio-temporal expression patterns of *MIR156* and *MIR157* genes, I was able to partially answer this question. It is now clear that individual *MIR156* and *MIR157* genes have distinct expression patterns and specialised roles during plant development. The photoperiod-dependent flowering response differed among *mir156* and *mir157* mutants and their influence on vegetative and reproductive shoot development varied. The distinct phenotypes correlated with differences in expression dynamics, which

suggests that diversity among *MIR156* and *MIR157* promoters contributes to this versatility.

An important future direction is to determine which SPL factors are negatively regulated by specific *MIR156/MIR157* genes. There are 11 *SPL* genes whose mRNAs are targets for miR156/miR157 and it remains unclear precisely which *SPL* genes are responsible for the early-flowering phenotypes of *mir156ac* mutants under long days, for the early flowering of *mir157cd* mutants under short days or for the increased cauline leaf number of *mir157cd* mutants under long and short days. Here, I found that SPL4 and SPL15 contribute to these phenotypes and might act sequentially. Determination of the responsible SPL factors will require careful epistasis genetics and expression analyses, and these experiments will be required to understand the mechanisms by which the miRNA156/157 pathways regulate reproductive development.

Many aspects of the interactions between miR156/miR157 and genes encoding SPL transcription factors are conserved between Arabidopsis and distantly related crop plants. Notably, mir156-regulated SPL transcription factors have been shown to influence inflorescence architecture and yield traits in a variety of crop plants. This includes soybean (Sun et al., 2019; Yue et al., 2021), tomato (Cui et al., 2020) and grasses such as maize, rice and wheat (Chuck et al., 2010, 2014; Jiao et al., 2010; Liu et al., 2017; Miao et al., 2019; Song et al., 2017). The miR156/miR157 module is also involved in various stress responses (Cui et al., 2014; Ma et al., 2021; Stief et al., 2014; Zhou and Tang, 2018), which are important to prevent yield loss (Zhang et al., 2018).

The manipulation of individual *MIR156* and *MIR157* genes might therefore allow the fine-tuning of shoot architecture by increasing the expression of specific SPL factors in particular domains without compromising other important traits, an approach that was already suggested for rice (Miao et al., 2019). In Arabidopsis, both *mir157d* and *ful* mutants develop additional secondary inflorescences from an extended I1 zone compared with wild-type plants. However, the loss of *FUL* function also impacts silique development and therefore seed yield (Ferrandiz et al., 2000; Gu et al., 1998; McCarthy et al., 2015). By contrast, siliques of *mir157d* appeared to develop normally. Similarly, other *MIR156* and *MIR157* genes are functional in *mir157d* mutants and are available for stress responses. The detailed characterization of the roles of individual

MIR156/*MIR157* genes presented here therefore suggests approaches to increase inflorescence branch number and yield in crops.

7. Materials and Methods

7.1. Plant material and growth conditions

7.1.1. Plant growth conditions

All flowering-time, confocal and quantification experiments were conducted under controlled conditions in growth cabinets. To synchronise germination, seeds were sown on soil in 9 x 9 cm pots and were stratified for 2–3 days at 4°C in darkness. The day of transfer to controlled growth conditions was set as day 0 in flowering-time experiments. For long-day (LD) experiments, the photoperiod consisted of 16 h light/8 h darkness cycles, whereas short-day conditions (SD) consisted of 8 h light/16 h darkness. All experiments were conducted in plant cultivation cabinets (AR75, Percival scientific) equipped with LED lights that generated an approximate light intensity of 170 µmol $m^{-2}s^{-1}$ (Figure 7.1). The cabinets maintained a constant growth temperature of 21°C.

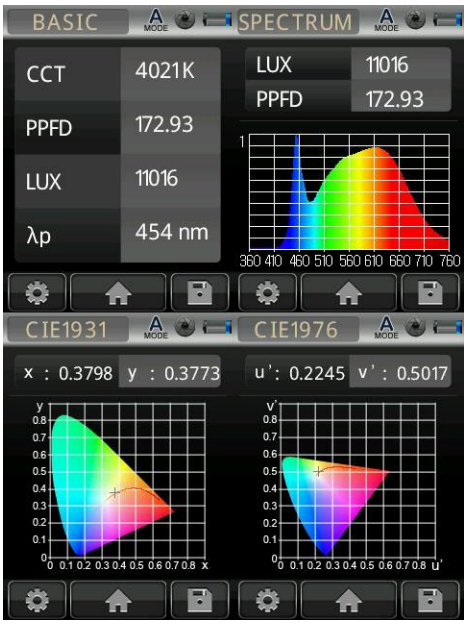

Figure 7.1. Recorded light spectrum and light intensity of growth cabinets used in flowering-time and sequencing experiments. PPFD = photosynthetic photon flux density (µmol $m^{-2}s^{-1}$).

The Basta (phosphinothricin, ppt) selection of transgenic lines occurred on soil by spraying seedlings with 1/1000 (v/v) Basta solution. To select on plates, seeds were surface sterilised by washing in 70% ethanol with 0.05% Tween20 for 10 min, followed by 10 min in 96% ethanol. After drying, seeds were sown on plates using full-strength

Murashige and Skoog (MS) plates supplemented with the appropriate antibiotic (15 ng μL^{-1} for ppt-selection or 50 ng μL^{-1} for kanamycin selection).

For confocal experiments, samples were harvested between Zeitgeber time (ZT) 2 and ZT 3 into 4% (w/v) PFA fixative buffered by PBS, pH 6.5 –7.0. Samples were fixed by vacuum infiltration for 1 h, followed by 2 h incubation at room temperature. To clear tissue, samples were washed in PBS buffer, transferred to ClearSee (Kurihara et al., 2015) and incubated for three days. Cell walls were stained by adding SCRI Renaissance 2200 (1 µL ml^{-1}) the day before imaging (Musielak et al., 2015).

For quantitative real-time PCR (qRT-PCR) and sRNA-sequencing experiments, apices were harvested by removing visible leaves, cotyledons and hypocotyl. The samples were then flash frozen in liquid nitrogen. Samples were harvested at ZT 2 and ZT 4. Approximately 50 apices were harvested for time points 1wSD, 2wSD, 4LD and 7LD. For later time points, this number was reduced to 30 or 20 samples. At least three biological replicates were harvested for each time point.

7.1.2. Plant material

The Arabidopsis accession Col-0 was used as a wild-type control and all mutants and transgenic lines used were in this background. The *spl4* mutant was generated and isolated by Dr. Youbong Hyun using the CRISPR/Cas9 strategy published in Hyun et al. (2015). The homozygous *spl4* mutant carries a 7-bp deletion allele in the first exon and is a transgene-free descendant of the published T1 generation (Hyun et al., 2015).

The CRISPR/Cas9-induced *mir156* and *mir157* deletion alleles were generated in the Coupland group by Dr. Serena Della Pina. The mutagenesis yielded *mir156a*, *mir156c*, *mir157ab* and *mir157cd* mutants, which were then combined as necessary for this work. Except for *mir157ab* and *mir157abc* mutants, these lines were free of the CRISPR/Cas9 transgene. The deletions were present in sequences encoding the pri-miRNA hairpin structure (Figure 4.1A). Table 7.1 lists the plant material used in this work. Primers used for genotyping are listed in Table 7.2.

Table 7.1. List of mutants and transgenic lines used in this work.

Mutant or transgenic line	Note	Reference
spl4 CRISPR mutant	The homozygous *spl4* mutant is a descendant of the T1 plant carrying a 7-bp deletion allele in the first exon.	Youbong Hyun, Coupland group (Hyun et al., 2015)
spl15-1	SALK T-DNA mutant	(Hyun et al., 2016)
ful-2	EMS mutant	(Ferrandiz et al., 2000)
pSPL15::9A:VENUS:SPL15/Col-0	Basta resistant	(Hyun et al., 2016)
pSPL15::9A:VENUS:rSPL15/Col-0	Basta resistant	(Hyun et al., 2016)
pFUL::FUL:9A:VENUS/ful-2	Basta resistant	Annabel van Driel, Coupland group (PhD thesis, van Driel, 2021)
mir172a-2 mir172b-3 mir172d-3	CRISPR/Cas9-induced alleles	(Ó'Maoiléidigh et al., 2021)
ft-10 tsf-1	SALK T-DNA mutant	(Jang et al., 2009)
mir156a, mir156c CRISPR mutants	CRISPR/Cas9-induced alleles	Serena Della Pina, Coupland group
mir157ab, mir157c, mir157d, CRISPR mutants	CRISPR/Cas9-induced alleles	Serena Della Pina, Coupland group
MIR156C::VENUS:GUS	Basta resistant	Youbong Hyun, Coupland group
MIR156B::VENUS:GUS	Basta resistant	Youbong Hyun, Coupland group
MIR156A::GFP	Basta resistant	Wang group, (Cheng et al., 2021)
MIR157A::VENUS:GUS	Basta resistant	Generated in this work
MIR157D::VENUS:GUS	Basta resistant	Generated in this work
pWUS::3xVENUS pCLV3::mCherry	Basta and Kanamycin resistant	Lohmann group (Pfeiffer et al., 2016)

7.1.3. Genotyping

For genotyping, genomic DNA (gDNA) was extracted using the BioSprint 96 DNA Plant Kit (QIAGEN, catalogue #941557) in combination with the Biosprint automation platform according to the manufacturer's instructions. Briefly, small rosette leaves were harvested into 96-well plates, submerged in lysis buffer and disrupted using Tissue Lyser II. The samples were then transferred to isopropanol and loaded into the

Biosprint 96 extraction robot, together with all required washing solutions. The extracted gDNA was eluted to a final volume of 100 µL with ddH_2O.

Genotyping PCR reactions were run in a final volume 10 µL (Table 7.3 and 7.4), which contained GoTaq and associated GoTaq Green buffer (Promega, catalogue #M300A, #M791A). Standard laboratory procedures were followed. The primers used to genotype each mutant are listed in Table 7.2.

Table 7.2. Primers used for genotyping.

Oligo-nucleotide Number	Oligo-nucleotide name	Sequence	Usage note
AR001	*LBb1.3*	ATTTTGCCGATTTCGGAAC	For SALK mutants. Binds to the left T-DNA border
AR002	*MIR156A-gt-F*	AAAGAGATCAGCACCGGAATC	Deletion allele
AR009	*MIR156A-gt-R*	AGTTGGGACAAGAGAAACGCA	Use with AR009.
AR056	*MIR156C-gt-F*	AAACGTGACCGGGACCGAAT	Deletion allele
AR011	*MIR156C-gt-R*	ACACCTTCAAAGTCTGCCTCC	Use with AR056
SDP422	*MIR157A-gt-F*	CATTTCGTTGCTCTCTATGTG	Deletion allele
SDP423	*MIR157A-gt-R*	AACTGTTTCAATCACTCTCGT	Use with SDP422
SDP426	*MIR157B-gt-F*	CTGGTGTTTAATCAAGTTCTTG	Deletion allele
SDP427	*MIR157B-gt-R*	CACTATTCAGATTGATAGGCATG	Use with SDP427
AR289	*MIR157C-gt-F*	GGTTTGAGAGTGATGTTGGTTGT	Deletion allele
AR180	*MIR157C-gt-R*	TTTATCATCCACATGCGGTG	Use with AR289
AR339	*MIR157D-wt-F*	AAGAAAGGTGATGACAGAAGCA	205 bp in wild type.
AR340	*MIR157D-wt-R*	AGTGGAGGGTGATAGTGTGGT	No amplification in the mutant.
AR099	*MIR157D-mt-F*	TCATGCTCTTAGGGTGCAGTT	Size: 126 bp for the mutant, 1.3 kb for wild type.
SDP433	*MIR157D-mt-R*	CTATGCATGTTCACGACACC	Difficult to amplify with GoTaq.
AR006	*cas9_geno_F*	GGACTTCCTGGACAACGAGG	Cas9 genotyping, binds to the central part of the gene.
AR007	*cas9_geno_R*	CGTTGATAAGCTTGCGGCTC	Product size: 194 bp
AR024	*VN + GFP F*	GAGCTGAAGGGCATCGACTT	Same as qRT-PCR primers
AR025	*VN + GFP R*	CTCGATGTTGTGGCGGATCT	147 bp product with AR24 on *VN* and *GFP*

AR052	*BaR_F*	CTGCCAGAAACCCACGTCAT	Basta resistance gene
AR053	*BaR_R*	TCGAGACAAGCACGGTCAAC	Basta resistance gene
AR350	*spl4-wt-F*	AAGTCTTACCTTGTGGAAGAA	7 bp deletion
AR352	*spl4-wt-R*	GCAACTTCTCTTAGCTTCATC	Use 3% agarose gel
AR032	*spl15-1-F*	TGCATCACTGATCTTGCGGTTG	Use with AR033 for wild type allele.
AR033	*spl15-1-R*	GGAGTTGTTAATGTGTTCGGGTCAG	Use with AR001 for T-DNA allele
AR371	*ful-2_amp-F*	TTGGCCGAGACGTTTCACAA	Amplify with AR401, sequence product with AR373
AR401	*ful-amp_3.5kb_R*	GTGAGAGATTCTCCGACAGGAA	Binds outside of the pFUL reporter
AR373	*ful-2_seq*	ATTAGAAGTTTGTATGTGCGACCC	Sequencing the ful-2 point mutation
AR175	*gabi-T-DNA*	CCCATTTGACGTGAATGTAGACAC	AR175 and AR176 for the T-DNA allele. GABI-Kat mutant.
AR176	*ft10-gabi-R*	TAAGCTCAATGATATTCCCGTACA	AR176 and AR177 for the wild-type allele
AR177	*ft10-gabi-F*	CAGGTTCAAAACAAGCCAAGA	
AR178	*tsf1-R*	CTGGCAGTTGAAGTAAGAG	Use with AR179 for wild-type allele.
AR179	*tsf1-F*	CACGAGGTTGGTCTCTCTTAAG	Use with AR001 for mutant allele.
AR248	*172A-F*	TCGACTATTCCGCCATGTTTG	(Ó'Maoiléidigh et al., 2021)
AR249	*172A-R*	ACCTACCTGAAGAAGATCTGGATG	(Ó'Maoiléidigh et al., 2021)
AR250	*172B-F*	TCAGCCCTTGGATTCGTGAGG	(Ó'Maoiléidigh et al., 2021)
AR251	*172B-R*	TAACGCCCTAATCCGTCATTGACC	(Ó'Maoiléidigh et al., 2021)
AR252	*172D-F*	CTTCACCCTAAATCTCTTCCTCTCCTTCAG	(Ó'Maoiléidigh et al., 2021)
AR253	*172D-R*	CACCTCAAGTTATCATATCGGAGG	(Ó'Maoiléidigh et al., 2021)

Table 7.3. GoTaq mixture for single reaction genotyping PCR.

Reagent	Volume/ amount
ddH_2O	To 10 µL
5× GoTaq Green buffer	2 µL
25 mM $MgCl_2$	1.0 µL
10 mM dNTPs	0.4 µL
Forward primer	0.4 µL
Reverse primer	0.4 µL
GoTaq polymerase (5U $µL^{-1}$)	0.05 µL
Template DNA	2.0 µL

Table 7.4. Standard GoTaq PCR program used for genotyping and colony screening.

PCR step		Temperature (°C)	Time
1.	Initial denaturation	95	2 min
2.	Denaturation	95	30 s
3.	Primer annealing	50 – 60	15 s
4.	Primer extension	72	1 min kb^{-1}
5.	Cycles	–	30 – 35×
6.	Final extension	72	5 min
7.	Hold	10	∞

7.2. Molecular cloning

7.2.1. Design and molecular cloning of reporter constructs

All *MIR156* and *MIR157* reporter constructs imaged during this project included the entire upstream and downstream intergenic regions of the respective genes. Following the design used in previous studies (Cheng et al., 2021; Ó'Maoiléidigh et al., 2021), the miRNA-encoding stem loop region was replaced by of the reporter gene.

Cloning of *MIR157* reporter constructs employed the Gibson Assembly method, which allows the combination of arbitrary PCR fragments and vector backbones, given that their DNA ends overlap by 15 to 30 bp (Gibson et al., 2009). The DNA fragments were recombined *in vitro* into a single plasmid through the combined action of a 5′ DNA exonuclease, a DNA polymerase and a DNA ligase. The Gibson Assembly mix

supplied by New England Biolabs (NEB, catalogue number: E5510S) and associated protocols were used for this cloning strategy. The reporter constructs were directly assembled into binary vectors, which were checked for integrity by Sanger sequencing.

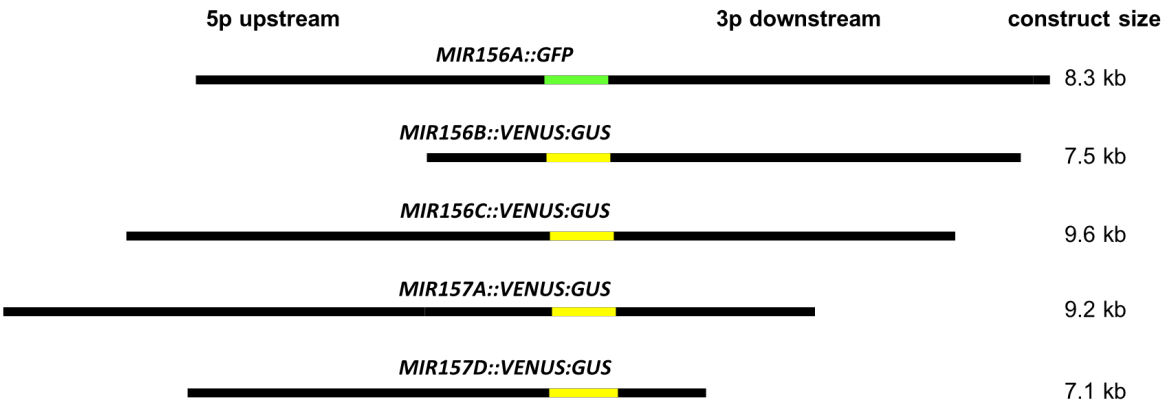

Figure 7.2. Design of *MIR156* and *MIR157* reporter constructs used in this work.

The cloning was initiated by pre-amplifying the upstream and downstream region with either PrimeSTAR GXL (TaKaRa, #R050A) or Phusion® High-Fidelity (NEB, # M0530L) DNA polymerases. Compatible overhangs were then added in a second PCR that used the previous reaction as template. After *Dpn*I digestion to remove residual template DNA, PCR products were purified using the Macherey-Nagel NucleoSpin Gel- and PCR Clean-up Kit (MN, #11992242).

The binary vector pBGW0 (a Gateway-compatible vector carrying a Basta-resistance gene, here referred to as V195) had to be modified for its use with Gibson assembly. It was linearised via restriction digestion by the EcoRI-HF enzyme (NEB catalogue #R3193), and then amplified using Phusion polymerase and primers AR218 and AR219. After *Dpn*I treatment and PCR-clean up, the linearised vector (pLV195) was used for Gibson cloning. The reaction mixture is listed in Table 7.11, using the protocol described below.

Table 7.5. Description of used and generated plasmids.

Plasmid name	Description	Size (bp)	Antibiotic resistance
V195 (pBGW0)	Gateway-compatible binary vector carrying a *ccdB* cassette	9,669	Spec, Basta (plant)
pLV195	V195 linearised for Gibson assembly. Does not carry the *ccdB* cassette,	8,016	Spec, Basta (plant)
V195 MIR156B::VNG	V195 vector containing the whole intergenic sequences of *MIR156B* fused to *VENUS-GUS*, which replaces the miR156 hairpin.	15,514	Spec, Basta (plant)
pLV195 MIR157A::VNG	pLV195 vector containing the whole intergenic sequences of *MIR157A* fused to *VENUS-GUS*, which replaces the miR157 hairpin.	17,034	Spec, Basta (plant)
pLV195 MIR157D::VNG	pLV195 vector containing the whole intergenic sequences of *MIR157D* fused to *VENUS-GUS*, which replaces the miR157 hairpin.	15,065	Spec, Basta (plant)

7.2.2. *Dpn*I treatment

The *Dpn*I restriction enzyme digests palindromic GATC sequences if the adenosine residue has been methylated. This is the case for plasmids isolated from standard lab strains, but not for DNA generated by PCR *in vitro*. The enzyme is therefore useful to remove template DNA from PCR products.

The digestion can be performed directly on PCR products. For example, 6 µL 10× CutSmart Buffer and 1 µL *Dpn*I-HF enzyme (New England Biolabs, catalogue #R0176S) were added to 65 µL PCR product, and the mixture was incubated at 37°C for 1 h. The enzyme was inactivated by incubating at 80°C for 20 min.

Table 7.6. Primers used for cloning and sequencing.

Oligonucleotide Number	Oligonucleotide name	Sequence	Usage note
AR036	V195F	GGCTTGTCCCGCGTCATCGG	Insert sequencing and colony PCR.

AR037	V195R	AACTGAAGGCGGGAAACGAC	Insert sequencing and colony PCR.
AR218	pLV195-F	AGCCTGCTTTTTTGTACAAACTTGTGATAT	Amplification of EcoRI-HF digested V195 plasmids. Modifies ATT sites.
AR219	pLV195-R	ACCCAGCTTTCTTGTACAAAGTGGTGATAT	Size of pLV195: 8,006 bp.
AR149	157A-5p-preamp-F	GTCCCGAGTTATACACCGTCC	Pre-amplification of *MIR157A* 5p intergenic region. Used with AR150.
AR150	157A-5p-preamp-R	TGTCAACACTATCAATGCCTCTCA	Pre-amplification of *MIR157A* 5p intergenic region. Used with AR149.
AR151	157A-3p-preamp-F	GCTCTCTAGCCTTCTGTCATCA	Pre-amplification of *MIR157A* 3p intergenic region. Used with AR151.
AR152	157A-3p-preamp-R	TCGAGATGATACCACAAGAAATCA	Pre-amplification of *MIR157A* 3p intergenic region. Used with AR151.
AR220	157A-5p_V195-F	ATATCACAAGTTTGTACAAAAAAGCAGGCTGTCCCGAGTTATACACCGTCC	Amplification of *MIR157A* 5p sequence. Adds overlap with V195 binary vector. Used with AR154.
AR154	157A-5p_NLS-R	GACCTTTCTCTTCTTCTTTGGAGCCATCACTATCAATGCCTCTCAATTCTCAAAC	Amplification of *MIR157A* 5p sequence. Adds overlap with NLS of the *VENUS-GUS* gene. Used with AR220.
AR369	157A-3p_GUS-F	CCGCAGCAGGGAGGCAAACAATGAACCTTTTATTTGCTTTATTGTCTC	Amplification of *MIR157A* 3p sequence. Adds overlap with the GUS stop codon. Used with AR221.
AR221	157A-3p-V195-R	ATATCACCACTTTGTACAAGAAAGCTGGGTGAAAAGAAGATGTACAACTTTTATTCAAGGATATTTCAG	Amplification of *MIR157A* 3p sequence. Adds overlap with V195 binary vector. Used with AR369.
AR370	VNG-157A-3p-R	GAGACAATAAAGCAAATAAAAGGTTCATTGTTTGCCTCCCTGCTGCGG	Amplification of *VENUS-GUS*. Adds overlap with *MIR157A*-3p. Used with Use with AR268.
AR266	157D-5p-preamp-F	GCGTTTGCGTTTGTGGTTTG	Pre-amplification of *MIR157D* 5p intergenic. Used with AR267.

AR267	157D-5p-preamp-R	GCAACCACACTATCACCCTCC	Used with AR266.
AR270	157D-3p-preamp-F	TCACCTTTCTTTCTCTATTTCTCTCTAC	Pre-amplification of *MIR157D* 3p intergenic region. Used with AR271
AR271	157D-5p-preamp-R	GACTGTTTCGTCACCGTCCA	Used with AR270
AR272	157D-5p_V195-F	ATATCACAAGTTTGTACAAAAAAGCAGGCTGAAATATTGCCGACTTAGCTGACATAA	Amplification of *MIR157D* 5p sequence. Adds overlap with V195 binary vector. Used with AR349.
AR349	157D-5p_NLS-R	GACCTTTCTCTTCTTCTTTGGAGCCATGCAACCACACTATCACCCTCC	Amplification of *MIR157D* 5p sequence. Adds overlap with NLS of the *VENUS-GUS* gene. Used with AR272.
AR274	157D-3p-GUS-F	CAAACAATGATCACCTTTCTTTCTCTATTTCTCTCTAC	Amplification of *MIR157D* 3p sequence. Adds overlap with the GUS stop codon. Used with AR275.
AR275	157D-3p-V195-R	ATATCACCACTTTGTACAAGAAAGCTGGGTCTAATTTCCCTCCGAGAATTTATTGGCT	Amplification of *MIR157D* 3p sequence. Adds overlap with V195 binary vector. Used with AR274.
AR268	VN-GUS-NLS-F	ATGGCTCCAAAGAAGAAGAGAAAGGTCATGGTGAGCAAGGGCGAGG	Amplification of *VENUS-GUS*, forward primer.
AR269	VNG-157D-3p-R	TGTAGAGAGAAATAGAGAAAGAAAGGTGATCATTGTTTGCCTCCCTGCTG	Amplification of *VENUS-GUS*. Adds overlap with *MIR157D*-3p. Used with AR268.
SDP309	miR156a-c-d_RGEN-A1	TTGTGTGCTCACTCTCTTCTACAATCACTACTTCGACTCTAGCT	Overlapping primers that were used to generate the single guide RNA (sgRNA) targeting *MIR156A, MIR156C* and *MIR156D.*
SDP310	miR156a-c-d_RGEN-A2	AGAAGAGAGTGAGCACACAAGTTTTAGAGCTAGAAATAGCAA	
SDP317	miR157c-d_RGEN-A1	TAGTGCTCTCTATCTTCTGTACAATCACTACTTCGACTCTAGCT	Overlapping primers that were used to generate sgRNA targeting *MIR157C* and *MIR157D.*
SDP318	miR157c-d_RGEN-A2	ACAGAAGATAGAGAGCACTAGTTTTAGAGCTAGAAATAGCAA	

SPL319	miR157a-b_RGEN-A1	TTGTGCTCTCTAGCCTTCTGACAATCACTACTTCGACTCTAGCT	Overlapping primers that were used to generate sgRNA targeting *MIR157A* and *MIR157B.*
SDP320	miR157a-b_RGEN-A2	CAGAAGGCTAGAGAGCACAAGTTTTAGAGCTAGAAATAGCAA	

Table 7.7. PCR mixture for a single reaction using the proofreading Phusion polymerase.

Reagent	Volume/ amount
ddH_2O	To 20 µL
5× Phusion HF buffer	4.0 µL
10 mM dNTPs	0.4 µL
Forward primer (10 µM)	0.4 µL
Reverse primer (10 µM)	0.4 µL
Phusion High-Fidelity Polymerase (2 U $µL^{-1}$)	0.1 µL
Template DNA	1.0 µL

Table 7.8. Standard Phusion PCR program used for cloning.

PCR step		Temperature (°C)	Time
1.	Initial denaturation	98	30 s
2.	Denaturation	98	10 s
3.	Primer annealing	50 – 60	20 s
4.	Primer extension	72	30 s kb^{-1}
5.	Cycles	–	30 – 35×
6.	Final extension	72	5 min
7.	Hold	10 °C	∞

Table 7.9. PCR mixture for a single reaction using the proofreading PrimeStar GXL polymerase.

Reagent	Volume/ amount
ddH_2O	To 20.5 µL
5× PrimeStar GXL buffer	4.0 µL
2.5 mM dNTPs	1.6 µL
Forward primer (10 µM)	0.6 µL

Reverse primer (10 µM)	0.6 µL
PrimeStar GXL polymerase (1.25 U μL^{-1})	0.4 µL
Template DNA	1.0 µL

Table 7.10. Standard PrimeStar GXL PCR program used for cloning.

PCR step	Temperature (°C)	Time	
1.	Initial denaturation	98	30 s
2.	Denaturation	98	10 s
3.	Primer annealing	50 – 60	15 s
4.	Primer extension	68	30 s kb^{-1}
5.	Cycles	-	15×
6.	Final extension	No final extension	
7.	Hold	10 °C	∞

7.2.3. Gibson Assembly

The Gibson Assembly mix supplied by New England Biolabs (NEB, catalogue #E5510S) and associated protocols were used for cloning. The reaction was prepared according to Table 7.11. Samples were incubated at 50°C for 1 h. After transfer to ice, 2 µL of the mixture was used to transform chemically competent DH10β cells via heat shock.

Table 7.11. Reagents for a single Gibson assembly reaction. According to manufacturer's recommendations.

Reagent	2–3 fragments	4–6 fragments
Total Amount of Fragments	X µL (0.05 to 0.5 pmol)	X µL (0.2 to 1.0 pmol)
Gibson Assembly Master Mix (2×)	10 µL	10 µL
ddH_2O	Up to 10 µL	Up to 10 µL
Total volume	20 µL	20 µL

7.2.4. Heat-shock transformation of chemically competent cells

Chemically competent DH10β TSSGT *E. coli* cells were used for molecular cloning. A 50-µL aliquot of competent cells was thawed on ice for 10 minutes and 2 µL DNA was added and mixed by stirring. After an additional incubation for 5 min on ice, samples were heat shocked for 45 s at 42°C, and then placed on ice again. For recovery of the cells, 400 mL Lysogeny Broth (LB) growth medium was added to the cells, which were then incubated at 37°C for 1 h. For selection, the mixture was transferred to LB agar plates supplemented with appropriate antibiotics. After overnight incubation at 37°C, positive clones were selected by colony PCR.

7.2.5. Electroporation of Agrobacterium tumefaciens

Electrocompetent GV3101 *A. tumefaciens* cells carrying pSOUP or pMP90RK helper plasmids were thawed on ice and 100 ng of the binary vector containing the desired construct was added. The bubble-free mixture was transferred to 1-mm electrocuvettes, and cells were transformed with a single 2.20 kV pulse. After the addition of 400 µL LB medium, samples were incubated at 28°C for 2 h and were plated onto LB agar plates supplemented with Rifampicin (Rif), Kanamycin (Kan), Gentamycin (Gent) and Spectinomycin (Spec) for GV3101 pMP90RK V195 transformations or with Rif, Tetracyclin (Tet), Gent, Spec for GV3101 pSOUP V195 transformations. Positive clones were selected via colony PCR.

7.2.6. *Agrobacterium tumefaciens*–mediated plant transformation

A modified version of the floral dip transformation method (Clough and Bent, 1998) was used to generate transgenic lines in the *Arabidopsis thaliana* Col-0 background. The *A. tumefaciens* strain GV3101 carrying the pSOUP or pMP90RK helper plasmids and the binary plasmid were pre-cultured in LB supplemented with appropriate antibiotics for 2 days at 28°C. A 250-mL overnight culture was inoculated the day before transformation. Prior to transformation, a 250 ml solution containing 20% sucrose (w/v) and 0.1% (v/v) Silwet L-77 (Loveland Industries LTD) were added to the overnight culture. Col-0 plants at the onset of anthesis were transformed by submerging shoots for 1 min into the mixture. Dipped plants were covered in bags and

kept in darkness overnight and were transferred to greenhouse conditions the following day.

Table 7.12. List of antibiotics and concentrations used.

Antibiotic	Concentration
Kanamycin	25 µg mL^{-1}
Rifampicin	50 µg mL^{-1}
Tetracyclin	5 µg mL^{-1}
Gentamycin	25 µg mL^{-1}
Spectinomycin	100 µg mL^{-1}

7.3. Plant phenotyping

7.3.1. Flowering time experiments

Flowering time was measured as the number of days to bolting and the number of days until the first flower opened. Bolting was defined as the time point at which the inflorescence stem reached 0.5 cm in height. The number of rosette leaves was counted after bolting. The number of cauline leaves on the primary inflorescence was counted. Leaves that subtended a flower were considered to be bracts. The height of the I1 zone was measured 2 weeks after the opening of the first flower, after I1 internodes ceased to elongate. The height of the I1 zone was defined as the distance from the rosette to the first silique. The number of cauline leaves on paraclades at the fifth I1 node was counted several weeks after flowering, after the secondary inflorescences had elongated and all cauline leaves had been initiated.

Internode length was measured as the stem length between nodes subtended by cauline leaves. If two nodes were present in close proximity, the corresponding internode had a length of zero centimetres. The mean rate of leaf initiation was approximated by dividing rosette leaf number by bolting time.

7.3.2. Rosette angle and leaf measurements

The divergence angle between successive rosette leaves was measured for plants grown for 5 weeks in short days. Plants were photographed from a top-down perspective using a Canon EOS 600D. The axis between the petiole and the midvein

was used to determine the divergence angle (Figure 7.3A). For leaf-shape scans, successive leaves of 4-week-old plants grown in short days were aligned on white paper, fixed with glue and scanned. Leaf shapes were visualized by thresholding the image contrast. The length/width ratio (LWR) was calculated from the maximum length and width dimensions of leaves (Figure 7.3B). All measurements were taken using the Fiji distribution of ImageJ software (Schindelin et al., 2012).

Figure 7.3. Examples of data acquisition for vegetative phenotypes. A) Divergence angle between two successive leaves in wild type. The angle was measured between the petiole/-midvein axes of successive leaves. B) Height and width parameters were taken from scans of aligned leaf blades.

7.4. Statistical analysis

All data were analysed using R version 4.0.3 and associated statistical packages (R core Team, 2020). Statistical differences were determined with one- or two-factor ANOVA comparisons. For clearly non-parametric data, a Kruskal-Wallis (KW) omnibus test was applied instead. If significant differences were identified, post-hoc multiple comparisons were performed. Tukey's HSD multiple comparison test was used to determine differences identified by ANOVA (both from base R) and a Nemenyi post-hoc test (PMCMRplus package) was used to analyse differences after the Kruskal-Wallis test (base R). A Levenes test of equal variance was employed to determine differences in sample variation. Each figure legend describes the statistical test that was applied. A bonferroni-corrected $p < 0.05$ was defined to determine significant differences.

Generalised additive models (GAMs, mgcv package Wood, 2012) were used to model and compare non-linear trends, including the abundance of miR156 and miR157 levels over time. The predicted 95% confidence interval was plotted alongside the GAM prediction. To determine statistically significant differences at specific time points, pairwise difference between GAM smoothing components were calculated according to the method used by Rose et al. (2012).

7.5. Expression analysis

7.5.1. cDNA synthesis using oligo(dT) primers

To quantify the expression of gene transcripts, total RNA was extracted using the RNeasy Plant Mini Kit (QIAGEN) and was subsequently treated with Ambion DNAse I (Thermo Fischer Scientific #AM2224) to remove contaminating gDNA. The first-strand cDNA was synthesised with SuperScript IV reverse transcriptase (Thermo Fischer Scientific catalogue #18090200), using 1 µg RNA and oligo(dT_{18}) primers. The resulting cDNA was diluted to 150 µL with distilled water.

7.5.2. cDNA synthesis using stem-loop primers

To quantify mature miR156 abundance via qRT-PCR, total RNA was extracted using the miRNAeasy Tissue/ Cells Advanced Mini Kit, following the manufacturer's protocol (QIAGEN, catalogue #217604). After extraction, the RNA was eluted to 30 µL RNase-free water and was treated with DNAse I.

Reverse transcription was performed using the SuperScript IV cDNA synthesis kit (ThermoFischer Scientific, catalogue #18091050), but followed a modified protocol using stem-loop primers, first introduced by Chen et al. (2005). Stem-loop primers are oligonucleotides that contain a secondary structure in addition to bases complementary to the miRNA of interest. To ensure consistent formation of secondary structures, the stem-loop primers were denatured at 95°C for 2 min followed by gradual cooling to 4°C as suggested by Tong et al. (2015). The subsequent pulsed reverse-transcription reaction followed the protocol described by Varkonyi-Gasic et al. (2007). The small nucleolar RNA 101 (snoR101) was included as a reference.

Table 7.13. Thermocycler program for pulsed reverse transcription.

Step		Temperature (°C)	Time
1.	Incubation	30	30 s
2.	Incubation	42	30 s
3.	Incubation	50	1 s
4.	Cycles		60×
5.	Inactivation	80	10 min

7.5.3. Quantification of gene expression via qRT-PCR

A single qPCR reaction consisted of 3 µL cDNA, 0.5 µL of each primer, 5 µL 5× iQ SYBR Green Supermix (Bio-Rad, #1708880) and 1 µL dH_2O. The primer efficiency was determined by qRT on a dilution series.

The ΔC_T method was used to calculate the relative expression (Livak and Schmittgen, 2001). The following equation was used to define ΔC_T:

$$\Delta\mathrm{CT} = \sqrt{\frac{eff_{Reference1}^{ctReference1} * eff_{Reference2}^{ctReference2}}{eff_{Target}^{ctTarget}}}$$

In cold-treatment experiments, $\Delta\Delta C_T$ values were calculated by normalising gene expression against that at the first experimental time point. *SERINE/THREONINE PROTEIN PHOSPHATASE 2A* (*PP2A*) and/or *PEROXIN4* (PEX4) were used as reference genes (Czechowski et al., 2005) in mRNA-based quantitative RT-PCR analyses. At least three independent biological replicates were included in each analysis. The qRT-PCR reactions used the iQ™ SYBR® green supermix (Bio-Rad catalogue #1708880) and the CFX386 Real Time Detection System (Bio-Rad catalogue #1855484).

Table 7.14. Mixture for a single qRT-PCR reaction using iQ-SYBR Green supermix.

Reagent	Volume/amount
ddH_2O	1.0 µL
iQ SYBR green supermix	5 µL
Forward primer (10 µM)	0.5 µL
Reverse primer (10 µM)	0.5 µL
Template cDNA	3 µL

Table 7.15. Thermocycler program for qRT-PCR.

PCR step		Temperature (°C)	Time
1.	Initial denaturation	95	3 min
2.	Denaturation	95	10 s
3.	Annealing and extension	60	40 s
4.	Plate read		
5.	Cycles		40×
6.	Melting curve	55 to 95	10 s/1°C

Table 7.16. List of oligonucleotides used for qPCR expression analysis.

Gene (accession)	Oligo-nucleotide number	Sequence	Notes
PP2A (At1g13320)	**AR216**	AAGCGGTTGTGGAGAACATGATACG	(Czechowski et al., 2005)
PP2A (At1g13320)	**AR217**	TGGAGAGCTTGATTTGCGAAATACCG	(Czechowski et al., 2005)
PEX4 (At5g25760)	**AR214**	TTACGAAGGCGGTGTTTTTC	(Czechowski et al., 2005)
PEX4(At5g25760)	**AR215**	GGCGAGGCGTGTATACATTT	(Czechowski et al., 2005)
AP1 (At1g69120)	**AR361**	ATGAGAGGTACTCTTACGCCGA	(Andrés et al., 2015)
AP1 (At1g69120)	**AR362**	CAAGTCTTCCCCAAGATAATGC	(Andrés et al., 2015)
SPL15 (At3g57920)	**AR336**	GCCACCGCCCATTTCAACCC	Annabel van Driel
SPL15 (At3g57920)	**AR337**	CGCCCGCGATGACTTCCCAA	Annabel van Driel
FUL (At5g60910)	**AR359**	TGGAGGAGGTTACGCAGTATTGA	Virginia Fernández

FUL (At5g60910)	**AR360**	TGCTCCAACTCTTCTTCAGTTCTTC	Virginia Fernández
SPL4 (At1g53160)	**AR367**	TGCGGCTTTGCCAAGTAGAT	This work
SPL4 (At1g53160)	**AR390**	ACACACTTTGTGTCTCCGGT	This work
MIR156A (At2g25095)	**AR283**	CTTCGTTCTCTATGTCTCAATCTCTC	(Yang et al., 2013)
MIR156A (At2g25095)	**AR284**	TGATTAAAGGCTAAAGGTCTCCTC	(Yang et al., 2013)
MIR156C (At4g31877)	**AR285**	GTGATAATGAGTGATGACTGATG	(Yang et al., 2013)
MIR156C (At4g31877)	**AR286**	GAAAACGTGACCGGGACCGAATCG	(Yang et al., 2013)
MIR157A (At1g66783)	**AR165**	AAAAGGTGATGACAGAAGGCTAGA	This work
MIR157A (At1g66783)	**AR166**	AGATGATGAGATACAATTCGGAGCA	This work
MIR157C (At3g18217)	**AR289**	CACACCGCATGTGGATGATAAAAT	This work
MIR157C (At3g18217)	**AR290**	AAGAGATAAAGGTGGTGACAGAAGT	This work
VENUS + GFP	**AR024**	GAGCTGAAGGGCATCGACTT	This work
VENUS + GFP	**AR025**	CTCGATGTTGTGGCGGATCT	This work
AtsnoR101	**AR300**	CTTCACAGGTAAGTTCGCTTG	(Porri et al., 2012)
AtsnoR101	**AR301**	AGCATCAGCAGACCAGTAGTT	(Porri et al., 2012)
miR156-F	**AR297**	TGACAGAAGAGAGTG	(Porri et al., 2012)
miR156-RT-key	**AR298**	CGCGAGCTCAGAATTAATACGACTCACTATACGCGGTGCTCAC	(Porri et al., 2012)
Universal reverse	**AR299**	CGCGAGCTCAGAATTAATACGA	(Varkonyi-Gasic et al., 2010)

7.5.4. sRNA sequencing experiment

At all time points, apices were harvested in three biological replicates. Samples were flash frozen in liquid nitrogen and were ground to a fine powder using a mortar and pestle. Small RNAs were extracted with the TraPR Small RNA Isolation Kit (Lexogen, catalogue number 128.24). Sample extraction and library preparation were carried out at the Max-Planck Genome Centre Cologne. Approximately 10 million single-end, 150-

bp reads were sequenced per sample using the Illumina HiSeq 3500 system. Raw reads were trimmed for adapter sequences using Cutadapt version 3.4. The parameters used selected for a minimum read length of 17 nucleotides and a minimum Illumina quality score of 20. Trimmed sequence reads were analysed with DeconSeq to filter out non-plant contaminations (Schmieder and Edwards, 2011).

Mapping of the sRNA reads to the Arabidopsis genome was performed with the Manatee tool (Handzlik et al., 2020) and used annotations from the Araport11 release (Cheng et al., 2017) that were supplemented with the miRbase 22 release (Kozomara et al., 2019). The annotations were limited to miRNAs, short-interfering RNAs and other non-coding RNAs. Other annotations, including protein-coding genes, were excluded from the analysis. The analysis was a collaboration with Dr. Vidya Oruganti.

7.5.5. Confocal imaging time courses

Samples were carefully dissected under a stereomicroscope and collected in 4% (w/v) paraformaldehyde in 1× phosphate-buffered saline solution (PBS, pH 7.0) on ice. Samples were vacuum-infiltrated at ~700 mbar for 30 minutes and subsequently fixed for 2 h at room temperature. After rinsing with 1× PBS, samples were placed in ClearSee (Kurihara et al., 2015) and were cleared for 2 to 5 days, depending on the sample thickness. Samples were stained by adding SCRI 2200 Renaissance (1 µL mL^{-1}) to the ClearSee solution and were incubated overnight.

Table 7.17. List of buffers used for confocal imaging.

Buffer	Components
10× PBS pH 7.0	1.5 M NaCl, 0.07M Na_2HPO_4, 0.03 M NaH_2PO_4 dissolved in dH_2O
Fixation buffer	1× PBS, 4 % (w/v) para-formaldehyde
ClearSee	10% (w/v) xylitol powder, 15% (w/v) sodium deoxycholate and 25% (w/v) urea dissolved in dH_2O

Confocal images were acquired with a Leica SP8 confocal. Samples were imaged with a 40× immersion objective (model HC PL APO CS2 40×/1.25 GLYC) on microscope slides using glycerol as immersion oil and ClearSee as mounting medium. SCRI 2200 Renaissance fluorescence was excited at 405 and emission with a wavelength between 430 nm and 470 nm was captured with PMT detectors. The VENUS, GFP and mCherry fluorophores were detected using more sensitive HyD detectors. GFP was excited at 488 nm and detected between 500 nm and 520 nm; VENUS was excited at 514 nm and detected between 520 nm and 535 nm and mCherry was excited at 552 nm and detected between 600 nm and 620 nm.

Images were acquired as Z-stacks in sequential mode. Images were processed in ImageJ, which involved applying consistent brightness settings and generating maximum intensity projections of 10 µm optical sections at the meristem centre. The imaging and processing parameters for fluorescent proteins were determined for the first time point and remained constant throughout the experiment, unless stated otherwise.

7.5.6. Data availability

All data and experimental procedures were stored on the electronic lab journal (Elab) and the biodata servers at the MPIPZ.

8. List of Abbreviations

Abbreviation	Definition
ABI3	ABSISIC ACID INSENSITIVE 3
AGL24	*AGAMOUS-LIKE 24*
AGO	ARGONAUTE
AMP1	ALTERED MERISTEM PROGRAM1
AP1	*APETALA1*
BRC1	BRANCHED1
bZIP	Basic Leucine Zipper
Cas9	CRISPR associated protein 9
CO	*CONSTANS*
CRISPR	Clustered Regularly Interspaced Short Palindromic Repeats
D-bodies	Dicing bodies
DCL1	DICER-like 1
ELA1	EUI-LIKE P450 A1
FAR1	FAR-RED IMPAIRED RESPONSE 1
FD	Transcription factor FD
FHY3	FAR-RED ELONGATED HYPOCOTYL3
FT	*FLOWERING LOCUS T*
FUL	*FRUITFULL*
FUSCA3	FUSCA3 transcription factor
GA	Gibberellic acid
Gent	Gentamycin
H3K27me3	Histone3 Lysin 27 trimethylation
HYL1	HYPONASTIC LEAVES 1
I1	Inflorescence phase 1
I2	Inflorescence phase 2
Kan	Kanamycin
LAFL	LEC1/ABI3/FUS3/LEC2 gene regulatory network
LEC2	LEAFY COTYLEDON 2
LFY	*LEAFY*
LWR	Length/Width Ratio
MIM156/MIM157	miR156/miR157-target mimicry
miR156	microRNA156
MIR156	*MICRORNA156* gene
MIR172	*MICRORNA172* gene
miRISC	miRNA-induced Silencing Complex
miRNA	MicroRNA

mRNA	Messenger RNA
msc-1D	*more and smaller cells 1-D*
NY-A8	NUCLEAR FACTOR Y subunit A8
PBS	phosphate-buffered saline solution
PFA	Paraformaldehyde
ppt	Phosphinothricin, Basta
PRC2	Polycomb Repressive Complex 2
pre-miRNA	precursor-microRNA
pri-miRNA	primary-microRNA
PTGS	Post-transcriptional gene silencing
Rif	Rifampicin
RISC	RNA-induced Silencing Complex
RNA	Ribonucleic acid
RNAPII	RNA Polymerase II
SAM	Shoot Apical Meristem
SBP	*SQUAMOSA PROMOTER BINDING PROTEIN*
SE	SERRATE
SL	Strigolactones
SMXL6/7/8	SUPPRESSOR OF MAX2 1-LIKE 6/7/8
SOC1	*SUPPRESSOR OF OVEREXPRESSION OF CONSTANS1*
Spec	Spectinomycin
SPL	*SQUAMOSA PROMOTER BINDING PROTEIN LIKE*
sRNAs	small RNAs
Tet	Tetracyclin
TPS1	Tre6P SYNTHETHASE 1
Tre6P	Trehalose-6-Phosphate
TSF	*TWIN SISTER OF FT*
VAL1/2	VIVIPAROUS/ABI3-LIKE1/2

9. List of Figures

10. References

Abe, M., Kobayashi, Y., Yamamoto, S., Daimon, Y., Yamaguchi, A., Ikeda, Y., Ichinoki, H., Notaguchi, M., Goto, K., and Araki, T. (2005). FD, a bZIP Protein Mediating Signals from the Floral Pathway Integrator FT at the Shoot Apex. Science *309*, 1052–1056. https://doi.org/10.1126/science.1115983.

Abe, M., Kosaka, S., Shibuta, M., Nagata, K., Uemura, T., Nakano, A., and Kaya, H. (2019). Transient activity of the florigen complex during the floral transition in Arabidopsis thaliana. Development *146*, dev171504. https://doi.org/10.1242/dev.171504.

Addo-Quaye, C., Eshoo, T.W., Bartel, D.P., and Axtell, M.J. (2008). Endogenous siRNA and miRNA Targets Identified by Sequencing of the Arabidopsis Degradome. Curr. Biol. *18*, 758–762. https://doi.org/10.1016/j.cub.2008.04.042.

Aguilar-Martínez, J.A., Poza-Carrión, C., and Cubas, P. (2007). Arabidopsis BRANCHED1 Acts as an Integrator of Branching Signals within Axillary Buds. Plant Cell *19*, 458–472. https://doi.org/10.1105/tpc.106.048934.

Andrés, F., Porri, A., Torti, S., Mateos, J., Romera-Branchat, M., García-Martínez, J.L., Fornara, F., Gregis, V., Kater, M.M., and Coupland, G. (2014). SHORT VEGETATIVE PHASE reduces gibberellin biosynthesis at the Arabidopsis shoot apex to regulate the floral transition. Proc. Natl. Acad. Sci. *111*, E2760–E2769. https://doi.org/10.1073/pnas.1409567111.

Andrés, F., Romera-Branchat, M., Martínez-Gallegos, R., Patel, V., Schneeberger, K., Jang, S., Altmüller, J., Nürnberg, P., and Coupland, G. (2015). Floral Induction in Arabidopsis by FLOWERING LOCUS T Requires Direct Repression of *BLADE-ON-PETIOLE* Genes by the Homeodomain Protein PENNYWISE. Plant Physiol. *169*, 2187–2199. https://doi.org/10.1104/pp.15.00960.

Arazi, T., Talmor-Neiman, M., Stav, R., Riese, M., Huijser, P., and Baulcombe, D.C. (2005). Cloning and characterization of micro-RNAs from moss. Plant J. *43*, 837–848. https://doi.org/10.1111/j.1365-313X.2005.02499.x.

Arribas-Hernández, L., Kielpinski, L.J., and Brodersen, P. (2016). mRNA Decay of Most Arabidopsis miRNA Targets Requires Slicer Activity of AGO11. Plant Physiol. *171*, 2620–2632. https://doi.org/10.1104/pp.16.00231.

Aukerman, M.J., and Sakai, H. (2003). Regulation of Flowering Time and Floral Organ Identity by a MicroRNA and Its *APETALA2-Like* Target Genes. Plant Cell *15*, 2730–2741. https://doi.org/10.1105/tpc.016238.

Axtell, M.J., Snyder, J.A., and Bartel, D.P. (2007). Common Functions for Diverse Small RNAs of Land Plants. Plant Cell *19*, 1750–1769. https://doi.org/10.1105/tpc.107.051706.

Balanzà, V., Martínez-Fernández, I., Sato, S., Yanofsky, M.F., Kaufmann, K., Angenent, G.C., Bemer, M., and Ferrándiz, C. (2018). Genetic control of meristem arrest and life span in Arabidopsis by a FRUITFULL-APETALA2 pathway. Nat. Commun. *9*, 1–9. https://doi.org/10.1038/s41467-018-03067-5.

Baranauskė, S., Mickutė, M., Plotnikova, A., Finke, A., Venclovas, Č., Klimašauskas, S., and Vilkaitis, G. (2015). Functional mapping of the plant small RNA methyltransferase: HEN1 physically interacts with HYL1 and DICER-LIKE 1 proteins. Nucleic Acids Res. *43*, 2802–2812. https://doi.org/10.1093/nar/gkv102.

Barrera-Rojas, C.H., Rocha, G.H.B., Polverari, L., Brito, D.A.P., Batista, D.S., Notini, M.M., da Cruz, A.C.F., Morea, E.G.O., Sabatini, S., Otoni, W.C., et al. (2019). miR156-targeted SPL10 controls root meristem activity and root-derived de novo shoot regeneration via cytokinin responses. J. Exp. Bot. https://doi.org/10.1093/jxb/erz475.

Barton, M.K. (2010). Twenty years on: The inner workings of the shoot apical meristem, a developmental dynamo. Dev. Biol. *341*, 95–113. https://doi.org/10.1016/j.ydbio.2009.11.029.

Basile, A., Fambrini, M., and Pugliesi, C. (2017). The vascular plants: open system of growth. Dev. Genes Evol. *227*, 129–157. https://doi.org/10.1007/s00427-016-0572-1.

Baum, D.A., and Day, C.D. (2004). Cryptic Bracts Exposed: Insights into the Regulation of Leaf Expansion. Dev. Cell *6*, 318–319. https://doi.org/10.1016/S1534-5807(04)00071-1.

Bäurle, I., and Dean, C. (2006). The Timing of Developmental Transitions in Plants. Cell *125*, 655–664. https://doi.org/10.1016/j.cell.2006.05.005.

Bergonzi, S., Albani, M.C., Themaat, E.V.L. van, Nordström, K.J.V., Wang, R., Schneeberger, K., Moerland, P.D., and Coupland, G. (2013). Mechanisms of Age-Dependent Response to Winter Temperature in Perennial Flowering of *Arabis alpina*. Science *340*, 1094–1097. https://doi.org/10.1126/science.1234116.

Bernier, G. (1988). The Control of Floral Evocation and Morphogenesis. Annu. Rev. Plant Physiol. Plant Mol. Biol. *39*, 175–219. https://doi.org/10.1146/annurev.pp.39.060188.001135.

Birkenbihl, R.P., Jach, G., Saedler, H., and Huijser, P. (2005). Functional Dissection of the Plant-specific SBP-Domain: Overlap of the DNA-binding and Nuclear Localization Domains. J. Mol. Biol. *352*, 585–596. https://doi.org/10.1016/j.jmb.2005.07.013.

Blázquez, M.A., Green, R., Nilsson, O., Sussman, M.R., and Weigel, D. (1998). Gibberellins Promote Flowering of Arabidopsis by Activating the *LEAFY* Promoter. Plant Cell *10*, 791–800. https://doi.org/10.1105/tpc.10.5.791.

Böhlenius, H., Huang, T., Charbonnel-Campaa, L., Brunner, A.M., Jansson, S., Strauss, S.H., and Nilsson, O. (2006). CO/FT Regulatory Module Controls Timing of Flowering and Seasonal Growth Cessation in Trees. Science *312*, 1040–1043. https://doi.org/10.1126/science.1126038.

Bologna, N.G., Mateos, J.L., Bresso, E.G., and Palatnik, J.F. (2009). A loop-to-base processing mechanism underlies the biogenesis of plant microRNAs miR319 and miR159. EMBO J. *28*, 3646–3656. https://doi.org/10.1038/emboj.2009.292.

Bologna, N.G., Schapire, A.L., Zhai, J., Chorostecki, U., Boisbouvier, J., Meyers, B.C., and Palatnik, J.F. (2013). Multiple RNA recognition patterns during microRNA biogenesis in plants. Genome Res. *23*, 1675–1689. https://doi.org/10.1101/gr.153387.112.

Bologna, N.G., Iselin, R., Abriata, L.A., Sarazin, A., Pumplin, N., Jay, F., Grentzinger, T., Dal Peraro, M., and Voinnet, O. (2018). Nucleo-cytosolic Shuttling of ARGONAUTE1 Prompts a Revised Model of the Plant MicroRNA Pathway. Mol. Cell *69*, 709-719.e5. https://doi.org/10.1016/j.molcel.2018.01.007.

Borner, R., Kampmann, G., Chandler, J., Gleißner, R., Wisman, E., Apel, K., and Melzer, S. (2000). A MADS domain gene involved in the transition to flowering in Arabidopsis. Plant J. *24*, 591–599. https://doi.org/10.1046/j.1365-313x.2000.00906.x.

Bowman, J.L., and Eshed, Y. (2000). Formation and maintenance of the shoot apical meristem. Trends Plant Sci. *5*, 110–115. https://doi.org/10.1016/S1360-1385(00)01569-7.

Breuil-Broyer, S., Morel, P., De Almeida-Engler, J., Coustham, V., Negrutiu, I., and Trehin, C. (2004). High-resolution boundary analysis during *Arabidopsis thaliana* flower development. Plant J. *38*, 182–192. https://doi.org/10.1111/j.1365-313X.2004.02026.x.

Brioudes, F., Jay, F., Sarazin, A., Grentzinger, T., Devers, E., and Voinnet, O. (2021). HASTY, the Arabidopsis EXPORTIN5 ortholog, regulates cell-to-cell and vascular microRNA movement. EMBO J. *40*, e107455. https://doi.org/10.15252/embj.2020107455.

Brodersen, P., Sakvarelidze-Achard, L., Bruun-Rasmussen, M., Dunoyer, P., Yamamoto, Y.Y., Sieburth, L., and Voinnet, O. (2008). Widespread Translational Inhibition by Plant miRNAs and siRNAs. Science *320*, 1185–1190. https://doi.org/10.1126/science.1159151.

Brosnan, C.A., and Voinnet, O. (2011). Cell-to-cell and long-distance siRNA movement in plants: mechanisms and biological implications. Curr. Opin. Plant Biol. *14*, 580–587. https://doi.org/10.1016/j.pbi.2011.07.011.

Buendía-Monreal, M., and Gillmor, C.S. (2017). Convergent repression of miR156 by sugar and the CDK8 module of Arabidopsis Mediator. Dev. Biol. *423*, 19–23. https://doi.org/10.1016/j.ydbio.2017.01.007.

Buhtz, A., Springer, F., Chappell, L., Baulcombe, D.C., and Kehr, J. (2008). Identification and characterization of small RNAs from the phloem of Brassica napus. Plant J. *53*, 739–749. https://doi.org/10.1111/j.1365-313X.2007.03368.x.

Cambiagno, D.A., Giudicatti, A.J., Arce, A.L., Gagliardi, D., Li, L., Yuan, W., Lundberg, D.S., Weigel, D., and Manavella, P.A. (2021). HASTY modulates miRNA biogenesis by linking pri-miRNA transcription and processing. Mol. Plant *14*, 426–439. https://doi.org/10.1016/j.molp.2020.12.019.

Cardon, G., Höhmann, S., Klein, J., Nettesheim, K., Saedler, H., and Huijser, P. (1999). Molecular characterisation of the Arabidopsis *SBP-box* genes. Gene *237*, 91–104. https://doi.org/10.1016/S0378-1119(99)00308-X.

Cardon, G.H., Höhmann, S., Nettesheim, K., Saedler, H., and Huijser, P. (1997). Functional analysis of the *Arabidopsis thaliana SBP-box* gene *SPL3*: a novel gene involved in the floral transition. Plant J. *12*, 367–377. https://doi.org/10.1046/j.1365-313X.1997.12020367.x.

Carlsbecker, A., Lee, J.-Y., Roberts, C.J., Dettmer, J., Lehesranta, S., Zhou, J., Lindgren, O., Moreno-Risueno, M.A., Vatén, A., Thitamadee, S., et al. (2010). Cell signalling by microRNA165/6 directs gene dose-dependent root cell fate. Nature *465*, 316–321. https://doi.org/10.1038/nature08977.

Chandler, J.W. (2012). Floral meristem initiation and emergence in plants. Cell. Mol. Life Sci. *69*, 3807–3818. https://doi.org/10.1007/s00018-012-0999-0.

Chao, L.-M., Liu, Y.-Q., Chen, D.-Y., Xue, X.-Y., Mao, Y.-B., and Chen, X.-Y. (2017). Arabidopsis Transcription Factors SPL1 and SPL12 Confer Plant Thermotolerance at Reproductive Stage. Mol. Plant *10*, 735–748. https://doi.org/10.1016/j.molp.2017.03.010.

Chen, X. (2004). A MicroRNA as a Translational Repressor of *APETALA2* in Arabidopsis Flower Development. Science *303*, 2022–2025. https://doi.org/10.1126/science.1088060.

Chen, C., Ridzon, D.A., Broomer, A.J., Zhou, Z., Lee, D.H., Nguyen, J.T., Barbisin, M., Xu, N.L., Mahuvakar, V.R., Andersen, M.R., et al. (2005). Real-time quantification of microRNAs by stem–loop RT–PCR. Nucleic Acids Res. *33*, e179. https://doi.org/10.1093/nar/gni178.

Chen, N., Veerappan, V., Abdelmageed, H., Kang, M., and Allen, R.D. (2018a). HSI2/VAL1 Silences *AGL15* to Regulate the Developmental Transition from Seed Maturation to Vegetative Growth in Arabidopsis. Plant Cell *30*, 600–619. https://doi.org/10.1105/tpc.17.00655.

Chen, Q., Payyavula, R.S., Chen, L., Zhang, J., Zhang, C., and Turgeon, R. (2018b). FLOWERING LOCUS T mRNA is synthesized in specialized companion cells in Arabidopsis and Maryland Mammoth tobacco leaf veins. Proc. Natl. Acad. Sci. *115*, 2830–2835. https://doi.org/10.1073/pnas.1719455115.

Cheng, C.-Y., Krishnakumar, V., Chan, A.P., Thibaud-Nissen, F., Schobel, S., and Town, C.D. (2017). Araport11: a complete reannotation of the *Arabidopsis thaliana* reference genome. Plant J. *89*, 789–804. https://doi.org/10.1111/tpj.13415.

Cheng, Y.-J., Shang, G.-D., Xu, Z.-G., Yu, S., Wu, L.-Y., Zhai, D., Tian, S.-L., Gao, J., Wang, L., and Wang, J.-W. (2021). Cell division in the shoot apical meristem is a trigger for miR156 decline and vegetative phase transition in Arabidopsis. Proc. Natl. Acad. Sci. *118*. https://doi.org/10.1073/pnas.2115667118.

Chitwood, D.H., Nogueira, F.T.S., Howell, M.D., Montgomery, T.A., Carrington, J.C., and Timmermans, M.C.P. (2009). Pattern formation via small RNA mobility. Genes Dev. *23*, 549–554. https://doi.org/10.1101/gad.1770009.

Cho, S.H., Coruh, C., and Axtell, M.J. (2012). miR156 and miR390 regulate tasiRNA accumulation and developmental timing in *Physcomitrella patens*. Plant Cell *24*, 4837–4849. https://doi.org/10.1105/tpc.112.103176.

Chorostecki, U., Moro, B., Rojas, A.M.L., Debernardi, J.M., Schapire, A.L., Notredame, C., and Palatnik, J.F. (2017). Evolutionary Footprints Reveal Insights into Plant MicroRNA Biogenesis. Plant Cell *29*, 1248–1261. https://doi.org/10.1105/tpc.17.00272.

Chuck, G., Cigan, A.M., Saeteurn, K., and Hake, S. (2007). The heterochronic maize mutant *Corngrass1* results from overexpression of a tandem microRNA. Nat. Genet. *39*, 544–549. https://doi.org/10.1038/ng2001.

Chuck, G., Whipple, C., Jackson, D., and Hake, S. (2010). The maize SBP-box transcription factor encoded by *tasselsheath4* regulates bract development and the establishment of meristem boundaries. Development *137*, 1243–1250. https://doi.org/10.1242/dev.048348.

Chuck, G.S., Brown, P.J., Meeley, R., and Hake, S. (2014). Maize SBP-box transcription factors unbranched2 and unbranched3 affect yield traits by regulating the rate of lateral primordia initiation. Proc. Natl. Acad. Sci. *111*, 18775–18780. https://doi.org/10.1073/pnas.1407401112.

Clark, S.E., Running, M.P., and Meyerowitz, E.M. (1995). *CLAVATA3* is a specific regulator of shoot and floral meristem development affecting the same processes as *CLAVATA1*. Development *121*, 2057–2067. https://doi.org/10.1242/dev.121.7.2057.

Clarke, J.H., Tack, D., Findlay, K., Van Montagu, M., and Van Lijsebettens, M. (1999). The *SERRATE* locus controls the formation of the early juvenile leaves and phase length in Arabidopsis. Plant J. *20*, 493–501. https://doi.org/10.1046/j.1365-313x.1999.00623.x.

Clough, S.J., and Bent, A.F. (1998). Floral dip: a simplified method for Agrobacterium-mediated transformation of *Arabidopsis thaliana*. Plant J. *16*, 735–743. https://doi.org/10.1046/j.1365-313x.1998.00343.x.

Cockcroft, C.E., den Boer, B.G.W., Healy, J.M.S., and Murray, J.A.H. (2000). Cyclin D control of growth rate in plants. Nature *405*, 575–579. https://doi.org/10.1038/35014621.

Collani, S., Neumann, M., Yant, L., and Schmid, M. (2019). FT Modulates Genome-Wide DNA-Binding of the bZIP Transcription Factor FD. Plant Physiol. *180*, 367–380. https://doi.org/10.1104/pp.18.01505.

Connell, J.P., and Furman, W. (1984). The Study of Transitions. In Continuities and Discontinuities in Development, R.N. Emde, and R.J. Harmon, eds. (Boston, MA: Springer US), pp. 153–173.

Conti, L., and Bradley, D. (2007). TERMINAL FLOWER1 Is a Mobile Signal Controlling Arabidopsis Architecture. Plant Cell *19*, 767–778. https://doi.org/10.1105/tpc.106.049767.

Corbesier, L., Vincent, C., Jang, S., Fornara, F., Fan, Q., Searle, I., Giakountis, A., Farrona, S., Gissot, L., Turnbull, C., et al. (2007). FT Protein Movement Contributes to Long-Distance Signaling in Floral Induction of Arabidopsis. Science *316*, 1030–1033. https://doi.org/10.1126/science.1141752.

Cui, L., Zheng, F., Wang, J., Zhang, C., Xiao, F., Ye, J., Li, C., Ye, Z., and Zhang, J. (2020). miR156a-targeted SBP-Box transcription factor SlSPL13 regulates inflorescence morphogenesis by directly activating *SFT* in tomato. Plant Biotechnol. J. *18*, 1670–1682. https://doi.org/10.1111/pbi.13331.

Cui, L.-G., Shan, J.-X., Shi, M., Gao, J.-P., and Lin, H.-X. (2014). The miR156-SPL9-DFR pathway coordinates the relationship between development and abiotic stress tolerance in plants. Plant J. *80*, 1108–1117. https://doi.org/10.1111/tpj.12712.

Czechowski, T., Stitt, M., Altmann, T., Udvardi, M.K., and Scheible, W.-R. (2005). Genome-wide identification and testing of superior reference genes for transcript normalization in Arabidopsis. Plant Physiol. *139*, 5–17. https://doi.org/10.1104/pp.105.063743.

Dalmadi, Á., Gyula, P., Bálint, J., Szittya, G., and Havelda, Z. (2019). AGO-unbound cytosolic pool of mature miRNAs in plant cells reveals a novel regulatory step at AGO1 loading. Nucleic Acids Res. *47*, 9803–9817. https://doi.org/10.1093/nar/gkz690.

Dong, Z., Han, M.-H., and Fedoroff, N. (2008). The RNA-binding proteins HYL1 and SE promote accurate in vitro processing of pri-miRNA by DCL1. Proc. Natl. Acad. Sci. *105*, 9970–9975. https://doi.org/10.1073/pnas.0803356105.

van Driel, A.D. (2021). Characterisation of Transcription Factor SPL15, an Integrator of Multiple Flowering Time Pathways. Doctoral dissertation. Universität zu Köln.

Eamens, A.L., Smith, N.A., Curtin, S.J., Wang, M.-B., and Waterhouse, P.M. (2009). The *Arabidopsis thaliana* double-stranded RNA binding protein DRB1 directs guide strand selection from microRNA duplexes. RNA *15*, 2219–2235. https://doi.org/10.1261/rna.1646909.

Eastmond, P.J., Van Dijken, A.J.H., Spielman, M., Kerr, A., Tissier, A.F., Dickinson, H.G., Jones, J.D.G., Smeekens, S.C., and Graham, I.A. (2002). Trehalose-6-phosphate synthase 1, which catalyses the first step in trehalose synthesis, is essential

for Arabidopsis embryo maturation. Plant J. *29*, 225–235. https://doi.org/10.1046/j.1365-313x.2002.01220.x.

Ebert, M.S., and Sharp, P.A. (2012). Roles for MicroRNAs in Conferring Robustness to Biological Processes. Cell *149*, 515–524. https://doi.org/10.1016/j.cell.2012.04.005.

Eriksson, S., Böhlenius, H., Moritz, T., and Nilsson, O. (2006). GA4 Is the Active Gibberellin in the Regulation of *LEAFY* Transcription and Arabidopsis Floral Initiation. Plant Cell *18*, 2172–2181. https://doi.org/10.1105/tpc.106.042317.

Fahlgren, N., Jogdeo, S., Kasschau, K.D., Sullivan, C.M., Chapman, E.J., Laubinger, S., Smith, L.M., Dasenko, M., Givan, S.A., Weigel, D., et al. (2010). *MicroRNA* Gene Evolution in *Arabidopsis lyrata* and *Arabidopsis thaliana*. Plant Cell *22*, 1074–1089. https://doi.org/10.1105/tpc.110.073999.

Fang, Y., and Spector, D.L. (2007). Identification of Nuclear Dicing Bodies Containing Proteins for MicroRNA Biogenesis in Living Arabidopsis Plants. Curr. Biol. *17*, 818–823. https://doi.org/10.1016/j.cub.2007.04.005.

Fang, X., Cui, Y., Li, Y., and Qi, Y. (2015). Transcription and processing of primary microRNAs are coupled by Elongator complex in Arabidopsis. Nat. Plants *1*, 1–9. https://doi.org/10.1038/nplants.2015.75.

Fátyol, K., Ludman, M., and Burgyán, J. (2016). Functional dissection of a plant Argonaute. Nucleic Acids Res. *44*, 1384–1397. https://doi.org/10.1093/nar/gkv1371.

Feng, S., Xu, Y., Guo, C., Zheng, J., Zhou, B., Zhang, Y., Ding, Y., Zhang, L., Zhu, Z., Wang, H., et al. (2016). Modulation of miR156 to identify traits associated with vegetative phase change in tobacco (*Nicotiana tabacum*). J. Exp. Bot. *67*, 1493–1504. https://doi.org/10.1093/jxb/erv551.

Ferrandiz, C., Gu, Q., Martienssen, R., and Yanofsky, M.F. (2000). Redundant regulation of meristem identity and plant architecture by *FRUITFULL*, *APETALA1* and *CAULIFLOWER*. Development *127*, 725–734. .

Fichtner, F., and Lunn, J.E. (2021). The Role of Trehalose 6-Phosphate (Tre6P) in Plant Metabolism and Development. Annu. Rev. Plant Biol. *72*, 737–760. https://doi.org/10.1146/annurev-arplant-050718-095929.

Fletcher, J.C., Brand, U., Running, M.P., Simon, R., and Meyerowitz, E.M. (1999). Signaling of Cell Fate Decisions by CLAVATA3 in Arabidopsis Shoot Meristems. Science *283*, 1911–1914. https://doi.org/10.1126/science.283.5409.1911.

Förderer, A., Zhou, Y., and Turck, F. (2016). The age of multiplexity: recruitment and interactions of Polycomb complexes in plants. Curr. Opin. Plant Biol. *29*, 169–178. https://doi.org/10.1016/j.pbi.2015.11.010.

Fouracre, J.P., He, J., Chen, V.J., Sidoli, S., and Poethig, R.S. (2021). *VAL* genes regulate vegetative phase change via miR156-dependent and independent

mechanisms. PLOS Genet. *17*, e1009626. https://doi.org/10.1371/journal.pgen.1009626.

Franco-Zorrilla, J.M., Valli, A., Todesco, M., Mateos, I., Puga, M.I., Rubio-Somoza, I., Leyva, A., Weigel, D., García, J.A., and Paz-Ares, J. (2007). Target mimicry provides a new mechanism for regulation of microRNA activity. Nat. Genet. *39*, 1033–1037. https://doi.org/10.1038/ng2079.

Fuchs, M., and Lohmann, J.U. (2020). Aiming for the top: non-cell autonomous control of shoot stem cells in Arabidopsis. J. Plant Res. *133*, 297–309. https://doi.org/10.1007/s10265-020-01174-3.

Galvão, V.C., Horrer, D., Küttner, F., and Schmid, M. (2012). Spatial control of flowering by DELLA proteins in *Arabidopsis thaliana*. Development dev.080879. https://doi.org/10.1242/dev.080879.

Gandikota, M., Birkenbihl, R.P., Höhmann, S., Cardon, G.H., Saedler, H., and Huijser, P. (2007). The miRNA156/157 recognition element in the 3′ UTR of the Arabidopsis SBP box gene *SPL3* prevents early flowering by translational inhibition in seedlings. Plant J. *49*, 683–693. https://doi.org/10.1111/j.1365-313X.2006.02983.x.

Gao, J., Zhang, K., Cheng, Y.-J., Yu, S., Shang, G.-D., Wang, F.-X., Wu, L.-Y., Xu, Z.-G., Mai, Y.-X., Zhao, X.-Y., et al. (2022). A robust mechanism for resetting juvenility during each generation in Arabidopsis. Nat. Plants *8*, 257–268. https://doi.org/10.1038/s41477-022-01110-4.

Gibson, D.G., Young, L., Chuang, R.-Y., Venter, J.C., Hutchison, C.A., and Smith, H.O. (2009). Enzymatic assembly of DNA molecules up to several hundred kilobases. Nat. Methods *6*, 343–345. https://doi.org/10.1038/nmeth.1318.

Grbić, V., and Bleecker, A.B. (2000). Axillary meristem development in *Arabidopsis thaliana*. Plant J. *21*, 215–223. https://doi.org/10.1046/j.1365-313x.2000.00670.x.

Grentzinger, T., Oberlin, S., Schott, G., Handler, D., Svozil, J., Barragan-Borrero, V., Humbert, A., Duharcourt, S., Brennecke, J., and Voinnet, O. (2020). A universal method for the rapid isolation of all known classes of functional silencing small RNAs. Nucleic Acids Res. *48*, e79–e79. https://doi.org/10.1093/nar/gkaa472.

Grosberg, R.K., and Strathmann, R.R. (2007). The Evolution of Multicellularity: A Minor Major Transition? Annu. Rev. Ecol. Evol. Syst. *38*, 621–654. https://doi.org/10.1146/annurev.ecolsys.36.102403.114735.

Gu, Q., Ferrandiz, C., Yanofsky, M.F., and Martienssen, R. (1998). The *FRUITFULL MADS-box* gene mediates cell differentiation during Arabidopsis fruit development. Development *125*, 1509–1517. https://doi.org/10.1242/dev.125.8.1509.

Guo, Z., Kuang, Z., Wang, Y., Zhao, Y., Tao, Y., Cheng, C., Yang, J., Lu, X., Hao, C., Wang, T., et al. (2020). PmiREN: a comprehensive encyclopedia of plant miRNAs. Nucleic Acids Res. *48*, D1114–D1121. https://doi.org/10.1093/nar/gkz894.

Han, M.-H., Goud, S., Song, L., and Fedoroff, N. (2004). The Arabidopsis double-stranded RNA-binding protein HYL1 plays a role in microRNA-mediated gene regulation. Proc. Natl. Acad. Sci. *101*, 1093–1098. https://doi.org/10.1073/pnas.0307969100.

Handzlik, J.E., Tastsoglou, S., Vlachos, I.S., and Hatzigeorgiou, A.G. (2020). Manatee: detection and quantification of small non-coding RNAs from next-generation sequencing data. Sci. Rep. *10*, 705. https://doi.org/10.1038/s41598-020-57495-9.

He, J., Xu, M., Willmann, M.R., McCormick, K., Hu, T., Yang, L., Starker, C.G., Voytas, D.F., Meyers, B.C., and Poethig, R.S. (2018). Threshold-dependent repression of *SPL* gene expression by miR156/miR157 controls vegetative phase change in *Arabidopsis thaliana*. PLoS Genet. *14*. https://doi.org/10.1371/journal.pgen.1007337.

Hempel, F.D. (1997). FORCING VEGETATIVE PRIMORDIA TO BECOME FLOWERS: ARABIDOPSIS “CONVERSIONS.” Flower. Newsl. 33–39. .

Hempel, F.D., and Feldman, L.J. (1994). Bi-directional inflorescence development in Arabidopsis thaliana: Acropetal initiation of flowers and basipetal initiation of paraclades. Planta *192*, 276–286. .

Hiraoka, K., Yamaguchi, A., Abe, M., and Araki, T. (2013). The Florigen Genes *FT* and *TSF* Modulate Lateral Shoot Outgrowth in *Arabidopsis thaliana*. Plant Cell Physiol. *54*, 352–368. https://doi.org/10.1093/pcp/pcs168.

Hu, T., Manuela, D., Hinsch, V., and Xu, M. (2022). PICKLE associates with histone deacetylase 9 to mediate vegetative phase change in Arabidopsis. New Phytol. *n/a*. https://doi.org/10.1111/nph.18174.

Hyun, Y., Kim, J., Cho, S.W., Choi, Y., Kim, J.-S., and Coupland, G. (2015). Site-directed mutagenesis in Arabidopsis thaliana using dividing tissue-targeted RGEN of the CRISPR/Cas system to generate heritable null alleles. Planta *241*, 271–284. https://doi.org/10.1007/s00425-014-2180-5.

Hyun, Y., Richter, R., Vincent, C., Martinez-Gallegos, R., Porri, A., and Coupland, G. (2016). Multi-layered Regulation of SPL15 and Cooperation with SOC1 Integrate Endogenous Flowering Pathways at the Arabidopsis Shoot Meristem. Dev. Cell *37*, 254–266. https://doi.org/10.1016/j.devcel.2016.04.001.

Hyun, Y., Vincent, C., Tilmes, V., Bergonzi, S., Kiefer, C., Richter, R., Martinez-Gallegos, R., Severing, E., and Coupland, G. (2019). A regulatory circuit conferring varied flowering response to cold in annual and perennial plants. Science *363*, 409–412. https://doi.org/10.1126/science.aau8197.

Immink, R.G.H., Posé, D., Ferrario, S., Ott, F., Kaufmann, K., Valentim, F.L., Folter, S. de, Wal, F. van der, Dijk, A.D.J. van, Schmid, M., et al. (2012). Characterization of SOC1’s Central Role in Flowering by the Identification of Its Upstream and Downstream Regulators. Plant Physiol. *160*, 433–449. https://doi.org/10.1104/pp.112.202614.

Iwata, Y., Takahashi, M., Fedoroff, N.V., and Hamdan, S.M. (2013). Dissecting the interactions of SERRATE with RNA and DICER-LIKE 1 in Arabidopsis microRNA precursor processing. Nucleic Acids Res. *41*, 9129–9140. https://doi.org/10.1093/nar/gkt667.

Jacqmard, A., Gadisseur, I., and Bernier, G. (2003). Cell Division and Morphological Changes in the Shoot Apex of *Arabidopsis thaliana* during Floral Transition. Ann. Bot. *91*, 571–576. https://doi.org/10.1093/aob/mcg053.

Jaeger, K.E., and Wigge, P.A. (2007). FT Protein Acts as a Long-Range Signal in Arabidopsis. Curr. Biol. *17*, 1050–1054. https://doi.org/10.1016/j.cub.2007.05.008.

Jang, S., Torti, S., and Coupland, G. (2009). Genetic and spatial interactions between *FT*, *TSF* and *SVP* during the early stages of floral induction in Arabidopsis. Plant J. *60*, 614–625. https://doi.org/10.1111/j.1365-313X.2009.03986.x.

Jia, H., Suzuki, M., and McCarty, D.R. (2014). Regulation of the seed to seedling developmental phase transition by the LAFL and VAL transcription factor networks. Wiley Interdiscip. Rev. Dev. Biol. *3*, 135–145. https://doi.org/10.1002/wdev.126.

Jiang, X., Lubini, G., Hernandes-Lopes, J., Rijnsburger, K., Veltkamp, V., de Maagd, R.A., Angenent, G.C., and Bemer, M. (2022). *FRUITFULL-like* genes regulate flowering time and inflorescence architecture in tomato. Plant Cell *34*, 1002–1019. https://doi.org/10.1093/plcell/koab298.

Jiao, Y., Wang, Y., Xue, D., Wang, J., Yan, M., Liu, G., Dong, G., Zeng, D., Lu, Z., Zhu, X., et al. (2010). Regulation of *OsSPL14* by OsmiR156 defines ideal plant architecture in rice. Nat. Genet. *42*, 541–544. https://doi.org/10.1038/ng.591.

Jones-Rhoades, M.W., and Bartel, D.P. (2004). Computational Identification of Plant MicroRNAs and Their Targets, Including a Stress-Induced miRNA. Mol. Cell *14*, 787–799. https://doi.org/10.1016/j.molcel.2004.05.027.

Jones-Rhoades, M.W., Bartel, D.P., and Bartel, B. (2006). MicroRNAs AND THEIR REGULATORY ROLES IN PLANTS. Annu. Rev. Plant Biol. *57*, 19–53. https://doi.org/10.1146/annurev.arplant.57.032905.105218.

Joshua-Tor, L., and Hannon, G.J. (2011). Ancestral Roles of Small RNAs: An Ago-Centric Perspective. Cold Spring Harb. Perspect. Biol. *3*, a003772. https://doi.org/10.1101/cshperspect.a003772.

Jung, J.-H., Seo, P.J., Kang, S.K., and Park, C.-M. (2011). miR172 signals are incorporated into the miR156 signaling pathway at the SPL3/4/5 genes in Arabidopsis developmental transitions. Plant Mol. Biol. *76*, 35–45. https://doi.org/10.1007/s11103-011-9759-z.

Jung, J.-H., Ju, Y., Seo, P.J., Lee, J.-H., and Park, C.-M. (2012). The SOC1-SPL module integrates photoperiod and gibberellic acid signals to control flowering time in Arabidopsis. Plant J. *69*, 577–588. https://doi.org/10.1111/j.1365-313X.2011.04813.x.

Jung, J.-H., Lee, H.-J., Ryu, J.Y., and Park, C.-M. (2016). SPL3/4/5 Integrate Developmental Aging and Photoperiodic Signals into the FT-FD Module in Arabidopsis Flowering. Mol. Plant *9*, 1647–1659. https://doi.org/10.1016/j.molp.2016.10.014.

Karim, Md.R., Hirota, A., Kwiatkowska, D., Tasaka, M., and Aida, M. (2009). A Role for Arabidopsis PUCHI in Floral Meristem Identity and Bract Suppression. Plant Cell *21*, 1360–1372. https://doi.org/10.1105/tpc.109.067025.

Kaufmann, K., and Airoldi, C.A. (2018). Master Regulatory Transcription Factors in Plant Development: A Blooming Perspective. In Plant Transcription Factors: Methods and Protocols, N. Yamaguchi, ed. (New York, NY: Springer), pp. 3–22.

Kawakatsu, T., Itoh, J.-I., Miyoshi, K., Kurata, N., Alvarez, N., Veit, B., and Nagato, Y. (2006). PLASTOCHRON2 Regulates Leaf Initiation and Maturation in Rice. Plant Cell *18*, 612. https://doi.org/10.1105/tpc.105.037622.

Kerstetter, R.A., and Poethig, R.S. (1998). The Specification of Leaf Identity During Shoot Development. Annu. Rev. Cell Dev. Biol. *14*, 373–398. https://doi.org/10.1146/annurev.cellbio.14.1.373.

Kidner, C.A., and Martienssen, R.A. (2004). Spatially restricted microRNA directs leaf polarity through ARGONAUTE1. Nature *428*, 81–84. https://doi.org/10.1038/nature02366.

Kim, J.J., Lee, J.H., Kim, W., Jung, H.S., Huijser, P., and Ahn, J.H. (2012). The microRNA156-SQUAMOSA PROMOTER BINDING PROTEIN-LIKE3 Module Regulates Ambient Temperature-Responsive Flowering via *FLOWERING LOCUS T* in Arabidopsis. Plant Physiol. *159*, 461–478. https://doi.org/10.1104/pp.111.192369.

Kim, W., Jun, A.R., and Ahn, J.H. (2016). Proximal disruption of base pairing of the second stem in the upper stem of pri-miR156a caused ambient temperature-sensitive flowering in Arabidopsis. Plant Signal. Behav. *11*. https://doi.org/10.1080/15592324.2016.1226455.

Kinoshita, A., Vayssières, A., Richter, R., Sang, Q., Roggen, A., van Driel, A.D., Smith, R.S., and Coupland, G. (2020). Regulation of shoot meristem shape by photoperiodic signaling and phytohormones during floral induction of Arabidopsis. ELife *9*, e60661. https://doi.org/10.7554/eLife.60661.

Klein, J., Saedler, H., and Huijser, P. (1996). A new family of DNA binding proteins includes putative transcriptional regulators of the *Antirrhinum majus* floral meristem identity gene *SQUAMOSA*. Mol. Gen. Genet. MGG *250*, 7–16. https://doi.org/10.1007/BF02191820.

Knauer, S., Holt, A.L., Rubio-Somoza, I., Tucker, E.J., Hinze, A., Pisch, M., Javelle, M., Timmermans, M.C., Tucker, M.R., and Laux, T. (2013). A Protodermal miR394 Signal Defines a Region of Stem Cell Competence in the Arabidopsis Shoot Meristem. Dev. Cell *24*, 125–132. https://doi.org/10.1016/j.devcel.2012.12.009.

Kozomara, A., Birgaoanu, M., and Griffiths-Jones, S. (2019). miRBase: from microRNA sequences to function. Nucleic Acids Res. *47*, D155–D162. https://doi.org/10.1093/nar/gky1141.

Kurihara, Y., and Watanabe, Y. (2004). Arabidopsis micro-RNA biogenesis through Dicer-like 1 protein functions. Proc. Natl. Acad. Sci. *101*, 12753–12758. https://doi.org/10.1073/pnas.0403115101.

Kurihara, D., Mizuta, Y., Sato, Y., and Higashiyama, T. (2015). ClearSee: a rapid optical clearing reagent for whole-plant fluorescence imaging. Development *142*, 4168–4179. https://doi.org/10.1242/dev.127613.

Kurihara, Y., Takashi, Y., and Watanabe, Y. (2006). The interaction between DCL1 and HYL1 is important for efficient and precise processing of pri-miRNA in plant microRNA biogenesis. RNA *12*, 206–212. https://doi.org/10.1261/rna.2146906.

Kwiatkowska, D. (2008). Flowering and apical meristem growth dynamics. J. Exp. Bot. *59*, 187–201. https://doi.org/10.1093/jxb/erm290.

Landrein, B., Refahi, Y., Besnard, F., Hervieux, N., Mirabet, V., Boudaoud, A., Vernoux, T., and Hamant, O. (2015). Meristem size contributes to the robustness of phyllotaxis in Arabidopsis. J. Exp. Bot. *66*, 1317–1324. https://doi.org/10.1093/jxb/eru482.

Lanet, E., Delannoy, E., Sormani, R., Floris, M., Brodersen, P., Crété, P., Voinnet, O., and Robaglia, C. (2009). Biochemical Evidence for Translational Repression by Arabidopsis MicroRNAs. Plant Cell *21*, 1762–1768. https://doi.org/10.1105/tpc.108.063412.

Laubinger, S., Sachsenberg, T., Zeller, G., Busch, W., Lohmann, J.U., Rätsch, G., and Weigel, D. (2008). Dual roles of the nuclear cap-binding complex and SERRATE in pre-mRNA splicing and microRNA processing in *Arabidopsis thaliana*. Proc. Natl. Acad. Sci. *105*, 8795–8800. https://doi.org/10.1073/pnas.0802493105.

Laufs, P., Peaucelle, A., Morin, H., and Traas, J. (2004). MicroRNA regulation of the *CUC* genes is required for boundary size control in Arabidopsis meristems. Development *131*, 4311–4322. https://doi.org/10.1242/dev.01320.

Leakey, A.D.B., Ainsworth, E.A., Bernacchi, C.J., Rogers, A., Long, S.P., and Ort, D.R. (2009). Elevated CO2 effects on plant carbon, nitrogen, and water relations: six important lessons from FACE. J. Exp. Bot. *60*, 2859–2876. https://doi.org/10.1093/jxb/erp096.

Lee, B., Yu, S., and Jackson, D. (2009). Control of Plant Architecture: The Role of Phyllotaxy and Plastochron. J. Plant Biol. *52*, 277–282. https://doi.org/10.1007/s12374-009-9034-x.

Lee, C., Kim, S.-J., Jin, S., Susila, H., Youn, G., Nasim, Z., Alavilli, H., Chung, K.-S., Yoo, S.J., and Ahn, J.H. (2019). Genetic interactions reveal the antagonistic roles of FT/TSF and TFL1 in the determination of inflorescence meristem identity in Arabidopsis. Plant J. *99*, 452–464. https://doi.org/10.1111/tpj.14335.

Lee, R.C., Feinbaum, R.L., and Ambros, V. (1993). The *C. elegans* heterochronic gene *lin-4* encodes small RNAs with antisense complementarity to *lin-14*. Cell *75*, 843–854. https://doi.org/10.1016/0092-8674(93)90529-Y.

Li, J., Gao, X., Zhang, X., and Liu, C. (2020). Dynamic Expansion and Functional Evolutionary Profiles of Plant Conservative Gene Family SBP-Box in Twenty Two Flowering Plants and the Origin of miR156. Biomolecules *10*, 757. https://doi.org/10.3390/biom10050757.

Li, M., Yu, H., Liu, K., Yang, W., Zhou, B., Gan, L., Li, S., Zhang, C., and Yu, B. (2021a). Serrate-Associated Protein 1, a splicing-related protein, promotes miRNA biogenesis in Arabidopsis. New Phytol. *232*, 1959–1973. https://doi.org/10.1111/nph.17691.

Li, Q., Liu, N., Liu, Q., Zheng, X., Lu, L., Gao, W., Liu, Y., Liu, Y., Zhang, S., Wang, Q., et al. (2021b). DEAD-box helicases modulate dicing body formation in Arabidopsis. Sci. Adv. https://doi.org/10.1126/sciadv.abc6266.

Li, S., Liu, L., Zhuang, X., Yu, Y., Liu, X., Cui, X., Ji, L., Pan, Z., Cao, X., Mo, B., et al. (2013). MicroRNAs Inhibit the Translation of Target mRNAs on the Endoplasmic Reticulum in Arabidopsis. Cell *153*, 562–574. https://doi.org/10.1016/j.cell.2013.04.005.

Lian, H., Wang, L., Ma, N., Zhou, C.-M., Han, L., Zhang, T.-Q., and Wang, J.-W. (2021). Redundant and specific roles of individual *MIR172* genes in plant development. PLOS Biol. *19*, e3001044. https://doi.org/10.1371/journal.pbio.3001044.

Liang, X., Nazarenus, T.J., and Stone, J.M. (2008). Identification of a Consensus DNA-Binding Site for the *Arabidopsis thaliana* SBP Domain Transcription Factor, AtSPL14, and Binding Kinetics by Surface Plasmon Resonance. Biochemistry *47*, 3645–3653. https://doi.org/10.1021/bi701431y.

Liljegren, S.J., Gustafson-Brown, C., Pinyopich, A., Ditta, G.S., and Yanofsky, M.F. (1999). Interactions among APETALA1, LEAFY, and TERMINAL FLOWER1 Specify Meristem Fate. Plant Cell *11*, 1007–1018. https://doi.org/10.2307/3870794.

Liu, C., Zhou, J., Bracha-Drori, K., Yalovsky, S., Ito, T., and Yu, H. (2007). Specification of Arabidopsis floral meristem identity by repression of flowering time genes. Development *134*, 1901–1910. https://doi.org/10.1242/dev.003103.

Liu, C., Chen, H., Er, H.L., Soo, H.M., Kumar, P.P., Han, J.-H., Liou, Y.C., and Yu, H. (2008). Direct interaction of AGL24 and SOC1 integrates flowering signals in Arabidopsis. Development *135*, 1481–1491. https://doi.org/10.1242/dev.020255.

Liu, J., Cheng, X., Liu, P., and Sun, J. (2017). miR156-Targeted SBP-Box Transcription Factors Interact with DWARF53 to Regulate *TEOSINTE BRANCHED1* and *BARREN STALK1* Expression in Bread Wheat. Plant Physiol. *174*, 1931–1948. https://doi.org/10.1104/pp.17.00445.

Liu, L., Farrona, S., Klemme, S., and Turck, F.K. (2014). Post-fertilization expression of *FLOWERING LOCUS T* suppresses reproductive reversion. Front. Plant Sci. *5*. .

Liu, L., Li, C., Teo, Z.W.N., Zhang, B., and Yu, H. (2019). The MCTP-SNARE Complex Regulates Florigen Transport in Arabidopsis. Plant Cell *31*, 2475–2490. https://doi.org/10.1105/tpc.18.00960.

Livak, K.J., and Schmittgen, T.D. (2001). Analysis of Relative Gene Expression Data Using Real-Time Quantitative PCR and the 2−ΔΔCT Method. Methods *25*, 402–408. https://doi.org/10.1006/meth.2001.1262.

Llave, C., Kasschau, K.D., Rector, M.A., and Carrington, J.C. (2002a). Endogenous and Silencing-Associated Small RNAs in Plants. Plant Cell *14*, 1605–1619. https://doi.org/10.1105/tpc.003210.

Llave, C., Xie, Z., Kasschau, K.D., and Carrington, J.C. (2002b). Cleavage of *Scarecrow-like* mRNA Targets Directed by a Class of Arabidopsis miRNA. Science *297*, 2053–2056. https://doi.org/10.1126/science.1076311.

Long, J., and Barton, M.K. (2000). Initiation of Axillary and Floral Meristems in Arabidopsis. Dev. Biol. *218*, 341–353. https://doi.org/10.1006/dbio.1999.9572.

Lyndon, R.F., and Battey, N.H. (1985). The growth of the shoot apical meristem during flower initiation. Biol. Plant. *27*, 339–349. https://doi.org/10.1007/BF02879875.

Ma, Y., Xue, H., Zhang, F., Jiang, Q., Yang, S., Yue, P., Wang, F., Zhang, Y., Li, L., He, P., et al. (2021). The miR156/SPL module regulates apple salt stress tolerance by activating MdWRKY100 expression. Plant Biotechnol. J. *19*, 311–323. https://doi.org/10.1111/pbi.13464.

Maher, C., Stein, L., and Ware, D. (2006). Evolution of Arabidopsis microRNA families through duplication events. Genome Res. *16*, 510–519. https://doi.org/10.1101/gr.4680506.

Manavella, P.A., Hagmann, J., Ott, F., Laubinger, S., Franz, M., Macek, B., and Weigel, D. (2012). Fast-Forward Genetics Identifies Plant CPL Phosphatases as Regulators of miRNA Processing Factor HYL1. Cell *151*, 859–870. https://doi.org/10.1016/j.cell.2012.09.039.

Mandel, M.A., Gustafson-Brown, C., Savidge, B., and Yanofsky, M.F. (1992). Molecular characterization of the Arabidopsis floral homeotic gene *APETALA1*. Nature *360*, 273–277. https://doi.org/10.1038/360273a0.

Mateos, J.L., Bologna, N.G., Chorostecki, U., and Palatnik, J.F. (2010). Identification of MicroRNA Processing Determinants by Random Mutagenesis of Arabidopsis MIR172a Precursor. Curr. Biol. *20*, 49–54. https://doi.org/10.1016/j.cub.2009.10.072.

Mathieu, J., Warthmann, N., Küttner, F., and Schmid, M. (2007). Export of FT Protein from Phloem Companion Cells Is Sufficient for Floral Induction in Arabidopsis. Curr. Biol. *17*, 1055–1060. https://doi.org/10.1016/j.cub.2007.05.009.

May, P., Liao, W., Wu, Y., Shuai, B., Richard McCombie, W., Zhang, M.Q., and Liu, Q.A. (2013). The effects of carbon dioxide and temperature on microRNA expression

in *Arabidopsis* development. Nat. Commun. *4*, 2145. https://doi.org/10.1038/ncomms3145.

McCarthy, E.W., Mohamed, A., and Litt, A. (2015). Functional Divergence of *APETALA1* and *FRUITFULL* is due to Changes in both Regulation and Coding Sequence. Front. Plant Sci. *6*, 1076. https://doi.org/10.3389/fpls.2015.01076.

McMaster, G.S. (2005). Phytomers, phyllochrons, phenology and temperate cereal development. J. Agric. Sci. *143*, 137–150. https://doi.org/10.1017/S0021859605005083.

Meicenheimer, R.D. (2014). The plastochron index: Still useful after nearly six decades. Am. J. Bot. *101*, 1821–1835. https://doi.org/10.3732/ajb.1400305.

Mi, S., Cai, T., Hu, Y., Chen, Y., Hodges, E., Ni, F., Wu, L., Li, S., Zhou, H., Long, C., et al. (2008). Sorting of Small RNAs into Arabidopsis Argonaute Complexes Is Directed by the 5′ Terminal Nucleotide. Cell *133*, 116–127. https://doi.org/10.1016/j.cell.2008.02.034.

Miao, C., Wang, Z., Zhang, L., Yao, J., Hua, K., Liu, X., Shi, H., and Zhu, J.-K. (2019). The grain yield modulator miR156 regulates seed dormancy through the gibberellin pathway in rice. Nat. Commun. *10*, 1–12. https://doi.org/10.1038/s41467-019-11830-5.

Mirabet, V., Besnard, F., Vernoux, T., and Boudaoud, A. (2012). Noise and Robustness in Phyllotaxis. PLOS Comput. Biol. *8*, e1002389. https://doi.org/10.1371/journal.pcbi.1002389.

Miura, K., Ikeda, M., Matsubara, A., Song, X.-J., Ito, M., Asano, K., Matsuoka, M., Kitano, H., and Ashikari, M. (2010). OsSPL14 promotes panicle branching and higher grain productivity in rice. Nat. Genet. *42*, 545–549. https://doi.org/10.1038/ng.592.

Miyashima, S., Koi, S., Hashimoto, T., and Nakajima, K. (2011). Non-cell-autonomous microRNA165 acts in a dose-dependent manner to regulate multiple differentiation status in the Arabidopsis root. Dev. Camb. Engl. *138*, 2303–2313. https://doi.org/10.1242/dev.060491.

Moon, J., Suh, S.-S., Lee, H., Choi, K.-R., Hong, C.B., Paek, N.-C., Kim, S.-G., and Lee, I. (2003). The *SOC1* MADS-box gene integrates vernalization and gibberellin signals for flowering in Arabidopsis. Plant J. *35*, 613–623. https://doi.org/10.1046/j.1365-313X.2003.01833.x.

Moraes, T.S., Dornelas, M.C., and Martinelli, A.P. (2019). FT/TFL1: Calibrating Plant Architecture. Front. Plant Sci. *10*. .

Moro, B., Chorostecki, U., Arikit, S., Suarez, I.P., Höbartner, C., Rasia, R.M., Meyers, B.C., and Palatnik, J.F. (2018). Efficiency and precision of microRNA biogenesis modes in plants. Nucleic Acids Res. *46*, 10709–10723. https://doi.org/10.1093/nar/gky853.

Mozgova, I., and Hennig, L. (2015). The Polycomb Group Protein Regulatory Network. Annu. Rev. Plant Biol. *66*, 269–296. https://doi.org/10.1146/annurev-arplant-043014-115627.

Musialak-Lange, M., Fiddeke, K., Franke, A., Kragler, F., Abel, C., and Wahl, V. (2021). Sugar Signaling Induces Dynamic Changes During Meristem Development to Regulate Flowering in Arabidopsis. 2021.04.12.439483. https://doi.org/10.1101/2021.04.12.439483.

Musielak, T.J., Schenkel, L., Kolb, M., Henschen, A., and Bayer, M. (2015). A simple and versatile cell wall staining protocol to study plant reproduction. Plant Reprod. *28*, 161–169. https://doi.org/10.1007/s00497-015-0267-1.

Niwa, M., Daimon, Y., Kurotani, K., Higo, A., Pruneda-Paz, J.L., Breton, G., Mitsuda, N., Kay, S.A., Ohme-Takagi, M., Endo, M., et al. (2013). BRANCHED1 Interacts with FLOWERING LOCUS T to Repress the Floral Transition of the Axillary Meristems in Arabidopsis. Plant Cell *25*, 1228–1242. https://doi.org/10.1105/tpc.112.109090.

Nodine, M.D., and Bartel, D.P. (2010). MicroRNAs prevent precocious gene expression and enable pattern formation during plant embryogenesis. Genes Dev. *24*, 2678–2692. https://doi.org/10.1101/gad.1986710.

Olas, J.J., Van Dingenen, J., Abel, C., Działo, M.A., Feil, R., Krapp, A., Schlereth, A., and Wahl, V. (2019). Nitrate acts at the Arabidopsis thaliana shoot apical meristem to regulate flowering time. New Phytol. *223*, 814–827. https://doi.org/10.1111/nph.15812.

Olsen, P.H., and Ambros, V. (1999). The *lin-4* regulatory RNA controls developmental timing in *Caenorhabditis elegans* by blocking *LIN-14* protein synthesis after the initiation of translation. Dev. Biol. *216*, 671–680. https://doi.org/10.1006/dbio.1999.9523.

Ó'Maoiléidigh, D.S., Driel, A.D. van, Singh, A., Sang, Q., Bec, N.L., Vincent, C., Olalla, E.B.G. de, Vayssières, A., Branchat, M.R., Severing, E., et al. (2021). Systematic analyses of the *MIR172* family members of Arabidopsis define their distinct roles in regulation of *APETALA2* during floral transition. PLOS Biol. *19*, e3001043. https://doi.org/10.1371/journal.pbio.3001043.

Pajoro, A., Biewers, S., Dougali, E., Leal Valentim, F., Mendes, M.A., Porri, A., Coupland, G., Van de Peer, Y., van Dijk, A.D.J., Colombo, L., et al. (2014). The (r)evolution of gene regulatory networks controlling Arabidopsis plant reproduction: a two-decade history. J. Exp. Bot. *65*, 4731–4745. https://doi.org/10.1093/jxb/eru233.

Palatnik, J.F., Allen, E., Wu, X., Schommer, C., Schwab, R., Carrington, J.C., and Weigel, D. (2003). Control of leaf morphogenesis by microRNAs. Nature *425*, 257–263. https://doi.org/10.1038/nature01958.

Palauqui, J.-C., and Laufs, P. (2011). Phyllotaxis: In Search of the Golden Angle. Curr. Biol. *21*, R502–R504. https://doi.org/10.1016/j.cub.2011.05.054.

Park, J.-Y., Kim, H., and Lee, I. (2017). Comparative analysis of molecular and physiological traits between perennial *Arabis alpina* Pajares and annual *Arabidopsis thaliana* Sy-0. Sci. Rep. *7*, 13348. https://doi.org/10.1038/s41598-017-13606-7.

Park, M.Y., Wu, G., Gonzalez-Sulser, A., Vaucheret, H., and Poethig, R.S. (2005). Nuclear processing and export of microRNAs in Arabidopsis. Proc. Natl. Acad. Sci. *102*, 3691–3696. https://doi.org/10.1073/pnas.0405570102.

Park, W., Li, J., Song, R., Messing, J., and Chen, X. (2002). CARPEL FACTORY, a Dicer Homolog, and HEN1, a Novel Protein, Act in microRNA Metabolism in *Arabidopsis thaliana*. Curr. Biol. CB *12*, 1484–1495. .

Pasquinelli, A.E., Reinhart, B.J., Slack, F., Martindale, M.Q., Kuroda, M.I., Maller, B., Hayward, D.C., Ball, E.E., Degnan, B., Müller, P., et al. (2000). Conservation of the sequence and temporal expression of *let-7* heterochronic regulatory RNA. Nature *408*, 86–89. https://doi.org/10.1038/35040556.

Pengelly, A.R., Copur, Ö., Jäckle, H., Herzig, A., and Müller, J. (2013). A Histone Mutant Reproduces the Phenotype Caused by Loss of Histone-Modifying Factor Polycomb. Science *339*, 698–699. https://doi.org/10.1126/science.1231382.

Pfeiffer, A., Janocha, D., Dong, Y., Medzihradszky, A., Schöne, S., Daum, G., Suzaki, T., Forner, J., Langenecker, T., Rempel, E., et al. (2016). Integration of light and metabolic signals for stem cell activation at the shoot apical meristem. ELife *5*, e17023. https://doi.org/10.7554/eLife.17023.

Picó, S., Ortiz-Marchena, M.I., Merini, W., and Calonje, M. (2015). Deciphering the Role of POLYCOMB REPRESSIVE COMPLEX1 Variants in Regulating the Acquisition of Flowering Competence in Arabidopsis. Plant Physiol. *168*, 1286–1297. https://doi.org/10.1104/pp.15.00073.

Plotnikova, A., Kellner, M.J., Mosiolek, M., Schon, M.A., and Nodine, M.D. (2019). MicroRNA Dynamics and Functions During Arabidopsis Embryogenesis. BioRxiv 633735. https://doi.org/10.1101/633735.

Poethig, R.S. (2013). Vegetative phase change and shoot maturation in plants. Curr. Top. Dev. Biol. *105*, 125–152. https://doi.org/10.1016/B978-0-12-396968-2.00005-1.

Ponnu, J., Schlereth, A., Zacharaki, V., Działo, M.A., Abel, C., Feil, R., Schmid, M., and Wahl, V. (2020). The trehalose 6-phosphate pathway impacts vegetative phase change in Arabidopsis thaliana. Plant J. *n/a*. https://doi.org/10.1111/tpj.14965.

Porri, A., Torti, S., Romera-Branchat, M., and Coupland, G. (2012). Spatially distinct regulatory roles for gibberellins in the promotion of flowering of Arabidopsis under long photoperiods. Development *139*, 2198–2209. https://doi.org/10.1242/dev.077164.

Pouteau, S., and Albertini, C. (2009). The significance of bolting and floral transitions as indicators of reproductive phase change in Arabidopsis. J. Exp. Bot. *60*, 3367–3377. https://doi.org/10.1093/jxb/erp173.

Preston, J.C., and Hileman, L. (2013). Functional Evolution in the Plant SQUAMOSA-PROMOTER BINDING PROTEIN-LIKE (SPL) Gene Family. Front. Plant Sci. *4*. https://doi.org/10.3389/fpls.2013.00080.

Qi, Y., He, X., Wang, X.-J., Kohany, O., Jurka, J., and Hannon, G.J. (2006). Distinct catalytic and non-catalytic roles of ARGONAUTE4 in RNA-directed DNA methylation. Nature *443*, 1008–1012. https://doi.org/10.1038/nature05198.

R core Team (2020). R: A Language and Environment for Statistical Computing (Vienna, Austria: R Foundation for Statistical Computing).

Raczynska, K.D., Stepien, A., Kierzkowski, D., Kalak, M., Bajczyk, M., McNicol, J., Simpson, C.G., Szweykowska-Kulinska, Z., Brown, J.W.S., and Jarmolowski, A. (2014). The SERRATE protein is involved in alternative splicing in Arabidopsis thaliana. Nucleic Acids Res. *42*, 1224–1244. https://doi.org/10.1093/nar/gkt894.

Reinhart, B.J., Weinstein, E.G., Rhoades, M.W., Bartel, B., and Bartel, D.P. (2002). MicroRNAs in plants. Genes Dev. *16*, 1616–1626. https://doi.org/10.1101/gad.1004402.

Rhoades, M.W., Reinhart, B.J., Lim, L.P., Burge, C.B., Bartel, B., and Bartel, D.P. (2002). Prediction of Plant MicroRNA Targets. Cell *110*, 513–520. https://doi.org/10.1016/S0092-8674(02)00863-2.

Rodrigues, A.S., and Miguel, C.M. (2017). The pivotal role of small non-coding RNAs in the regulation of seed development. Plant Cell Rep. *36*, 653–667. https://doi.org/10.1007/s00299-017-2120-5.

Rogers, K., and Chen, X. (2013). Biogenesis, Turnover, and Mode of Action of Plant MicroRNAs. Plant Cell *25*, 2383. https://doi.org/10.1105/tpc.113.113159.

Romera-Branchat, M., Severing, E., Pocard, C., Ohr, H., Vincent, C., Née, G., Martinez-Gallegos, R., Jang, S., Andrés, F., Madrigal, P., et al. (2020). Functional Divergence of the Arabidopsis Florigen-Interacting bZIP Transcription Factors FD and FDP. Cell Rep. *31*, 107717. https://doi.org/10.1016/j.celrep.2020.107717.

Rose, N.L., Yang, H., Turner, S.D., and Simpson, G.L. (2012). An assessment of the mechanisms for the transfer of lead and mercury from atmospherically contaminated organic soils to lake sediments with particular reference to Scotland, UK. Geochim. Cosmochim. Acta *82*, 113–135. https://doi.org/10.1016/j.gca.2010.12.026.

Rougvie, A.E., and Moss, E.G. (2013). Chapter Six - Developmental Transitions in *C. elegans* Larval Stages. In Current Topics in Developmental Biology, A.E. Rougvie, and M.B. O'Connor, eds. (Academic Press), pp. 153–180.

Roussin-Léveillée, C., Silva-Martins, G., and Moffett, P. (2020). ARGONAUTE5 Represses Age-Dependent Induction of Flowering Through Physical and Functional Interaction with miR156 in Arabidopsis. Plant Cell Physiol. *61*, 957–966. https://doi.org/10.1093/pcp/pcaa022.

Ruvkun, G., and Giusto, J. (1989). The *Caenorhabditis elegans* heterochronic gene *lin-14* encodes a nuclear protein that forms a temporal developmental switch. Nature *338*, 313–319. https://doi.org/10.1038/338313a0.

Ruvkun, G., Wightman, B., and Ha, I. (2004). The 20 years it took to recognize the importance of tiny RNAs. Cell *116*, S93–S98. https://doi.org/10.1016/S0092-8674(04)00034-0.

Samach, A., Onouchi, H., Gold, S.E., Ditta, G.S., Schwarz-Sommer, Z., Yanofsky, M.F., and Coupland, G. (2000). Distinct Roles of CONSTANS Target Genes in Reproductive Development of Arabidopsis. Science *288*, 1613–1616. https://doi.org/10.1126/science.288.5471.1613.

Sang, Q., Vayssières, A., Ó'Maoiléidigh, D.S., Yang, X., Vincent, C., Bertran Garcia de Olalla, E., Cerise, M., Franzen, R., and Coupland, G. (2022). MicroRNA172 controls inflorescence meristem size through regulation of APETALA2 in Arabidopsis. New Phytol. *253*, 356–371. https://doi.org/10.1111/nph.18111.

Schauer, S.E., Jacobsen, S.E., Meinke, D.W., and Ray, A. (2002). DICER-LIKE1: blind men and elephants in Arabidopsis development. Trends Plant Sci. *7*, 487–491. https://doi.org/10.1016/S1360-1385(02)02355-5.

Schindelin, J., Arganda-Carreras, I., Frise, E., Kaynig, V., Longair, M., Pietzsch, T., Preibisch, S., Rueden, C., Saalfeld, S., Schmid, B., et al. (2012). Fiji: an open-source platform for biological-image analysis. Nat. Methods *9*, 676–682. https://doi.org/10.1038/nmeth.2019.

Schmieder, R., and Edwards, R. (2011). Fast Identification and Removal of Sequence Contamination from Genomic and Metagenomic Datasets. PLOS ONE *6*, e17288. https://doi.org/10.1371/journal.pone.0017288.

Schultz, E.A., and Haughn, G.W. (1991). *LEAFY*, a Homeotic Gene That Regulates Inflorescence Development in Arabidopsis. Plant Cell *3*, 771–781. https://doi.org/10.1105/tpc.3.8.771.

Schwab, R., Palatnik, J.F., Riester, M., Schommer, C., Schmid, M., and Weigel, D. (2005). Specific Effects of MicroRNAs on the Plant Transcriptome. Dev. Cell *8*, 517–527. https://doi.org/10.1016/j.devcel.2005.01.018.

Schwarz, S., Grande, A.V., Bujdoso, N., Saedler, H., and Huijser, P. (2008). The microRNA regulated SBP-box genes *SPL9* and *SPL15* control shoot maturation in Arabidopsis. Plant Mol. Biol. *67*, 183–195. https://doi.org/10.1007/s11103-008-9310-z.

Skopelitis, D.S., Benkovics, A.H., Husbands, A.Y., and Timmermans, M.C.P. (2017). Boundary Formation through a Direct Threshold-Based Readout of Mobile Small RNA Gradients. Dev. Cell *43*, 265-273.e6. https://doi.org/10.1016/j.devcel.2017.10.003.

Skopelitis, D.S., Hill, K., Klesen, S., Marco, C.F., Born, P. von, Chitwood, D.H., and Timmermans, M.C.P. (2018). Gating of miRNA movement at defined cell-cell

interfaces governs their impact as positional signals. Nat. Commun. *9*, 1–10. https://doi.org/10.1038/s41467-018-05571-0.

Smyth, D.R., Bowman, J.L., and Meyerowitz, E.M. (1990). Early Flower Development in Arabidopsis. Plant Cell *2*, 755–767. https://doi.org/10.2307/3869174.

Song, L., Han, M.-H., Lesicka, J., and Fedoroff, N. (2007). Arabidopsis primary microRNA processing proteins HYL1 and DCL1 define a nuclear body distinct from the Cajal body. Proc. Natl. Acad. Sci. *104*, 5437–5442. https://doi.org/10.1073/pnas.0701061104.

Song, X., Lu, Z., Yu, H., Shao, G., Xiong, J., Meng, X., Jing, Y., Liu, G., Xiong, G., Duan, J., et al. (2017). IPA1 functions as a downstream transcription factor repressed by D53 in strigolactone signaling in rice. Cell Res. *27*, 1128–1141. https://doi.org/10.1038/cr.2017.102.

Song, X., Li, Y., Cao, X., and Qi, Y. (2019). MicroRNAs and Their Regulatory Roles in Plant–Environment Interactions. Annu. Rev. Plant Biol. *70*, 489–525. https://doi.org/10.1146/annurev-arplant-050718-100334.

Stief, A., Altmann, S., Hoffmann, K., Pant, B.D., Scheible, W.-R., and Bäurle, I. (2014). Arabidopsis miR156 Regulates Tolerance to Recurring Environmental Stress through SPL Transcription Factors. Plant Cell *26*, 1792–1807. https://doi.org/10.1105/tpc.114.123851.

Stirnberg, P., Chatfield, S.P., and Leyser, H.M.O. (1999). *AXR1* Acts after Lateral Bud Formation to Inhibit Lateral Bud Growth in Arabidopsis. Plant Physiol. *121*, 839–847. https://doi.org/10.1104/pp.121.3.839.

Suárez-López, P., Wheatley, K., Robson, F., Onouchi, H., Valverde, F., and Coupland, G. (2001). CONSTANS mediates between the circadian clock and the control of flowering in Arabidopsis. Nature *410*, 1116–1120. https://doi.org/10.1038/35074138.

Suh, S.-S., Choi, K.-R., and Lee, I. (2003). Revisiting Phase Transition during Flowering in Arabidopsis. Plant Cell Physiol. *44*, 836–843. https://doi.org/10.1093/pcp/pcg109.

Sun, Z., Su, C., Yun, J., Jiang, Q., Wang, L., Wang, Y., Cao, D., Zhao, F., Zhao, Q., Zhang, M., et al. (2019). Genetic improvement of the shoot architecture and yield in soya bean plants via the manipulation of GmmiR156b. Plant Biotechnol. J. *17*, 50–62. https://doi.org/10.1111/pbi.12946.

Suzuki, M., Wang, H.H.-Y., and McCarty, D.R. (2007). Repression of the *LEAFY COTYLEDON 1/B3* Regulatory Network in Plant Embryo Development by *VP1/ABSCISIC ACID INSENSITIVE 3-LIKE* B3 Genes. Plant Physiol. *143*, 902–911. https://doi.org/10.1104/pp.106.092320.

Tal, L., Friedlander, G., Gilboa, N.S., Unger, T., Gilad, S., and Eshed, Y. (2017). Coordination of Meristem Doming and the Floral Transition by Late Termination, a Kelch Repeat Protein. Plant Cell *29*, 681–696. https://doi.org/10.1105/tpc.17.00030.

Talbert, P.B., Adler, H.T., Parks, D.W., and Comai, L. (1995). The *REVOLUTA* gene is necessary for apical meristem development and for limiting cell divisions in the leaves and stems of Arabidopsis thaliana. Development *121*, 2723–2735. https://doi.org/10.1242/dev.121.9.2723.

Taoka, K., Ohki, I., Tsuji, H., Furuita, K., Hayashi, K., Yanase, T., Yamaguchi, M., Nakashima, C., Purwestri, Y.A., Tamaki, S., et al. (2011). 14-3-3 proteins act as intracellular receptors for rice Hd3a florigen. Nature *476*, 332–335. https://doi.org/10.1038/nature10272.

Teper-Bamnolker, P., and Samach, A. (2005). The Flowering Integrator FT Regulates *SEPALLATA3* and *FRUITFULL* Accumulation in Arabidopsis Leaves. Plant Cell *17*, 2661–2675. https://doi.org/10.1105/tpc.105.035766.

Thieme, C., Schudoma, C., May, P., and Walther, D. (2012). Give It AGO: The Search for miRNA-Argonaute Sorting Signals in *Arabidopsis thaliana* Indicates a Relevance of Sequence Positions Other than the 5′-Position Alone. Front. Plant Sci. *3*. .

Thomas, B., and Vince-Prue, D. (1996). Photoperiodism in Plants (Elsevier).

Tian, R., Wang, F., Zheng, Q., Niza, V.M.A.G.E., Downie, A.B., and Perry, S.E. (2020). Direct and indirect targets of the arabidopsis seed transcription factor ABSCISIC ACID INSENSITIVE3. Plant J. *103*, 1679–1694. https://doi.org/10.1111/tpj.14854.

Todesco, M., Rubio-Somoza, I., Paz-Ares, J., and Weigel, D. (2010). A Collection of Target Mimics for Comprehensive Analysis of MicroRNA Function in *Arabidopsis thaliana*. PLOS Genet. *6*, e1001031. https://doi.org/10.1371/journal.pgen.1001031.

Tong, L., Xue, H., Xiong, L., Xiao, J., and Zhou, Y. (2015). Improved RT-PCR Assay to Quantitate the Pri-, Pre-, and Mature microRNAs with Higher Efficiency and Accuracy. Mol. Biotechnol. *57*, 939–946. https://doi.org/10.1007/s12033-015-9885-y.

Tooke, F., Ordidge, M., Chiurugwi, T., and Battey, N. (2005). Mechanisms and function of flower and inflorescence reversion. J. Exp. Bot. *56*, 2587–2599. https://doi.org/10.1093/jxb/eri254.

Torti, S., and Fornara, F. (2012). AGL24 acts in concert with SOC1 and FUL during Arabidopsis floral transition. Plant Signal. Behav. *7*, 1251–1254. https://doi.org/10.4161/psb.21552.

Torti, S., Fornara, F., Vincent, C., Andrés, F., Nordström, K., Göbel, U., Knoll, D., Schoof, H., and Coupland, G. (2012). Analysis of the Arabidopsis Shoot Meristem Transcriptome during Floral Transition Identifies Distinct Regulatory Patterns and a Leucine-Rich Repeat Protein That Promotes Flowering. Plant Cell *24*, 444–462. https://doi.org/10.1105/tpc.111.092791.

Tsukagoshi, H., Morikami, A., and Nakamura, K. (2007). Two B3 domain transcriptional repressors prevent sugar-inducible expression of seed maturation genes in Arabidopsis seedlings. Proc. Natl. Acad. Sci. *104*, 2543–2547. https://doi.org/10.1073/pnas.0607940104.

Tsukaya, H., Shoda, K., Kim, G.T., and Uchimiya, H. (2000). Heteroblasty in *Arabidopsis thaliana* (L.) Heynh. Planta *210*, 536–542. https://doi.org/10.1007/s004250050042.

Usami, T., Horiguchi, G., Yano, S., and Tsukaya, H. (2009). The *more and smaller cells* mutants of *Arabidopsis thaliana* identify novel roles for *SQUAMOSA PROMOTER BINDING PROTEIN-LIKE* genes in the control of heteroblasty. Development *136*, 955–964. https://doi.org/10.1242/dev.028613.

Valverde, F., Mouradov, A., Soppe, W., Ravenscroft, D., Samach, A., and Coupland, G. (2004). Photoreceptor Regulation of CONSTANS Protein in Photoperiodic Flowering. Science *303*, 1003–1006. https://doi.org/10.1126/science.1091761.

Varkonyi-Gasic, E., Wu, R., Wood, M., Walton, E.F., and Hellens, R.P. (2007). Protocol: a highly sensitive RT-PCR method for detection and quantification of microRNAs. Plant Methods *3*, 12. https://doi.org/10.1186/1746-4811-3-12.

Varkonyi-Gasic, E., Gould, N., Sandanayaka, M., Sutherland, P., and MacDiarmid, R.M. (2010). Characterisation of microRNAs from apple (Malus domestica'Royal Gala') vascular tissue and phloem sap. BMC Plant Biol. *10*, 159. https://doi.org/10.1186/1471-2229-10-159.

Vaucheret, H. (2008). Plant ARGONAUTES. Trends Plant Sci. *13*, 350–358. https://doi.org/10.1016/j.tplants.2008.04.007.

Vazquez, F., Gasciolli, V., Crété, P., and Vaucheret, H. (2004). The Nuclear dsRNA Binding Protein HYL1 Is Required for MicroRNA Accumulation and Plant Development, but Not Posttranscriptional Transgene Silencing. Curr. Biol. *14*, 346–351. https://doi.org/10.1016/j.cub.2004.01.035.

Visentin, I., Pagliarani, C., Deva, E., Caracci, A., Turečková, V., Novák, O., Lovisolo, C., Schubert, A., and Cardinale, F. (2020). A novel strigolactone-miR156 module controls stomatal behaviour during drought recovery. Plant Cell Environ. *43*, 1613–1624. https://doi.org/10.1111/pce.13758.

Wahl, V., Ponnu, J., Schlereth, A., Arrivault, S., Langenecker, T., Franke, A., Feil, R., Lunn, J.E., Stitt, M., and Schmid, M. (2013). Regulation of Flowering by Trehalose-6-Phosphate Signaling in Arabidopsis thaliana. Science *339*, 704–707. https://doi.org/10.1126/science.1230406.

Wang, F., and Perry, S.E. (2013). Identification of Direct Targets of FUSCA3, a Key Regulator of Arabidopsis Seed Development. Plant Physiol. *161*, 1251–1264. https://doi.org/10.1104/pp.112.212282.

Wang, J.-W., Schwab, R., Czech, B., Mica, E., and Weigel, D. (2008). Dual Effects of miR156-Targeted *SPL* Genes and *CYP78A5/KLUH* on Plastochron Length and Organ Size in *Arabidopsis thaliana*. Plant Cell *20*, 1231–1243. https://doi.org/10.1105/tpc.108.058180.

Wang, J.-W., Czech, B., and Weigel, D. (2009). miR156-Regulated SPL Transcription Factors Define an Endogenous Flowering Pathway in *Arabidopsis thaliana*. Cell *138*, 738–749. https://doi.org/10.1016/j.cell.2009.06.014.

Wang, J.-W., Park, M.Y., Wang, L.-J., Koo, Y., Chen, X.-Y., Weigel, D., and Poethig, R.S. (2011). MiRNA Control of Vegetative Phase Change in Trees. PLOS Genet. *7*, e1002012. https://doi.org/10.1371/journal.pgen.1002012.

Wang, L., Song, X., Gu, L., Li, X., Cao, S., Chu, C., Cui, X., Chen, X., and Cao, X. (2013). NOT2 Proteins Promote Polymerase II–Dependent Transcription and Interact with Multiple MicroRNA Biogenesis Factors in Arabidopsis. Plant Cell *25*, 715–727. https://doi.org/10.1105/tpc.112.105882.

Wang, Y., Hindemitt, T., and Mayer, K.F.X. (2006). Significant sequence similarities in promoters and precursors of *Arabidopsis thaliana* non-conserved microRNAs. Bioinformatics *22*, 2585–2589. https://doi.org/10.1093/bioinformatics/btl437.

Wei, X., Ke, H., Wen, A., Gao, B., Shi, J., and Feng, Y. (2021). Structural basis of microRNA processing by Dicer-like 1. Nat. Plants *7*, 1389–1396. https://doi.org/10.1038/s41477-021-01000-1.

Weigel, D., Alvarez, J., Smyth, D.R., Yanofsky, M.F., and Meyerowitz, E.M. (1992). *LEAFY* controls floral meristem identity in Arabidopsis. Cell *69*, 843–859. https://doi.org/10.1016/0092-8674(92)90295-N.

Werner, S., Wollmann, H., Schneeberger, K., and Weigel, D. (2010). Structure Determinants for Accurate Processing of miR172a in *Arabidopsis thaliana*. Curr. Biol. *20*, 42–48. https://doi.org/10.1016/j.cub.2009.10.073.

Wightman, B., Ha, I., and Ruvkun, G. (1993). Posttranscriptional regulation of the heterochronic gene *lin-14* by *lin-4* mediates temporal pattern formation in *C. elegans*. Cell *75*, 855–862. https://doi.org/10.1016/0092-8674(93)90530-4.

Willmann, M.R., Mehalick, A.J., Packer, R.L., and Jenik, P.D. (2011). MicroRNAs Regulate the Timing of Embryo Maturation in Arabidopsis. Plant Physiol. *155*, 1871–1884. https://doi.org/10.1104/pp.110.171355.

Wilson, R.N., Heckman, J.W., and Somerville, C.R. (1992). Gibberellin Is Required for Flowering in *Arabidopsis thaliana* under Short Days. Plant Physiol. *100*, 403–408. https://doi.org/10.1104/pp.100.1.403.

Wood, S. (2012). mgcv: Mixed GAM Computation Vehicle with GCV/AIC/REML smoothness estimation.

Wu, G., and Poethig, R.S. (2006). Temporal Regulation of Shoot Development in *Arabidopsis thaliana* By miR156 and Its Target *SPL3*. Dev. Camb. Engl. *133*, 3539–3547. https://doi.org/10.1242/dev.02521.

Wu, G., Park, M.Y., Conway, S.R., Wang, J.-W., Weigel, D., and Poethig, R.S. (2009). The Sequential Action of miR156 and miR172 Regulates Developmental Timing in Arabidopsis. Cell *138*, 750–759. https://doi.org/10.1016/j.cell.2009.06.031.

Wu, M.-F., Tian, Q., and Reed, J.W. (2006). Arabidopsis microRNA167 controls patterns of *ARF6* and *ARF8* expression, and regulates both female and male reproduction. Development *133*, 4211–4218. https://doi.org/10.1242/dev.02602.

Xie, D., Chen, M., Niu, J., Wang, L., Li, Y., Fang, X., Li, P., and Qi, Y. (2021). Phase separation of SERRATE drives dicing body assembly and promotes miRNA processing in Arabidopsis. Nat. Cell Biol. *23*, 32–39. https://doi.org/10.1038/s41556-020-00606-5.

Xie, K., Wu, C., and Xiong, L. (2006). Genomic organization, differential expression, and interaction of SQUAMOSA promoter-binding-like transcription factors and microRNA156 in rice. Plant Physiol. *142*, 280–293. https://doi.org/10.1104/pp.106.084475.

Xie, Y., Zhou, Q., Zhao, Y., Li, Q., Liu, Y., Ma, M., Wang, B., Shen, R., Zheng, Z., and Wang, H. (2020a). FHY3 and FAR1 Integrate Light Signals with the miR156-SPL Module-Mediated Aging Pathway to Regulate Arabidopsis Flowering. Mol. Plant *13*, 483–498. https://doi.org/10.1016/j.molp.2020.01.013.

Xie, Y., Liu, Y., Ma, M., Zhou, Q., Zhao, Y., Zhao, B., Wang, B., Wei, H., and Wang, H. (2020b). Arabidopsis FHY3 and FAR1 integrate light and strigolactone signaling to regulate branching. Nat. Commun. *11*, 1955. https://doi.org/10.1038/s41467-020-15893-7.

Xie, Z., Allen, E., Fahlgren, N., Calamar, A., Givan, S.A., and Carrington, J.C. (2005). Expression of Arabidopsis *MIRNA* Genes. Plant Physiol. *138*, 2145–2154. https://doi.org/10.1104/pp.105.062943.

Xing, S., Salinas, M., Höhmann, S., Berndtgen, R., and Huijser, P. (2010). miR156-Targeted and Nontargeted SBP-Box Transcription Factors Act in Concert to Secure Male Fertility in Arabidopsis. Plant Cell *22*, 3935–3950. https://doi.org/10.1105/tpc.110.079343.

Xing, S., Salinas, M., and Huijser, P. (2011). New players unveiled in early anther development. Plant Signal. Behav. *6*, 934–938. https://doi.org/10.4161/psb.6.7.15668.

Xu, M., Hu, T., Smith, M.R., and Poethig, R.S. (2016a). Epigenetic Regulation of Vegetative Phase Change in Arabidopsis. Plant Cell *28*, 28–41. https://doi.org/10.1105/tpc.15.00854.

Xu, Y., Guo, C., Zhou, B., Li, C., Wang, H., Zheng, B., Ding, H., Zhu, Z., Peragine, A., Cui, Y., et al. (2016b). Regulation of Vegetative Phase Change by SWI2/SNF2 Chromatin Remodeling ATPase BRAHMA. Plant Physiol. *172*, 2416–2428. https://doi.org/10.1104/pp.16.01588.

Yamaguchi, A., Kobayashi, Y., Goto, K., Abe, M., and Araki, T. (2005). TWIN SISTER OF FT (TSF) Acts as a Floral Pathway Integrator Redundantly with FT. Plant Cell Physiol. *46*, 1175–1189. https://doi.org/10.1093/pcp/pci151.

Yamaguchi, A., Wu, M.-F., Yang, L., Wu, G., Poethig, R.S., and Wagner, D. (2009). The MicroRNA-Regulated SBP-Box Transcription Factor SPL3 Is a Direct Upstream Activator of *LEAFY*, *FRUITFULL*, and *APETALA1*. Dev. Cell *17*, 268–278. https://doi.org/10.1016/j.devcel.2009.06.007.

Yamaguchi, N., Winter, C.M., Wu, M.-F., Kanno, Y., Yamaguchi, A., Seo, M., and Wagner, D. (2014). Gibberellin Acts Positively Then Negatively to Control Onset of Flower Formation in Arabidopsis. Science *344*, 638–641. https://doi.org/10.1126/science.1250498.

Yamasaki, H., Hayashi, M., Fukazawa, M., Kobayashi, Y., and Shikanai, T. (2009). SQUAMOSA Promoter Binding Protein–Like7 Is a Central Regulator for Copper Homeostasis in Arabidopsis. Plant Cell *21*, 347–361. https://doi.org/10.1105/tpc.108.060137.

Yang, L., Liu, Z., Lu, F., Dong, A., and Huang, H. (2006). SERRATE is a novel nuclear regulator in primary microRNA processing in Arabidopsis. Plant J. Cell Mol. Biol. *47*, 841–850. https://doi.org/10.1111/j.1365-313X.2006.02835.x.

Yang, L., Conway, S.R., and Poethig, R.S. (2011). Vegetative phase change is mediated by a leaf-derived signal that represses the transcription of miR156. Development dev.058578. https://doi.org/10.1242/dev.058578.

Yang, L., Wu, G., and Poethig, R.S. (2012). Mutations in the GW-repeat protein SUO reveal a developmental function for microRNA-mediated translational repression in Arabidopsis. Proc. Natl. Acad. Sci. *109*, 315–320. https://doi.org/10.1073/pnas.1114673109.

Yang, L., Xu, M., Koo, Y., He, J., and Poethig, R.S. (2013). Sugar promotes vegetative phase change in *Arabidopsis thaliana* by repressing the expression of *MIR156A* and *MIR156C*. ELife *2*, e00260. https://doi.org/10.7554/eLife.00260.

Yang, X., Dong, W., Ren, W., Zhao, Q., Wu, F., and He, Y. (2021). Cytoplasmic HYL1 modulates miRNA-mediated translational repression. Plant Cell *33*, 1980–1996. https://doi.org/10.1093/plcell/koab090.

Yoo, S.K., Chung, K.S., Kim, J., Lee, J.H., Hong, S.M., Yoo, S.J., Yoo, S.Y., Lee, J.S., and Ahn, J.H. (2005). CONSTANS Activates *SUPPRESSOR OF OVEREXPRESSION OF CONSTANS 1* through FLOWERING LOCUS T to Promote Flowering in Arabidopsis. Plant Physiol. *139*, 770–778. https://doi.org/10.1104/pp.105.066928.

Yu, H., Ito, T., Wellmer, F., and Meyerowitz, E.M. (2004). Repression of *AGAMOUS-LIKE 24* is a crucial step in promoting flower development. Nat. Genet. *36*, 157–161. https://doi.org/10.1038/ng1286.

Yu, S., Galvão, V.C., Zhang, Y.-C., Horrer, D., Zhang, T.-Q., Hao, Y.-H., Feng, Y.-Q., Wang, S., Schmid, M., and Wang, J.-W. (2012). Gibberellin regulates the Arabidopsis floral transition through miR156-targeted SQUAMOSA promoter binding-like transcription factors. Plant Cell *24*, 3320–3332. https://doi.org/10.1105/tpc.112.101014.

Yu, S., Cao, L., Zhou, C.-M., Zhang, T.-Q., Lian, H., Sun, Y., Wu, J., Huang, J., Wang, G., and Wang, J.-W. (2013). Sugar is an endogenous cue for juvenile-to-adult phase transition in plants. ELife *2*. https://doi.org/10.7554/eLife.00269.

Yuan, L., Song, X., Zhang, L., Yu, Y., Liang, Z., Lei, Y., Ruan, J., Tan, B., Liu, J., and Li, C. (2021). The transcriptional repressors VAL1 and VAL2 recruit PRC2 for genome-wide Polycomb silencing in Arabidopsis. Nucleic Acids Res. *49*, 98–113. https://doi.org/10.1093/nar/gkaa1129.

Yue, Y., Sun, S., Li, J., Yu, H., Wu, H., Sun, B., Li, T., Han, T., and Jiang, B. (2021). GmFULa improves soybean yield by enhancing carbon assimilation without altering flowering time or maturity. Plant Cell Rep. *40*, 1875–1888. https://doi.org/10.1007/s00299-021-02752-y.

Žádníková, P., and Simon, R. (2014). How boundaries control plant development. Curr. Opin. Plant Biol. *17*, 116–125. https://doi.org/10.1016/j.pbi.2013.11.013.

Zhang, H., Xia, R., Meyers, B.C., and Walbot, V. (2015). Evolution, functions, and mysteries of plant ARGONAUTE proteins. Curr. Opin. Plant Biol. *27*, 84–90. https://doi.org/10.1016/j.pbi.2015.06.011.

Zhang, H., Li, Y., and Zhu, J.-K. (2018). Developing naturally stress-resistant crops for a sustainable agriculture. Nat. Plants *4*, 989–996. https://doi.org/10.1038/s41477-018-0309-4.

Zhang, Q.-Q., Wang, J.-G., Wang, L.-Y., Wang, J.-F., Wang, Q., Yu, P., Bai, M.-Y., and Fan, M. (2020). Gibberellin repression of axillary bud formation in Arabidopsis by modulation of DELLA-SPL9 complex activity. J. Integr. Plant Biol. *n/a*, 421–432. https://doi.org/10.1111/jipb.12818.

Zhang, S., Xie, M., Ren, G., and Yu, B. (2013). CDC5, a DNA binding protein, positively regulates posttranscriptional processing and/or transcription of primary microRNA transcripts. Proc. Natl. Acad. Sci. *110*, 17588–17593. https://doi.org/10.1073/pnas.1310644110.

Zhang, X., Niu, D., Carbonell, A., Wang, A., Lee, A., Tun, V., Wang, Z., Carrington, J.C., Chang, C.A., and Jin, H. (2014). ARGONAUTE PIWI domain and microRNA duplex structure regulate small RNA sorting in Arabidopsis. Nat. Commun. *5*, 5468. https://doi.org/10.1038/ncomms6468.

Zhao, H., Lin, K., Ma, L., Chen, Q., Gan, S., and Li, G. (2020). Arabidopsis NUCLEAR FACTOR Y A8 inhibits the juvenile-to-adult transition by activating transcription of MIR156s. J. Exp. Bot. *71*, 4890–4902. https://doi.org/10.1093/jxb/eraa197.

Zhou, M., and Tang, W. (2018). MicroRNA156 amplifies transcription factor-associated cold stress tolerance in plant cells. Mol. Genet. Genomics 1–15. https://doi.org/10.1007/s00438-018-1516-4.

Zhou, C.-M., Zhang, T.-Q., Wang, X., Yu, S., Lian, H., Tang, H., Feng, Z.-Y., Zozomova-Lihová, J., and Wang, J.-W. (2013a). Molecular Basis of Age-Dependent Vernalization in *Cardamine flexuosa*. Science *340*, 1097–1100. https://doi.org/10.1126/science.1234340.

Zhou, Y., Tan, B., Luo, M., Li, Y., Liu, C., Chen, C., Yu, C.-W., Yang, S., Dong, S., Ruan, J., et al. (2013b). HISTONE DEACETYLASE19 Interacts with HSL1 and Participates in the Repression of Seed Maturation Genes in Arabidopsis Seedlings. Plant Cell *25*, 134–148. https://doi.org/10.1105/tpc.112.096313.

Zhu, H., Hu, F., Wang, R., Zhou, X., Sze, S.-H., Liou, L.W., Barefoot, A., Dickman, M., and Zhang, X. (2011). Arabidopsis Argonaute10 Specifically Sequesters miR166/165 to Regulate Shoot Apical Meristem Development. Cell *145*, 242–256. https://doi.org/10.1016/j.cell.2011.03.024.

Zhu, H., Zhou, Y., Castillo-González, C., Lu, A., Ge, C., Zhao, Y.-T., Duan, L., Li, Z., Axtell, M.J., Wang, X.-J., et al. (2013). Bidirectional processing of pri-miRNAs with branched terminal loops by Arabidopsis Dicer-like1. Nat. Struct. Mol. Biol. *20*, 1106–1115. https://doi.org/10.1038/nsmb.2646.

Zhu, Y., Klasfeld, S., Jeong, C.W., Jin, R., Goto, K., Yamaguchi, N., and Wagner, D. (2020). TERMINAL FLOWER 1-FD complex target genes and competition with FLOWERING LOCUS T. Nat. Commun. *11*, 5118. https://doi.org/10.1038/s41467-020-18782-1.

11. Acknowledgements

First and foremost, I am extremely grateful to Prof. Dr. George Coupland, who gave me the opportunity to work on this exciting topic. George, thanks for your patience, plenty of fruitful discussions and advice mixed with light-hearted comments. And yes, I very much appreciated your models on inflorescence development.

To my Prof. Dr. Ute Höcker, Prof. Dr. Martin Hülskamp and Dr. John Chandler for being part of my examination committee and taking time to assess my thesis and defence. I am also grateful to John for language editing of the thesis.

Thanks to Dr. Maria Albani and Prof. Dr. Youbong Hyun for following my journey as part of the Thesis Advisory Committee and offering advice and encouragement along the way. Youbong thanks for your supervision and help during the initial phase of this project. Maria thanks for inspiring and encouraging me to pursue a PhD.

Thanks to Dr. Vidya Oruganti for carefully analysing the sRNA-seq experiment, great discussions and sharing her bioinformatics knowledge with me.

I would like to extend my thanks to Wei, Clara, Imke and Julia, who gave me the opportunity to gain experience in supervising. You made me realise that teaching can be fun and that I know a lot about seemingly less important things in the lab.

Thanks to the MPIPZ, greenhouse, genome centre, CeMic and technical service teams for making the experimental life easier. Special thanks to Renate for mastering the difficult task of keeping the growth cabinets in Halle 14 up and running.

Thanks to our PhD coordinator Dr. Stephan Wagner for organising the IMPRS program, sending out gentle reminders and knowing the answer to every question.

Thanks to all current and former members of the Coupland group that created such a welcoming and collaborative environment.

To my friends in office F-O3. Thanks to Dr. Annabel van Driel and Dr. Eva Herrero Madrid for welcoming me from day one on. Thanks to Annabel and Enric Bertran Garcia de Olalla for transforming the office F-O3 into the unofficial social room with a

constant supply of cakes, snacks and coffee. It was a unique experience and definitively one of the many highlights during my PhD. And yes, Nein Mann was a good way to finish work on a Friday.

I am grateful to Dr. Yohanna Miotto and Dr. Alba Lloret Compañ for taking over experiments during the writing phase and for vivid and inspiring discussions. I am even more grateful for your friendship.

Thanks to the Saladomics: Vítor, Jana, Marty, Andrea, Niha, Enric, Yohanna, Nick, Alba, Andrès and Jasmin. We had a great harvest this year and additionally, you were a great audience to try out jokes on.

Danke an Nora, Timo und Linnea, die mit viel Spiel und Spaß für die nötige Ablenkung gesorgt haben und mir beigebracht haben, wie man nach forscher Aufforderung („jau!“) unzählige Katzenzeichungen anfertigt.

An meine Schwester und insbesondere meine Eltern, für die fortwährende Unterstützung während der Promotion. Mama, Papa, danke für euren bedingungslosen Rückhalt und dass ihr mir ermöglicht habt meinen eigenen Weg zu gehen.

Abschließend geht mein ganz besonderer Dank an Carolin. Ohne deine Heiterkeit, deine Unterstützung und dein Verständnis ging es nicht. Danke, dass du immer für mich da warst und mich auch mal auf andere Gedanken gebracht hast.